Low-Cost Masonry for the Design of Barrel-Vaulted Flooring Systems

by

Nebyu Samuel Haile

B.S. in Civil Engineering
Massachusetts Institute of Technology, 2022

Submitted to the Department of Architecture in Partial Fulfillment of the Requirements for the Degree of

MASTER OF SCIENCE IN BUILDING TECHNOLOGY

at the

Massachusetts Institute of Technology

May 2024

Authored by: Nebyu Samuel Haile
Department of Architecture
April 29, 2024

Certified by: John A. Ochsendorf
Class of 1942 Professor
Professor of Architecture
Professor of Civil & Environmental Engineering
Thesis Supervisor

Accepted by: Leslie K. Norford
Chair, Department Committee on Graduate Students
Professor of Building Technology

Low-Cost Masonry for the Design of Barrel-Vaulted Flooring Systems

by

Nebyu Samuel Haile

Submitted to the Department of Architecture on
April 29, 2024
in Partial Fulfillment of the Requirements for the Degree of
Master of Science in Building Technology

ABSTRACT

The world's population is projected to grow rapidly in urban areas, with a projected 2.5 billion more urban dwellers by 2050 (UN-DESA, 2019). This urban growth will notably concentrate in Less Economically Developed Countries (LEDCs), where 16 of the top 20 most populous cities are anticipated to be situated by 2100 (Hoornweg & Pope, 2017). LEDCs face a critical challenge in meeting the demand for affordable housing due to various factors, notably the high material costs, which can make up to 90% of residential construction expenses (Meikle, 2011). Most multi-story housing in LEDCs relies on reinforced concrete frames with flat slabs. This structurally inefficient system heavily depends on imported cement and steel for many locations. Compounding this issue, in LEDCs, the construction sector contributes significantly to their annual carbon emissions, sometimes doubling the global average and exacerbating the climate crisis (Yokoo et al., 2016). Addressing the pressing need for affordable housing requires alternative, more efficient structural systems that utilize affordable and environmentally conscious materials.

This thesis aims to address the challenge of affordable housing by proposing the implementation of unreinforced barrel-vaulted earthen floor systems as an alternative to conventional concrete flat slabs, which are often cost-prohibitive in LEDCs. While existing research predominantly focuses on thin concrete shells for vaulted floors, this study emphasizes earthen vaulted floor systems, utilizing locally available and cost-effective materials. Specifically, it analyzes the maximum spanning capacity of three shallow unreinforced earthen barrel-vaulted floor typologies, examining their associated costs and carbon footprints. Furthermore, the thesis investigates the feasibility of one of these typologies by constructing and evaluating a physical 3m span prototype subjected to international building code loads. The outcomes highlight the structural integrity, cost-effectiveness, and reduced carbon footprint of earthen vaulted floor systems, offering insights into a more environmentally conscious and economically feasible floor system typology for building construction in LEDCs.

Thesis Supervisor: John A. Ochsendorf
Title: Class of 1942 Professor
Professor of Architecture
Professor of Civil & Environmental Engineering

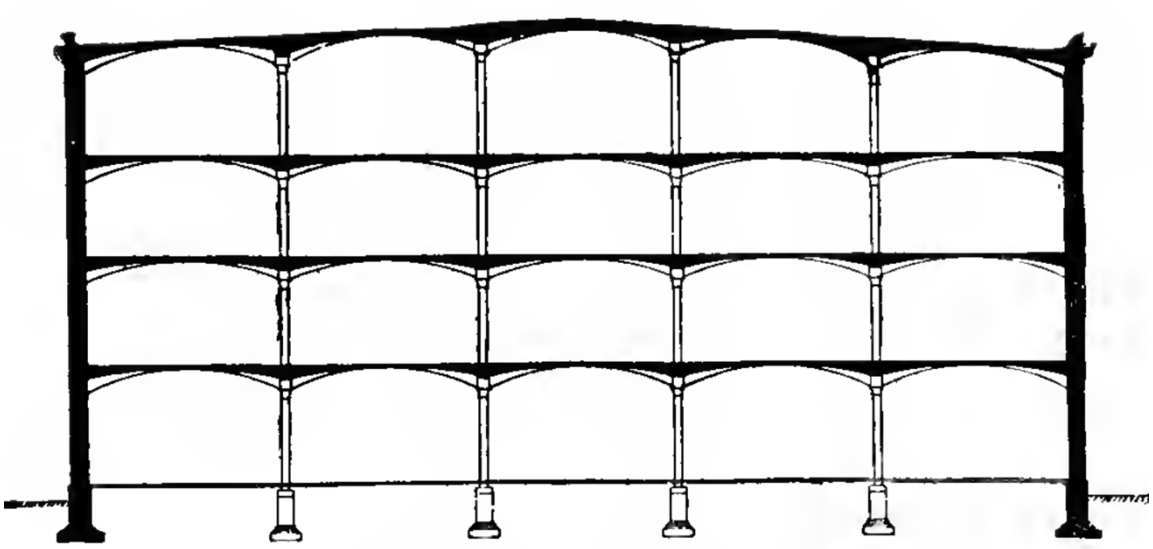

Vaulted factory building - Rafael Guastavino Sr., 1891

Build your architecture from what is beneath your feet.

– Hassan Fathy

Acknowledgements

It takes a village – I am grateful to all those who have helped me in this journey.

First, I would like to thank my Advisor and mentor, Professor John Ochsendorf. It has been my pleasure to have continually learned from you these past two years about my research, structural design as a whole field, and how to teach structural design to students. Thank you for giving me the resources, advice, and continued support to push my research and partake in programs toward furthering my work and career.

To the Building Technology Faculty: Professors Caitlin Mueller, Christopher Reinhart, Leslie Norford, and Leon Glicksman, thank you for the opportunity to learn from you. Many things I have learned in your classes have helped me a great deal in my work and research. To Jennifer Roesch, thank you for always being available to answer questions and help organize catering for meetings and class reviews.

I want to give additional thanks to Professor Norford for allowing me to be a teaching assistance for his class D-Lab Schools which not only provided me valuable teaching experience but allowed me to further my investigation on compressed earth as part of the class which was vital for my thesis work.

I thank all my Building Technology lab mates, past and present, for creating a friendly, open, and inspiring atmosphere to collaborate and learn from. I would like to give a special thanks to Mohamed Ismail, who took me on as a UROP almost five years ago, introduced me to the Lab, and allowed me to work and learn from him. I would also like to thank Natasha Hirt; I enjoyed taking many classes and working on many projects with you over these years.

Much of my work would not have been possible without the many labs who helped me. I want to give a big thanks to Stephen Rudolph and Chris Dewart who provided valuable advice and assistance to help me realize my prototypes. To my partners and friends in Ethiopia, who allowed me to carry out field tests, I want to thank Professor Asgedome Haile and greater EiABC for giving me the resources and support for my work in Ethiopia. I would also like to thank my Uncle Yonas, and his friend Solomon, for all their help in collecting and testing soil samples for my work.

I thank the Roger Foundation for supporting my undergraduate and graduate studies and helping provide the financial assistance that allowed me to focus on my research and intellectual growth. I would also like to thank the PKG Center at MIT for helping fund my IAP project in Ethiopia.

I thank all my friends and my brother Dagm, who motivated me, shared many fun conversations, always reminded me to take breaks, and were always there to help, whether it be reading a paper, rolling up their sleeves, helping me build, or even coming along to my research meetings with John.

Lastly, I want to thank my loved ones for their never-ending support throughout my time at MIT. To my mom, Emebet, thank you for continuously checking in on me. To my dad, Samuel, thank you for always being ready to help, even coming to Ethiopia and playing in the dirt with me. And to my siblings, Dagm and Tsedenya, thank you for all our talks about everything and nothing.

LIST OF FIGURES **7**

LIST OF TABLES **9**

1. INTRODUCTION **10**

1.1. MOTIVATION 10
1.2. BACKGROUND & RELATED WORKS 12
1.2.1. Current Floor Systems Standard *12*
1.2.2. Historic Efficient Floor Systems *14*
1.2.3. Modern Efficient Floor Systems *15*
1.2.4. Compressed Stabilized Earth Bricks *17*
1.3. RESEARCH OBJECTIVE & CONTRIBUTIONS 18

2. SPAN LIMITS OF EARTHEN MASONRY BARREL-VAULTED FLOORS **19**

2.1. METHODOLOGY 19
2.1.1. Floor Typologies *19*
2.1.2. Analysis Assumptions *20*
2.2. RESULTS 22
2.3. DISCUSSION 23

3. COMPRESSED STABILIZED EARTH BRICK PRODUCTION AND PERFORMANCE **24**

3.1. CSEBS IN BOSTON 24
3.1.1. Brick Production & Material Properties *24*
3.1.2. Retesting Bricks and Brick Prisms *27*
3.2. CSEBS IN ETHIOPIA 28
3.2.1. Soil Selection & Brick Production *28*
3.2.2. Brick Material Properties *32*
3.3. DISCUSSION 34

4. EARTHEN MASONRY BARREL VAULTED FLOOR PROTOTYPE **35**

4.1. METHODOLOGY 35
4.1.1. General Design *35*
4.1.2. Preliminary Structural Analysis *37*
4.1.2.1. 2D Analysis *37*
4.1.2.2. 3D Analysis *39*
4.2. TESTING RESULTS 40
4.3. COLLAPSE ANALYSIS 45
4.3.1. Deformations *45*
4.3.2. 2D Analysis Revisited *46*
4.3.3. Explanation for Failure *48*
4.4. DISCUSSION 52

5. CASE STUDY: COST & CARBON SAVINGS **53**

5.1. CONTEXT 53
5.1.1. Integrated Housing Development Programme *53*
5.1.2. Shortcomings of Integrated Housing Development Programme *55*
5.2. METHODOLOGY 56
5.2.1. Floor Designs *56*
5.2.2. Embodied Carbon Coefficients and Material Costs *58*
5.3. RESULTS 59
5.4. DISCUSSION 62

6. CONCLUSION **63**

6.1. SUMMARY OF CONTRIBUTIONS 63
6.2. LIMITATIONS AND FUTURE WORK 63
6.3. CLOSING REMARKS 64

BIBLIOGRAPHY **65**

APPENDIX A – CSEBS 68

PROCEDURE FOR MAKING CSEB 68
BOSTON CSEB 14 DAY STRESS STRAIN PLOTS - COMPRESSION DIRECTION 73
BOSTON CSEB 14 DAY STRESS STRAIN PLOTS - TALL DIRECTION 79
BOSTON 3NG CSEB 50 DAY STRESS STRAIN PLOTS 85
BOSTON 3NG CSEB 8 MONTH STRESS STRAIN PLOTS 88
BOSTON CSEB PRISMS STRESS STRAIN PLOTS - COMPRESSION DIRECTION 89
ETHIOPIAN SOIL SIEVE ANALYSIS 93

APPENDIX B – PROTOTYPE STRUCTURAL ANALYSIS 97

2D EQUILIBRIUM ANALYSIS OF PROTOTYPE 97

List of Figures

FIGURE 1: (A) MOST POPULOUS CITIES BY 2100 (HOORNWEG & POPE, 2017); (B) EXPECTED INCREASE OF FLOOR AREA BY 2050 BY REGION (WEBER ET AL., 2021) 10
FIGURE 2: HOUSING CONSTRUCTION COST BREAKDOWN BY MATERIAL AND LABOR (MEIKLE, 2011) 11
FIGURE 3: (A) PRICE OF CEMENT IN VARIOUS COUNTRIES COMPARED TO USA WITH AFRICAN COUNTRIES IN GREEN; (B) PRICE OF STEEL IN VARIOUS COUNTRIES COMPARED TO USA WITH AFRICAN COUNTRIES IN GREEN (LEONE ET AL., 2021) 11
FIGURE 4: (A) CONCRETE FLAT SLAB IN ETHIOPIA; (B) COMPOSITE METAL DECK FLOOR SYSTEM IN BOSTON (BAILEY, 2003) 13
FIGURE 5: "CONCRETE STRESSES IN A SINGLE-SPANNING RC SLAB AT THE POINT OF BENDING FAILURE …" (HAWKINS, 2020). THE FIGURE HIGHLIGHTS THE LARGE PORTION OF THE SLAB (WHITE) THAT IS NOT UTILIZED UNDER LOADING. 13
FIGURE 6: (A) WAFFLE SLAB [HOLEDECK]; BUBBLE DECK SLAB [TECHNOLOGY IN ARCHITECTURE]; (C) HOLLOW CORE SLAB 13
FIGURE 7: (A) GUASTAVINO TILE ARCH FLOOR SYSTEM (OCHSENDORF, 2010); (B) THRUST LINE UNDER MOVING POINT LOAD IS ALWAYS CONTAINED INSIDE THE STIFFENING WALL OR FILL (GUASTAVINO, 1893) 14
FIGURE 8: (A) RIBBED BARREL-VAULTED FLOOR/ROOF SYSTEM IN BOSTON PUBLIC LIBRARY (OCHSENDORF, 2010); (B) SHALLOW DOUBLE CURVED THIN TILE VAULTED ROOF SYSTEM IN BOSTON PUBLIC LIBRARY (1895) 14
FIGURE 9: (A) HILO PROTOTYPE; (B) EXPLODE VIEW OF HILO PROTOTYPE FORMWORK (LIEW ET AL., 2017) 15
FIGURE 10: DETAILS OF HILO PROTOTYPE EMPLOYED IN HILO RESEARCH & INNOVATION UNIT (RANAUDO ET AL., 2021) 15
FIGURE 11: HAWKING'S VAULTED FLOOR SYSTEM CONCEPTUAL DESIGN AND BUILT PROTOTYPE (HAWKINS, 2020) 16
FIGURE 12: GAITAN PROPOSED EARTHEN VAULT SYSTEM FOR A PARABOLIC ARCH (GAITAN, 2021) 16
FIGURE 13: SHAPED ONE-WAY RIBBED SLAB BY MOHAMED ISMAIL (ISMAIL, 2023) 17
FIGURE 14: VARIOUS COMPRESSED STABILIZED EARTH BRICKS IN ADDIS ABABA, ETHIOPIA AND BOSTON, MASSACHUSETTS 17
FIGURE 15: EARTHEN VAULTED FLOOR TYPOLOGIES; RED SURFACES (A), (B) REPRESENT IMPOSED FINISHING SURFACE LOADS. 19
FIGURE 16: (A) OPTIONS FOR RESOLVING OUTWARD THRUST (HAWKINS, 2020); (B) PROPOSED RING BEAM SYSTEM 20
FIGURE 17: EARTHEN VAULTED FLOOR DETAILS AND TERMINOLOGY 20
FIGURE 18: WORKED EXAMPLE OF CALCULATING MAXIMUM WORKING STRESS IN SAMPLE 5-METER SR TYPOLOGY VAULT. 21
FIGURE 19: WORKING STRESSES OF EARTHEN VAULTED FLOOR TYPOLOGIES; FOLLOWING ON THE WORK OF (GAITAN, 2021) 22
FIGURE 20: PROCEDURE TO PREPARE BOSTON BLUE CLAY FOR MIXING. 24
FIGURE 21: INCREMENTAL MOISTENING OF SOIL MIXTURE 25
FIGURE 22: OPTIMAL WATER CHECK OF MIX USING FIELD DROP TEST 25
FIGURE 23: SUMMARIZED PROCEDURE FOR BRICK COMPACTION 25
FIGURE 24: TESTING DIRECTION FOR COMPRESSIVE STRENGTH OF CSEBS 26
FIGURE 25: (A) 500 3NG BRICKS DURING LEFT TO AIR DRY; (B) BRICK DURING 24-HOUR SOAK BEFORE COMPRESSIVE TESTING 27
FIGURE 26: (A) CEMENT PRISM POST 30-DAY CURING; (B) CRUSHED PRISM; (C) CRUSHED PRISM HIGHLIGHTING 45 DEGREE TYPICAL SHEAR FAILURE 28
FIGURE 27: (A) SOIL MAP OF ADDIS, ABABA [ETHIOPIA MINISTRY OF AGRICULTURE (MOA)]; (B) SOIL SAMPLE LOCATIONS 29
FIGURE 28: (A) SIEVING SOILS IN ETHIOPIA THROUGH 9.5MM SIEVE; (B) ADDING ADDITIONAL SAND TO EACH SOIL TYPE. 30
FIGURE 29: (A) COMPACTION OF BRICKS USING HYDRAULIC PRESS; (B) ADDITIONAL STEEL "LIP" MADE TO OVER FILL MOLD TO BE PRESSED IN ONE PASS. 31
FIGURE 30: (A) CONSTRUCTION OF PRISM; (B) PRISMS DURING AIR DRYING PERIOD. 32
FIGURE 31: (A) BRICKS DURING 24-HOUR SOAK; (B) BRICKS DISSOLVING DURING 24-HOUR SOAK 32
FIGURE 32: EXPLODED AXONOMETRIC DRAWING OF PROTOTYPE 35
FIGURE 33: TECHNICAL DRAWING OF PROTOTYPE [M] 36

FIGURE 34: FORCES AND THRUST LINE IN PROTOTYPE UNDER 4 KN/M² ASYMMETRIC LIVE LOAD 37
FIGURE 35: STRESS CONCENTRATION ANALYSIS; THRUST AND REACTION FORCES SOLVED IN APPENDIX B - "SIZING STEEL TIE" 38
FIGURE 36: TNO ANALYSIS FOR 4 KN/M2 SYMMETRICALLY LOADED 39
FIGURE 37: FIGURE 36: TNO ANALYSIS FOR 4 KN/M2 ASYMMETRICALLY LOADED 40
FIGURE 38: COMPLETED VAULT FLOOR PROTOTYPE PERSPECTIVE VIEW 41
FIGURE 39: COMPLETED VAULT FLOOR PROTOTYPE ELEVATION VIEW 41
FIGURE 40: COMPLETED VAULTED FLOOR PROTOTYPE WITH AUTHOR WALKING ON TOP 42
FIGURE 41: TWENTY-FIVE BUCKETS BEING FILLED WITH WATER DURING 2 KN/M2 ASYMMETRICAL LOADING 43
FIGURE 42: 2 KN/M2 SYMMETRIC LOAD CASE WITH 1.25 KN POINT LOAD AT CENTER 43
FIGURE 43: FIFTY BUCKETS FULL OF WATER ON HALF OF VAULT DURING 4 KN/M2 ASYMMETRICAL LOADING 44
FIGURE 44: VAULT AT MOMENT OF COLLAPSE SHOWCASING THREE BAR HINGE MECHANISM 44
FIGURE 45: ANALYSIS APPROACH FOR CALCULATING DEFORMED GEOMETRY OF VAULT 45
FIGURE 46: DEFORMED GEOMETRIES OF PROTOTYPE DURING LOADING 46
FIGURE 47: FORCES AND THRUST LINE IN 0.47 CM STRIP OF DEFORMED PROTOTYPE UNDER 4 KN/M² ASYMMETRIC LIVE LOAD 46
FIGURE 48: LIMIT ANALYSIS OF A 0.47 CM WIDE STRIP OF DEFORMED PROTOTYPE. 47
FIGURE 49: DEFORMED SHAPE OF PROTOTYPE AFTER TIE ELONGATION 48
FIGURE 50: STRESSES IN PROTOTYPE AFTER TIE ELONGATION 49
FIGURE 51: STRESS - STRAIN CURVE OF MUD PRISM 3 49
FIGURE 52: SIMPLIFIED 2 BAR REPRESENTATION OF DEFORMED VAULT 50
FIGURE 53: ANALYSIS OF DEFORMED VAULT TO MEET SHRINKAGE REQUIREMENTS 50
FIGURE 54: A) 10/90 CONDOMINIUM; (B) 20/80 CONDOMINIUM; (C) 40/60 CONDOMINIUM 53
FIGURE 55: FINISHED 40/60 CONDOMINIUMS ON OUTSKIRTS OF ADDIS ABABA 54
FIGURE 56: 40/60 CONDOMINIUMS UNDER CONSTRUCTION ON OUTSKIRTS OF ADDIS ABABA [CHARLIE ROSSER, 2017] 54
FIGURE 57: AS BUILT TWO-WAY FLAT SLAB DETAILS (MM) 56
FIGURE 58: EARTHEN VAULTED FLOOR DESIGN 1 (MM) 57
FIGURE 59: EARTHEN VAULTED FLOOR DESIGN 2 (MM) 57
FIGURE 60: COST PER M² BREAKDOWN OF CASE STUDY FLOOR SYSTEMS 59
FIGURE 61: EMBODIED CARBON PER M² BREAKDOWN OF CASE STUDY FLOOR SYSTEMS 60
FIGURE 62: WEIGHT PER M² BREAKDOWN OF CASE STUDY FLOOR SYSTEMS 61

**All other figures by Author unless otherwise noted*

List of Tables

Table 1: Applied Loading on Earthen Vaulted Floors by Typology 21
Table 2: Boston CSEB Mix Designs 24
Table 3: Boston CSEB 14 Day Ultimate Strength and Stiffness – Compressed Direction 26
Table 4: Boston CSEB 14 Day Ultimate Strength and Stiffness – Tall Direction 26
Table 5: 3NG 50 Day Dry Ultimate Strength and Stiffness – Compressed Direction 27
Table 6: 3NG 50 Day Wet Ultimate Strength and Stiffness – Compressed Direction 27
Table 7: 3NG 8 Month Dry Ultimate Strength and Stiffness - Compressed Direction 28
Table 8: 3NG Prism Ultimate Strength and Stiffness - Compressed Direction 28
Table 9: Ethiopia Soil Characterization 29
Table 10: Ethiopia CSEB Mix Designs 31
Table 11: Ethiopia CSEB 14 Day Dry Ultimate Strength – Compressed Direction 33
Table 12: Ethiopia CSEB 14 Day Wet Ultimate Strength – Compressed Direction 33
Table 13: Ethiopia CSEB 30 Day Dry Ultimate Strength – Compressed Direction 33
Table 14: Ethiopia CSEB 30 Day Wet Ultimate Strength – Compressed Direction 33
Table 15: Ethiopia CSEB Prism Ultimate Strength - Compressed Direction 33
Table 16: Max Working Stresses in Prototype Vault Under Various Load Cases 38
Table 17: Critical Stress Based on Stress Block 38
Table 18: Deformations of Prototype Compared to Original Sate During Loading 45
Table 19: Deformations of Already Deformed Vault Due to Tie Lengthening 48
Table 20: Summary of Elastic Vault Deformations 51
Table 21: Embodied Carbon Coefficients 58
Table 22: Cost of Material and Labor 58
Table 23: Cost per m^2 Breakdown of Case Study Floor Systems by Percentage of Total 59
Table 24: Embodied Carbon per m^2 Breakdown of Case Study Floor Systems by Percentage of Total 60
Table 25: Weight per m^2 Breakdown of Case Study Floor Systems by Percentage of Total 61

1. Introduction

1.1. Motivation

Over the coming three decades, the United Nations forecasts a migration of an additional 2.5 billion individuals to urban areas (UN-DESA, 2019). This urban expansion is notably concentrated in Less Economically Developed Countries (LEDCs), where it is projected that by 2100, 16 of the top 20 most populous cities will be situated (Hoornweg & Pope, 2017). Among all LEDCs, those in Africa hold significant prominence, as approximately 1.12 billion of the projected 2.5 billion new urban inhabitants are expected to reside in African cities (UN-DESA, 2019). The rapid urban population growth necessitates a substantial increase in infrastructure, particularly in housing infrastructure. Corresponding to the substantial rise in urban population, the International Energy Agency (IEA) estimates a global increase in built floor area of 235 billion m^2 by 2050. Approximately 80% of this anticipated growth until 2030 is expected to occur in emerging countries (Weber et al., 2021).

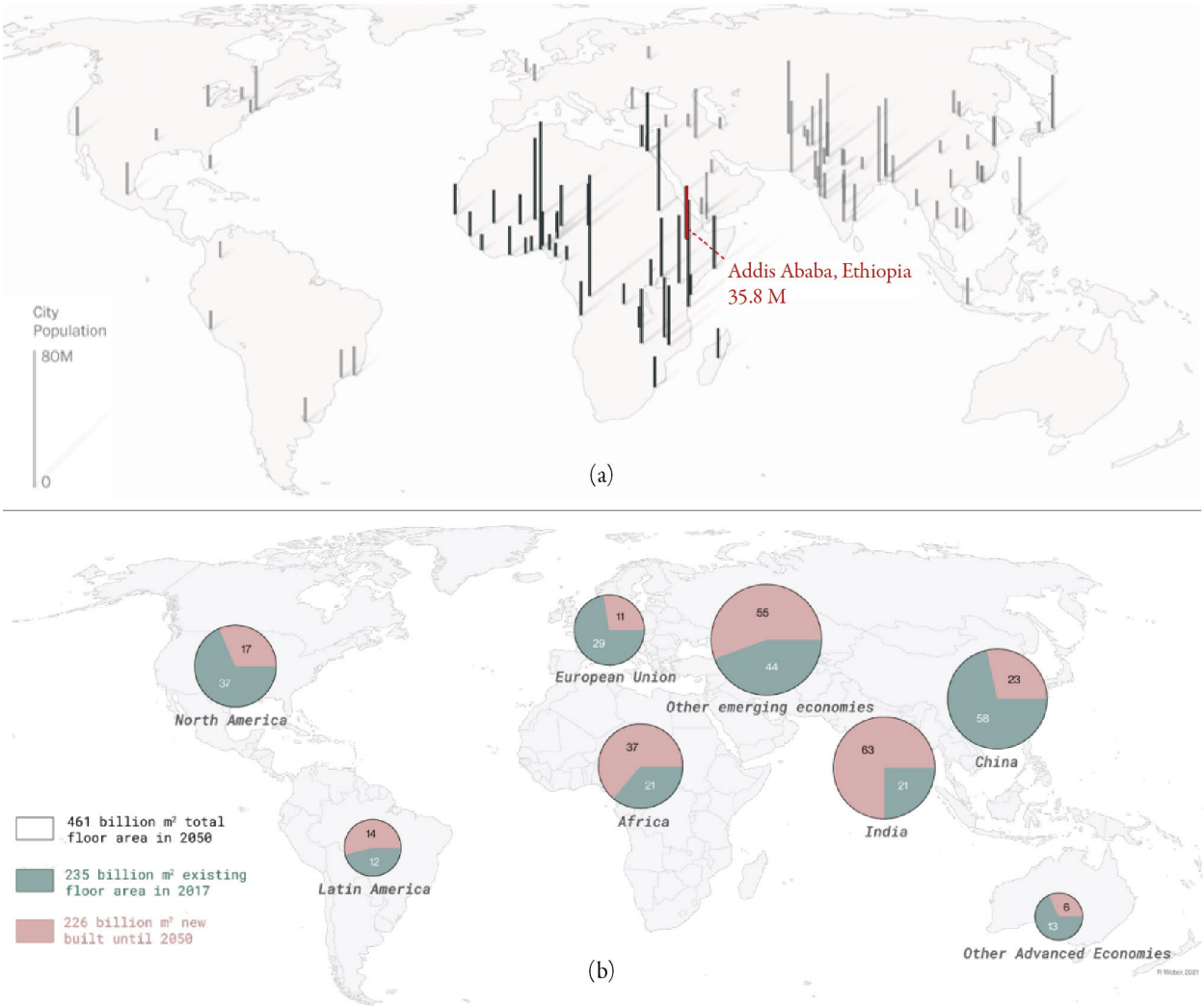

Figure 1: (a) Most populous cities by 2100 (Hoornweg & Pope, 2017); (b) Expected increase of floor area by 2050 by region (Weber et al., 2021)

A study conducted by the World Bank reveals that, among the 88 countries categorized as low-income or low-middle income, the average Gross Domestic Product (GDP) per capita ranges from $1,026 to $4,035. When focusing solely on the 45 United Nations-designated least developed countries, this figure diminishes to a range of $355 to $1,268 (World Bank Open Data, 2024). Consequently, in light of constrained economic conditions, burgeoning population growth, and the imperative for housing, LEDCs confront the urgent challenge of constructing a substantial volume of affordable housing in the coming decades.

Meeting the housing demands of densely populated urban areas necessitates a shift towards multi-story housing projects rather than single-family dwellings. Globally, the construction of multi-story housing predominantly relies on reinforced concrete frames with flat slabs. Unlike in more economically developed nations, where labor costs often dominate, construction expenditures in LEDCs are primarily dictated by material costs, particularly those related to the importation and production of cement and steel. Studies indicate that materials can account for 60-90% of the total cost of new construction in LEDCs (Meikle, 2011; Bah et al., 2018).

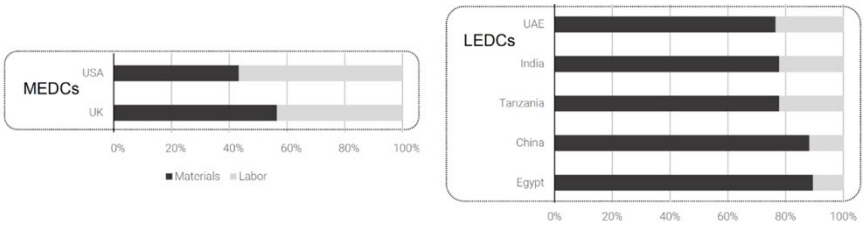

Figure 2: Housing construction cost breakdown by material and labor (Meikle, 2011)

The majority of construction materials, like cement and steel rebar utilized in reinforced concrete design, are imported in LEDCs. For instance, data from the World Bank indicates that, on average, Sub-Saharan African countries allocate approximately 11% of their annual imports towards metals (World Bank Country Profile, 2021). While LEDCs are increasingly expanding local cement production, particularly in Africa, many still lack sufficient production capacity and consequently rely heavily on imports. For instance, a study conducted in 2017 revealed that, across Africa, the total production capacity for cement was 10.2 million metric tons (Mt), while the actual consumption amounted to 81.7 Mt (Leone et al., 2021). The necessity to import these primary construction materials, compounded by the heightened costs associated with local production due to inadequate scale, results in substantial markups, highlighted in Figure 3, and contributes to inflated market rates, thereby elevating construction costs.

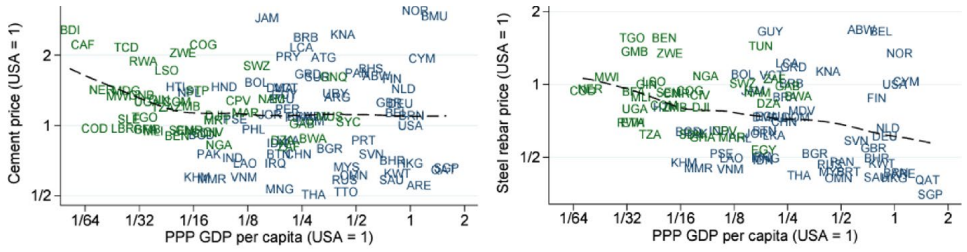

(a) (b)

Figure 3: (a) Price of cement in various countries compared to USA with African countries in green; (b) Price of steel in various countries compared to USA with African countries in green (Leone et al., 2021)

The International Comparison Program (ICP) in 2011 revealed that the average construction cost for a low-rise mass market apartment building and a high-rise (11+ story) mass market building in Africa amounted to $\$54/ft^2$ and $\$70/ft^2$, respectively (World Bank ICP, 2011). By comparison, construction costs in the United States can range from $100 to $400 per square foot (Kilroy, 2024). This discrepancy underscores the relatively high construction costs in LEDCs, considering their significantly lower GDPs, which are often 20 to 30 times lower than that of the USA. However, construction costs in LEDCs are only 3 to 5 times lower (Leone et al., 2021).

Reducing the amount of high-cost construction materials, namely cement and steel rebar, presents the most apparent avenue for cutting construction expenses. In the context of a reinforced concrete frame and flat slab structural system, a study investigating a theoretical 10-story concrete frame building identified the floor system as a key area for potential reduction (De Wolf et al., 2016). Two separate studies examining embodied carbon and embodied energy (direct proxies for the mass of material) in over 600 built buildings across various programs demonstrated that, for a concrete superstructure including foundations, 40-50% of the structural mass can be attributed to the slabs (Huberman et al., 2015; Hattan, 2019). Additionally, recent data-driven modeling of over 100,000 parametric-designed concrete buildings revealed that in residential buildings, 48% of the building's embodied carbon is in the slabs (Sory, 2023).

Furthermore, beyond the immediate goal of cost reduction, minimizing the use of cement and steel also results in a significant reduction in embodied carbon. This is particularly crucial considering the Intergovernmental Panel on Climate Change's (IPCC) plan outlined in 2018 to limit global warming to 1.5°C. This plan entails reducing global CO_2 emissions to 45% of 2010 levels by 2030 and achieving zero emissions by 2050 (IPCC, 2018). Given that the built environment accounts for nearly 40% of global CO_2 emissions, with construction and building materials (primarily steel and concrete) alone responsible for 13%, the reduction of embodied carbon in construction materials becomes imperative (Architecture 2030, 2022).

Given the material and cost concentration in floor systems, this thesis focuses on reducing housing costs in LEDCs by proposing an alternative to the traditional flat slab floor system. Specifically, it introduces an unreinforced barrel-vaulted compression-only masonry floor system. Exploiting the compression-only nature of vaults, this system significantly reduces steel usage while incorporating low-strength materials like earthen masonry units instead of concrete or fired clay bricks, thereby reducing costs compared to traditional floor systems. While this study emphasizes cost reduction, the decreased reliance on cement and steel also aligns with global goals to reduce CO_2 emissions.

1.2. Background & Related Works

1.2.1. Current Floor Systems Standard

The standard for floor systems consists of slab systems, which may be entirely concrete (Figure 4-A), typical in concrete frame buildings, or a combination of concrete and metal decking in steel frame constructions (Figure 4-B). Slab-based floor systems are widely favored due to their straightforward construction, simple formwork, architectural preferences, and shallow depths. However, these structural systems function primarily under bending, resulting in higher stresses that necessitate more material. Moreover, stress distribution in systems activated by bending tends to be uneven (Figure 5), often leaving portions of the slab underutilized, thus constituting an overall material inefficiency (Hawkins, 2020).

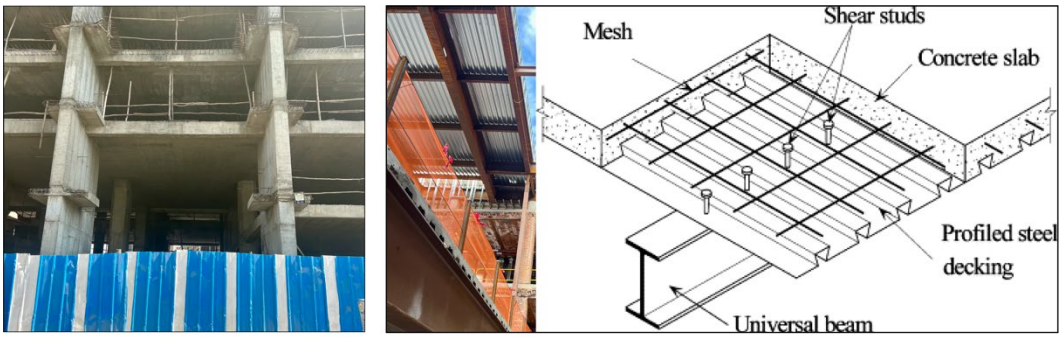

Figure 4: (a) Concrete flat slab in Ethiopia; (b) Composite metal deck floor system in Boston (Bailey, 2003)

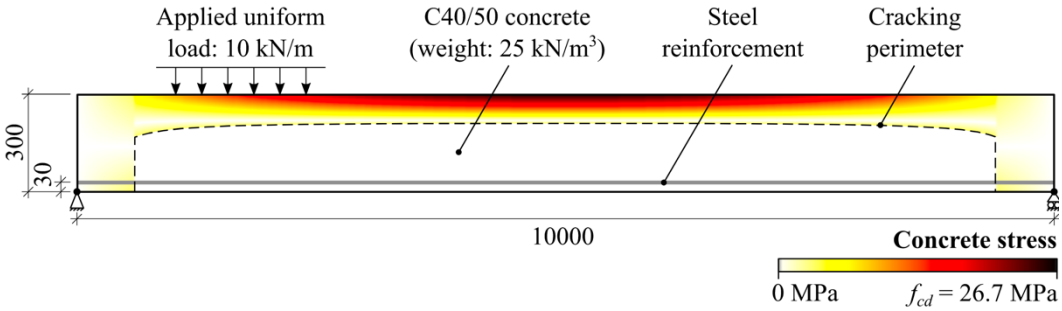

Figure 5: "Concrete stresses in a single-spanning RC slab at the point of bending failure …" (Hawkins, 2020). The figure highlights the large portion of the slab (white) that is not utilized under loading.

Certain contemporary slab systems, such as waffles, bubble decks, and hollow core slabs, have recognized this inefficiency and introduced voids in areas of minimal utilization (Figure 6). Nonetheless, these systems require additional formwork, entail more labor-intensive processes, or necessitate materials like inflated plastic balls. In many LEDCs, facilities for producing prefabricated systems such as hollow core slabs or materials like inflated plastic balls for bubble slabs are not readily available, thus perpetuating the predominant use of simple concrete flat slabs (Ismail, 2023).

Figure 6: (a) Waffle slab [Holedeck]; Bubble deck slab [Technology in Architecture]; (c) Hollow core slab

1.2.2. Historic Efficient Floor Systems

The structural efficiency of vaults lies in their reliance on axial compression rather than bending, enabling the use of brittle materials like stone and brick to span large distances. Arches and vaults derive strength from their geometry, resulting in low internal stresses compared to masonry strength, thereby minimizing the risk of crushing failure (Heyman, 1995). This characteristic led ancient civilizations such as the Nubians and Romans to effectively employ arches and vaults for spanning structures. Even in concrete flat slabs, a strut and tie model can be envisaged where the high compressive force at the top (Figure 5) forms an internal compressive membrane (arch), while the rebar at the bottom acts as a tie for the arch.

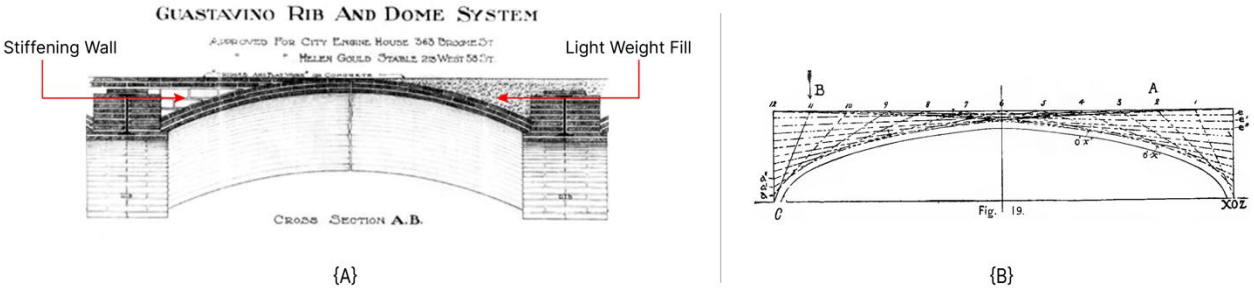

Figure 7: (a) Guastavino Tile Arch Floor System (Ochsendorf, 2010); (b) Thrust line under moving point load is always contained inside the stiffening wall or fill (Guastavino, 1893)

Leveraging the benefits of a vaulted form, In the late 19th to the mid-20th century, Spanish master builders Rafael Guastavino Sr. and Jr. employed their "Tile Arch System," utilizing layers of thin clay tiles to make vaulted roofs and floor systems (Figure 7-A). The floor systems comprised shallow tile vaults with a series of stiffening ribs, on top of which a flat walking surface spanned, or in lieu of the stiffening ribs a lightweight fill was sometimes used (Figure 8). Beyond allowing for a spanning surface, the stiffening walls and fill also play a significant role in allowing for a deeper structural envelope allowing the vault to remain stable under asymmetrical or point loads. Due to their vaulted systems' cost-effectiveness and fireproof nature, The Guastavino Company constructed thousands of such vaults until the mid-20th century, when they closed due to rising labor costs and the popularization of concrete (Ochsendorf, 2010).

Figure 8: (a) Ribbed barrel-vaulted floor/roof system in Boston Public Library (Ochsendorf, 2010); (b) Shallow double curved thin tile vaulted roof system in Boston Public Library (1895)

1.2.3. Modern Efficient Floor Systems

The imperative to combat climate change has spurred a renewed interest in utilizing geometric principles for low-carbon construction techniques. The Block Research Group (BRG) at ETH – Zurich exemplifies this paradigm shift through their prototypes, such as the Hilo Prototype, which employs digital fabrication to create thin, doubly curved shell floor systems with vertical stiffeners and post-tensioned rods or stiff corners to manage thrust (Figure 9-A). HiLo features a 20 mm thick concrete shell made of fiber-reinforced, ultra-high-strength, self-compacting concrete optimized through constrained optimization in a Thrust Network Analysis tool (Liew et al., 2017).

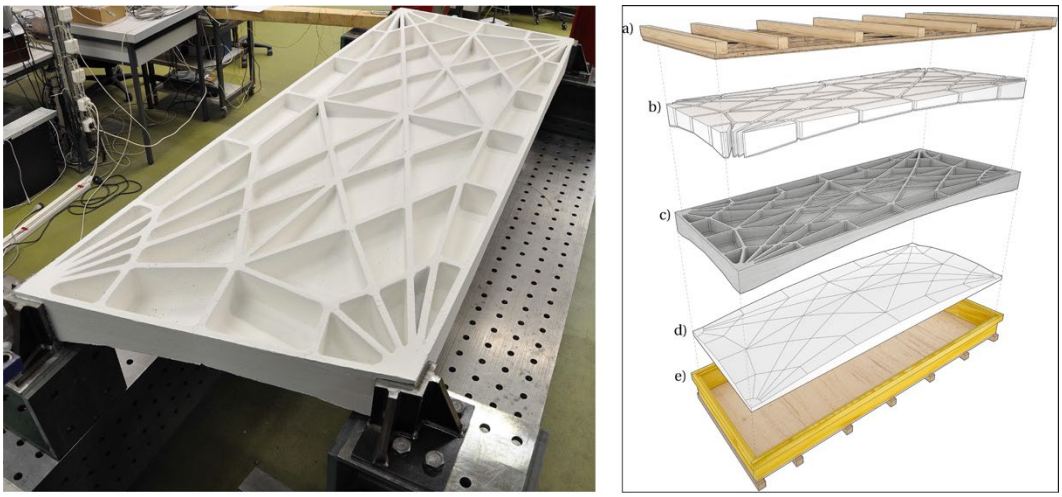

Figure 9: (a) HiLo Prototype; (b) Explode view of HiLo prototype formwork (Liew et al., 2017)

CNC milling, and wire-cutting techniques are utilized to produce double-sided formwork from expanded polystyrene foam and timber (Figure 9-B). The success of these prototypes is evidenced in their application at the building scale within the HiLo research and innovation unit in Dubendorf, Switzerland. The incorporation of two funicular floors covering approximately 20 m2 with a maximum span of 5.2 m resulted in a 70% reduction in concrete usage and a 90% reduction in steel compared to conventional slab structures (Liew et al., 2017).

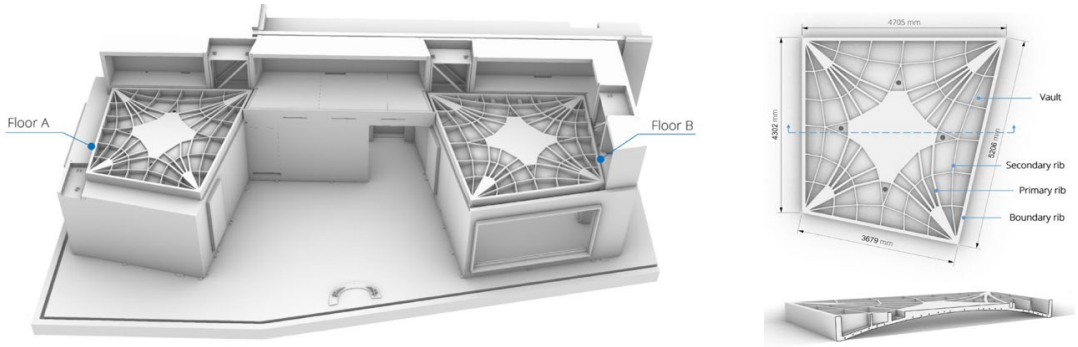

Figure 10: Details of HiLo prototype employed in HiLo research & innovation unit (Ranaudo et al., 2021)

Another efficient floor system proposed by Professor William Hawkins of the University of Bath (Figure 11) entails a doubly curved mesh-reinforced thin concrete shell with a foamed concrete topping surface. (Hawkins, 2020) suggests resolving thrust in the vaults through steel ties spanning between columns or being positioned above the vault, albeit at the expense of introducing bending forces in the columns. Prototype testing demonstrated the system's ability to withstand typical building loads while achieving a 50% reduction in embodied carbon compared to flat slab structures.

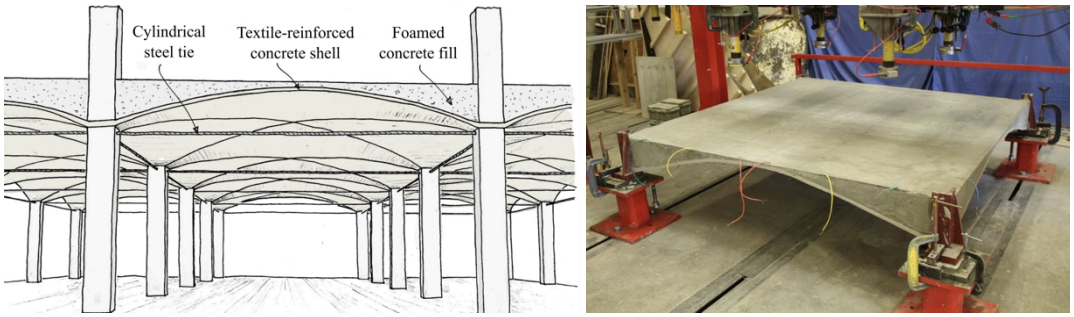

Figure 11: Hawking's vaulted floor system conceptual design and built prototype (Hawkins, 2020)

Inspired by The Guastavino Company's "Tile Arch System," a recent master's thesis by Sabrina Gaitan from the Massachusetts Institute of Technology explores the feasibility of parabolic barrel-vaulted Earthen floor systems. The proposed system (Figure 12) comprises a shallow barrel vault constructed from compressed earth bricks (CEBs), followed by an infill material, and finished with a CEB slab (Gaitan, 2021).

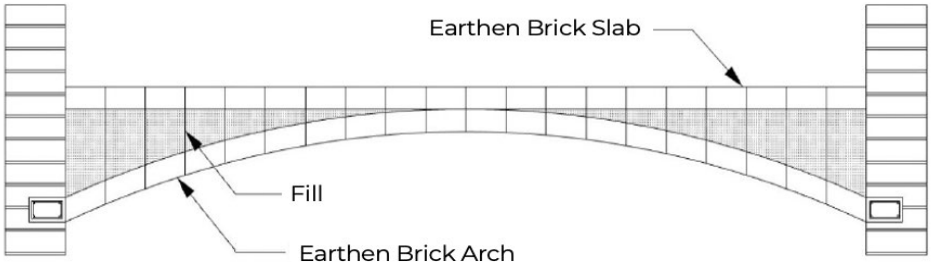

Figure 12: Gaitan proposed earthen vault system for a parabolic arch (Gaitan, 2021)

Gaitan's work emphasizes the low stresses that result from utilizing vaults allows for the use of earthen masonry units that are relatively weak but are much more affordable and have a lower environmental impact. (Gaitan, 2021) explored various aspect ratios (span/5,10,20) as well as various fill densities (1400 kg/m^3 and 2400 kg/m^3) and was able to show that a compressed earth brick with a factored strength of 1.2 MPa could span was far as 7-9 meters under a typical live load of 1.9 kN/m^2.

Another contemporary example (Figure 13) by Professor Mohamed Ismail moves away from vaulted forms but instead focuses on reducing materials in bending activated systems. The system utilizes numerical optimization to shape one-way ribbed slabs according to internal moments and stresses minimizing material usage showcasing up to a 50% reduction in embodied energy compared to a flat two-way slab (Ismail, 2023).

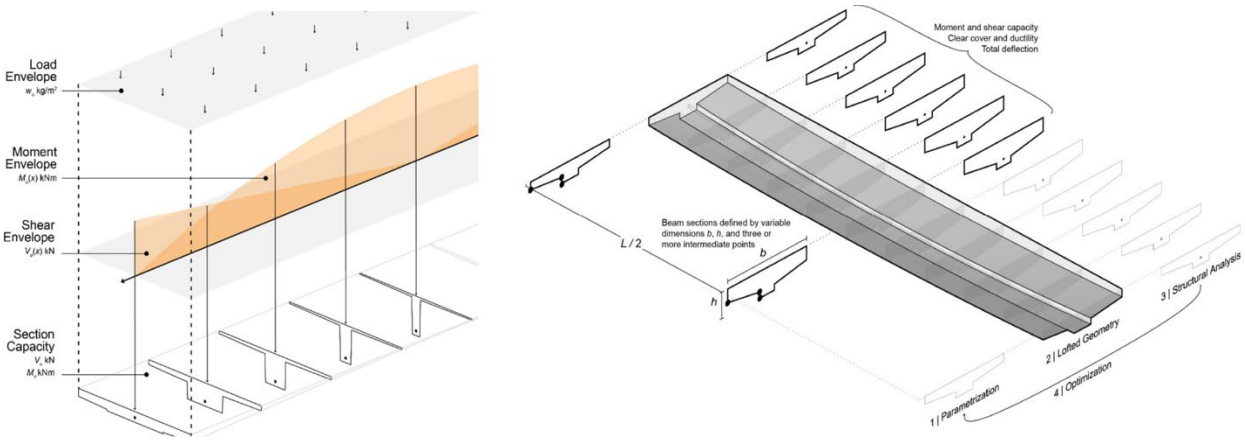

Figure 13: Shaped one-way ribbed slab by Mohamed Ismail (Ismail, 2023)

1.2.4. Compressed Stabilized Earth Bricks

Compressed earth bricks (CEBs) and compressed stabilized earth bricks (CSEB) are low carbon low-cost masonry units that are produced by compressing soil, sand, and small amounts of stabilizing agents, such as cement or lime, under pressure. The properties of CSEBs, including density and strength (ranging from 1500-2200 kg/m3 and 1-40 MPa), vary based on factors like soil composition, compaction pressure, and stabilization amount (Murmu & Patel, 2018). Recently, there has been growing interest in CSEBs for affordable housing due to their sustainability and cost-effectiveness. These bricks utilize locally available materials, demand lower energy inputs than conventional alternatives, and exhibit reduced embodied carbon. CSEBs typically contain 5-7% cement, in contrast to the 10-15% found in conventional concrete used for structural slabs (Murmu & Patel, 2018). Furthermore, unlike fired clay bricks, CSEBs do not require firing, significantly reducing production energy. A case study by the MASS Design Group on the Rwanda Institute for Conservation Agriculture project compared CSEBs and fired clay bricks, revealing that a 5% CSEB had a global warming potential nearly five times lower than a locally sourced fired clay brick (0.04 kgCO2e/kg vs. 0.20 kgCO2e/kg) (Kitchin, 2021). Although the regional cost of CSEBs varies, recent literature consistently demonstrates savings ranging from 15-40% compared to fired clay bricks across various countries (Abdel et al., 2023).

Figure 14: Various compressed stabilized earth bricks in Addis Ababa, Ethiopia and Boston, Massachusetts

1.3. Research Objective & Contributions

Section 1.1 underscores the pressing need for affordable and environmentally sustainable housing solutions within the next three decades, particularly in emerging economies. Additionally, Section 1.2 examines recent construction endeavors demonstrating substantial carbon reductions and presenting promising options for eco-conscious buildings. However, existing research on efficient vaulted floors, exemplified by projects such as HiLo and Hawkins, primarily relies on thin concrete shells utilizing advanced technologies like 3D printing and custom high-strength concrete mixtures (Hawkins, 2020; Liew et al., 2017; Ranaudo et al., 2021). While these approaches enhance carbon efficiency, their cost premiums render them economically unfeasible for many Less Economically Developed Countries, where urban growth is concentrated. Moreover, prior work on earthen vaulted floors, exemplified by Gaitan, is limited in scope, necessitating further exploration into floor typologies, quantifying cost-effectiveness and embodied carbon, structural analysis under building code loads, and validation of theoretical frameworks through physical testing.

Given the exigent demand for housing in emerging economies, there is a distinct necessity for flooring systems that mitigate carbon emissions while prioritizing affordability. This thesis advances the concept of earthen barrel-vaulted floor systems as a viable alternative. Specifically, it introduces three shallow earthen barrel-vaulted floor typologies and assesses their maximum spanning capacity under typical building loads. In particular this thesis focuses on single curvature vaults because they are simple, efficient, and easy to construct in a multitude of environments. Furthermore, it quantifies an earthen floor system's cost and carbon savings through a comparative case study with a conventional concrete flat slab in Addis Ababa, Ethiopia, a representative LEDC context. Finally, the thesis investigates the structural viability of one of these typologies by constructing and evaluating a physical 3m span prototype subjected to international building code loads.

The overarching goal and primary contribution of this thesis are to address the following key questions:

1. **How do unreinforced earthen vaulted floor systems perform in terms of spanning capacity under typical loads?**

2. **Are unreinforced earthen vaulted floor systems structurally viable based on full-scale testing?**

3. **What are the cost and carbon savings associated with unreinforced earthen vaulted floors compared to concrete flat slabs?**

By addressing these questions, this thesis aims to underscore the structural integrity, cost-effectiveness, and reduced carbon footprint of earthen vaulted floor systems, providing valuable insights into a more environmentally conscious and economically viable typology for building construction in LEDCs.

2. Span Limits of Earthen Masonry Barrel-Vaulted Floors

An essential contribution of this thesis is examining the spanning capacity of earthen vaulted floor systems under typical building loads. This section introduces three distinct shallow unreinforced earthen barrel-vaulted floor typologies and employs a parametric workflow to explore their design space. Utilizing 2D equilibrium analysis methods, the stresses within these systems are calculated across different aspect ratios and spans.

2.1. Methodology

2.1.1. Floor Typologies

Figure 15 depicts the three proposed floor typologies. Each typology comprises a primary 5 cm thick unreinforced CSEB parabolic barrel vault. Analogous to the Guastavino "Tile Arch System" (Figure 7), Typologies SR (sparse ribs) and DR (dense ribs) incorporate stiffening walls to support asymmetrical loads and provide a level surface for finishing. Typology SR features 10-centimeter-thick stiffening walls spaced at 1 meter, while typology DR employs 5-centimeter-thick walls at 30-centimeter intervals. Conversely, typology LF (light fill) substitutes stiffening walls with a lightweight filler slab, akin to Figure 12.

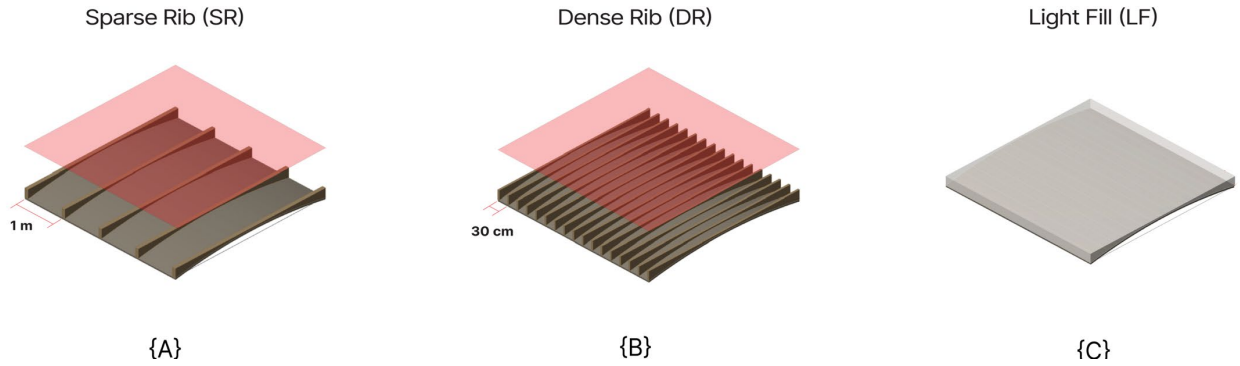

Figure 15: Earthen vaulted floor typologies; red surfaces (a), (b) represent imposed finishing surface loads.

All typologies assume a CSEB density of 2000 kg/m^3 based on experimental results, as highlighted in Chapter 3, and a literature review on CSEBs [26]. In typologies SR and DR, instead of specifying a finishing surface, the analysis imposes finishing surface dead loads of 1 kN/m^2 and 0.5 kN/m^2, respectively. This acknowledges the unique context of each location, where finishing surfaces can vary. For typology LF (Light Fill), no specific material is prescribed for the lightweight fill; instead, the fill density is estimated at 1400 kg/m^3, deemed reasonable for materials like aerated concrete or crushed construction waste.

For structural safety, each barrel vault must resolve its outward thrust (Figure 16). While many possible solutions exist for restraining the vault thrust this paper employs steel ties at each stiffening wall (Figure 17) or in the case of typology LF which has no stiffening walls ties are spaced every 1 meter. Alternatives to ties include a ring beam or buttressing walls; a combination of systems can be employed to increase redundancy (Figure 16-A). Figure 16-B shows a concrete ring beam system which resolves thrust in both directions and is self-contained so if one bay fails the adjacent remains.

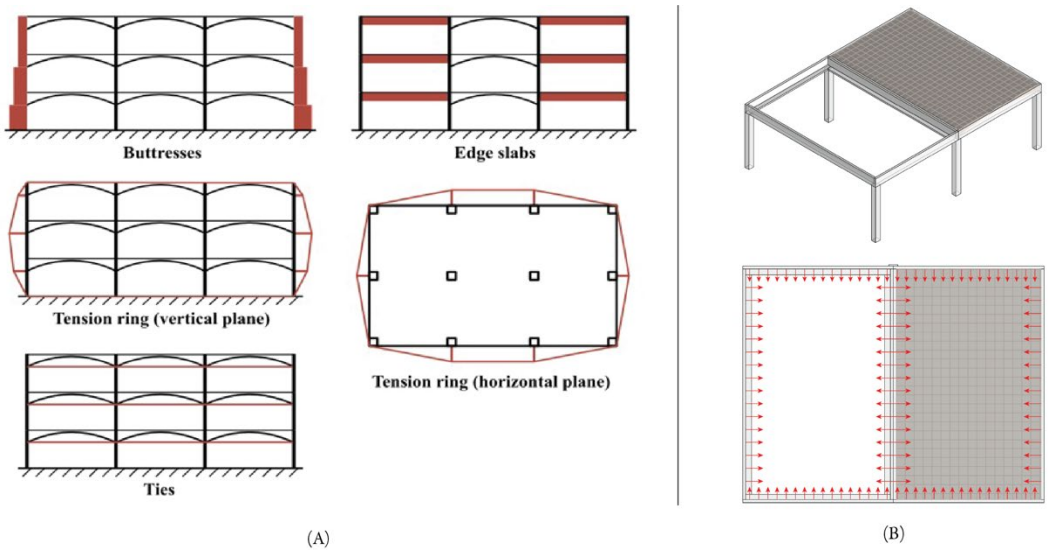

Figure 16: (a) Options for resolving outward thrust (Hawkins, 2020); (b) Proposed ring beam system

2.1.2. Analysis Assumptions

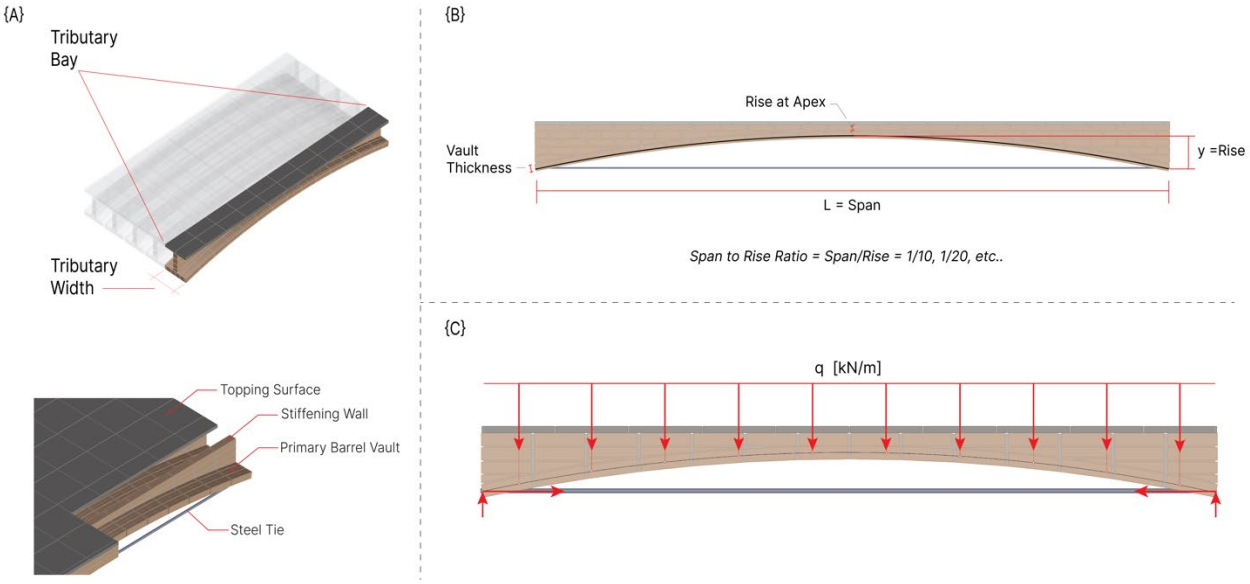

Figure 17: Earthen vaulted floor details and terminology

To analyze the forces in the vaulted floors, a 2D equilibrium analysis is performed on a single tributary bay (Figure 17-A) for each floor system. This bay includes one stiffening wall segment, a segment equivalent to the tributary width of the primary barrel vault, and a segment equivalent to the tributary width of the topping surface. The tributary width, determined by the spacing between stiffening walls, is set at 1 meter for typology SR, 30 centimeters for typology DR, and 1 meter for typology LF, aligning with tie spacing due to the absence of stiffening walls. The primary CSEB barrel vaults possess a uniform thickness (as defined in Figure 17-B) of 5cm, with stiffening walls rising to a height of 5 centimeters at the center, referred to as the apex rise (Figure 17-B). Furthermore, span measurement is taken from the centerline of the primary vault.

Loading conditions encompass self-weight, finishing loads, and factored live and dead loads in line with the International Building Codes (IBC) (International Code Council, 2021). During the analysis the self-weight of the tributary bay is computed from a 3D model on top of which the applied loading, Table 1, according to IBC is added.

Table 1: Applied Loading on Earthen Vaulted Floors by Typology

Floor Typology	Dead [kN/m²]	Partition [kN/m²]	Safety Factor	Live [kN/m²]	Safety Factor	Finishing [kN/m²]	Safety Factor	Total [kN/m²]
SR	1.5	1.5	1.35	2	1.5	1	1	8
DR	1.5	1.5		2		0.5		7.5
LF	1.5	1.5		2		0		7

For analysis, all loading is linearly projected along the span of the tributary bay, assuming that loads are transferred vertically to the primary barrel vault. Given a parabolic shape of the primary barrel vault and linearly projected loads, the forces in the vault are computed as a three-hinge arch under uniform loading (q), span (L), and rise (y):

$$\text{Thrust} = \frac{qL^2}{8y} \qquad (1)$$

$$\text{Vertical} = \frac{qL}{2} \qquad (2)$$

Since the stiffening walls and fill are assumed to only transfer loads vertically, they are excluded from the tributary area. Thus, for calculating working stresses, the tributary area is taken as the tributary width multiplied by the thickness of the primary barrel vault. Figure 18 shows a worked example of how the calculation of maximum stresses is computed for a 5-meter SR typology vault.

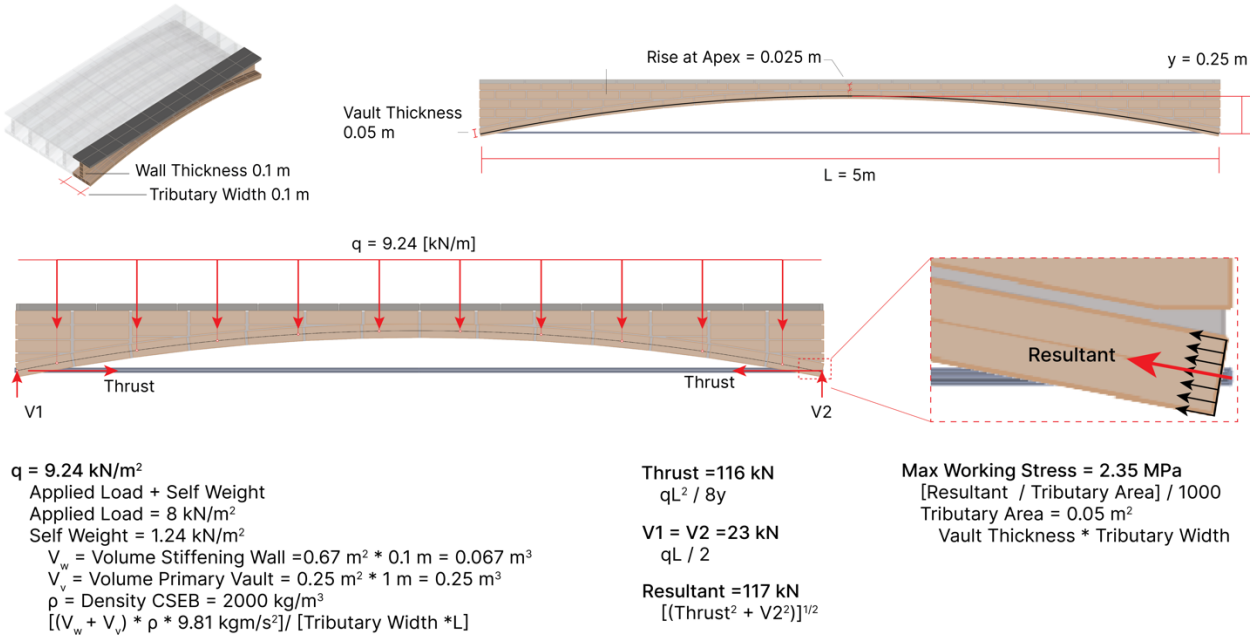

Figure 18: Worked example of calculating maximum working stress in sample 5-meter SR typology vault.

A parametric model was created in Rhinoceros 3D to represent each floor typology. This model served as the basis for the 2D equilibrium analysis shown in Figure 18. Each floor system was sampled in 0.01 meters interval over a 0.5 -10.5 meter range for the vault span. Additionally, two shallowness ratios, defined as the ratio of span to rise, are examined, with one set to span/10 and the other to span/20.

2.2. Results

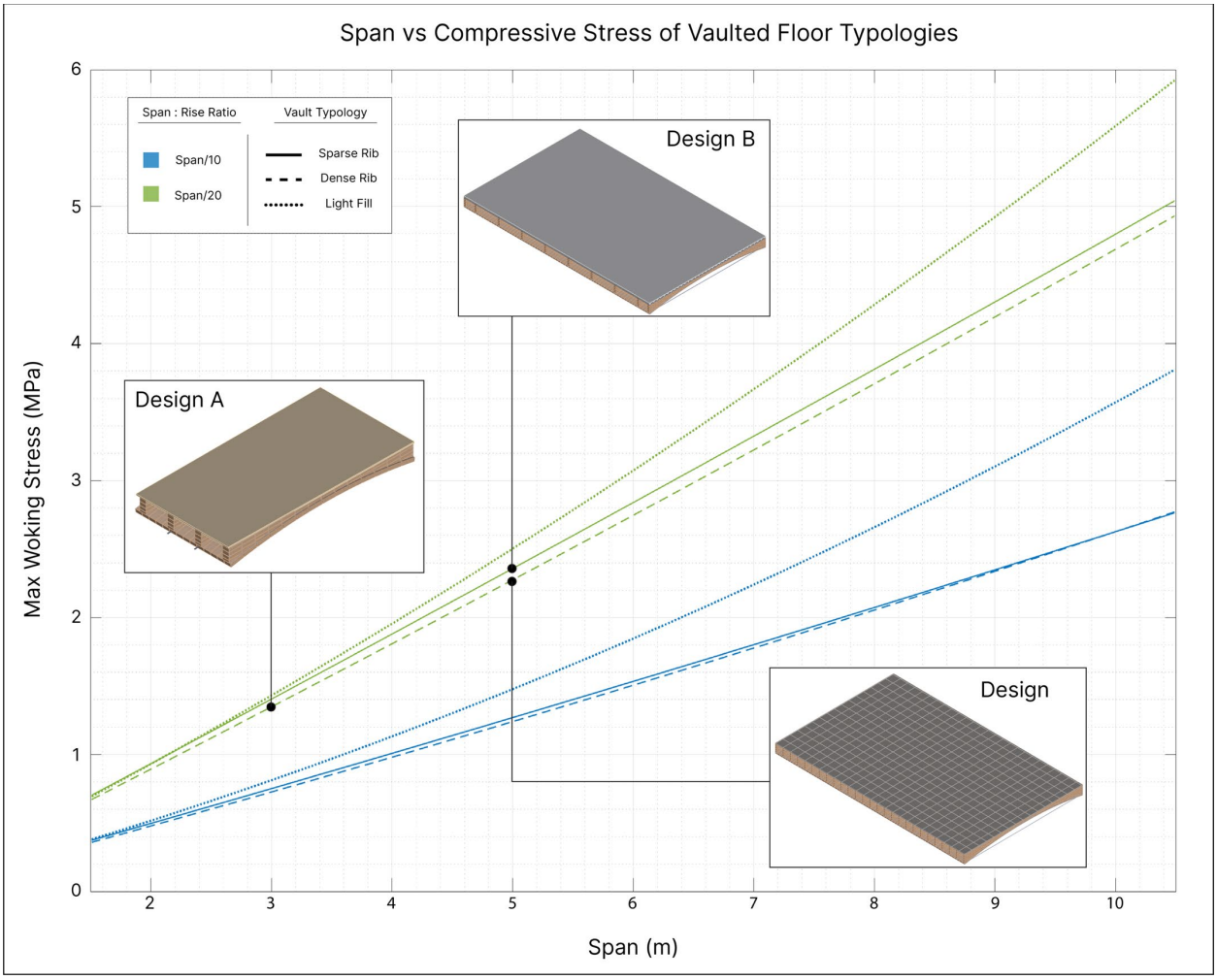

Figure 19: Working stresses of earthen vaulted floor typologies; following on the work of (Gaitan, 2021)

Figure 19 illustrates that all floor typologies can span distances commonly found in mid-rise buildings while maintaining low maximum working stresses. For instance, designs B and C, which represent designs that are discussed in Chapter 5's case study, show that even at a shallow aspect ratio of *span/20,* both designs span a 5-meter distance while keeping maximum stresses under 2.5 MPa, as per the assumptions in section 2.1. This underscores the feasibility of utilizing CSEBs as affordable, low-carbon masonry. The validity of these findings is further shown by the 3-meter scale prototype discussed in Chapter 4, highlighted as Design A in Figure 19.

A notable aspect of the results depicted in Figure 19 is that low stresses are observed across various typologies, spans, and aspect ratios. While soil properties and CSEB strengths vary across different locations (Murmu & Patel, 2018), the results indicate the feasibility of adapting the design to diverse contexts by adjusting the typology or aspect ratio. Although only *span/10* and *span/20* are plotted, additional ratios can be interpolated. Thus, as brick properties vary, a different typology can be selected, the span-to-rise ratio can be reduced, or vault thickness can be increased. Moreover, while this thesis focuses on CSEBs, other readily available construction alternatives, such as masonry units made from construction waste or more traditional fired clay bricks can be employed in the proposed system.

2.3. Discussion

This chapter has shown that various earthen vaulted floor typologies can span typical building spans while maintaining low stress values. Notably, even at shallow aspect ratios of span/20, all three typologies are able to maintain stresses below 6 MPa at extreme spans of 10+ meters, decreasing to 2.5 MPa and below at more typical building spans of 5 meters. These stress values are within the strength range of typical CSEBs as shown in (Murmu & Patel, 2018) and later in Chapter 3, proving that earthen masonry units can be applied to a vaulted floor form.

While confirming the structural feasibility of earthen vaulted floor systems, these findings have limitations. A primary limitation is that the static analysis is confined to uniform loading condition. With vaulted structures the primary failure mode is rarely crushing as highlighted by the low stresses in Figure 19, but rather stability failure as described by (Heyman, 1995). Therefore, to make this analysis more robust future analysis should consider asymmetrical loading as well as point loads proving that the system stays stable in a similar fashion as Figure 7-B. Furthermore, this analysis is confined to static behavior of the floor systems necessitating future exploration on the seismic behavior.

Another point of discussion with the results is that despite the low stresses in Figure 19, it is critical to emphasize that CSEBs exhibit inherent variability, demanding heightened safety considerations. The vast range of strengths shown in (Murmu & Patel, 2018) as well as the results in Chapter 3 highlight this variability. As a result of this variability, this thesis gives the design recommendation that a safety factor of 3 be used on CSEB strengths. For example, if the maximum working stress in the vault is 2.5 MPa, then a CSEB with at least 7.5 MPa strength is advised. Furthermore, it is important to note that masonry construction especially vaults are more difficult to construct and given they derive their strength from their geometry proper construction is critical. Therefore, while smaller span-to-rise ratios such as 1/20 gives thinner floor profiles, it allows for little room for construction error, prompting a recommendation of a 1/10 span-to-rise ration if concerns about construction quality arise.

In summary, this chapter establishes the viability of earthen vaulted floor typologies for spanning typical building distances with low-stress levels. It highlights the suitability of earthen masonry units for vaulted floor constructions. However, it also points out the need for further, more comprehensive research on the structural stability of the proposed systems.

3. Compressed Stabilized Earth Brick Production and Performance

Chapter 2 establishes that the stresses within the proposed vaulted floor system remain within or below the strength parameters documented for typical CSEBs in existing scientific literature. In Chapter 4, a prototype of one of the floor typologies is presented. Chapter 5 of this thesis conducts a comparative case study examining the cost and carbon footprint associated with flat slab versus vaulted earthen floor systems within the Ethiopian context. Chapter 3 addresses the production and properties of the CSEBs produced in Boston which were used in the prototype, as well as CSEBs produced in Addis Ababa, Ethiopia where the case study is contextualized.

3.1. CSEBS in Boston

3.1.1. Brick Production & Material Properties

The CSEBs comprise four main constituents: Boston blue clay, Quikrete All-purpose sand, Soil Cover brand crushed marble gravel, and Portland Cement. Boston blue clay sourced from a construction site was sun-dried, ground, and passed through a 4.75 mm mesh sieve, as illustrated in Figure 20.

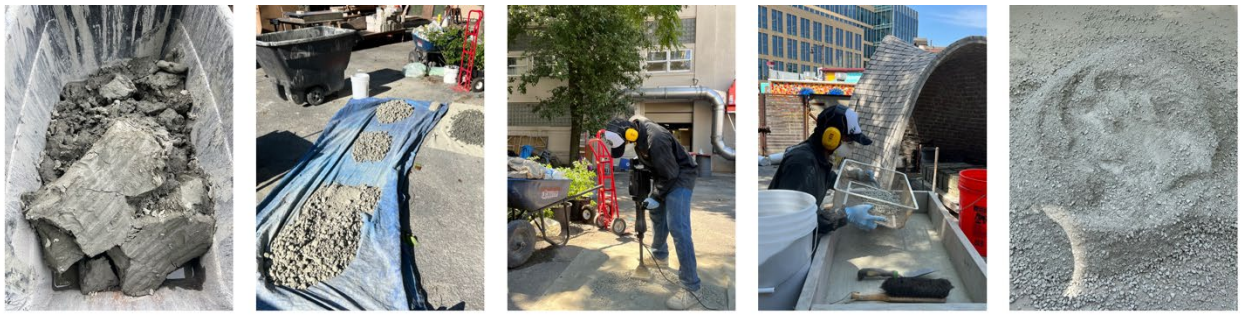

Figure 20: Procedure to prepare Boston blue clay for mixing.

Four mix designs were examined, with varying ratios of clay, sand, gravel, and cement determined by mass, as outlined in Table 2. The dry mixing of brick components was done using a concrete mixer.

Table 2: Boston CSEB Mix Designs

Mix	Sand	Clay	Gravel	Cement
3% Gravel (3G)	35%	42%	20%	3%
3% No Gravel (3NG)	45%	52%	0%	3%
5% Gravel (5G)	40%	40%	20%	5%
5% No Gravel (5NG)	50%	45%	0%	5%

Following dry mixing, the soil was gradually moistened in a bin, with water added incrementally at 5% by mass intervals. Hand mixing was preferred due to the high clay content, which can lead to clumping and uneven water distribution when using a concrete mixer (Figure 21). Optimal water content was determined through a drop test, guided by (Niazi et al., 2020), ensuring the mixture maintained neither excessive cohesion nor disintegration upon impact (Figure 22).

Figure 21: Incremental moistening of soil mixture

Figure 22: optimal water check of mix using field drop test

An aluminum mold measuring 10cm x 20cm x 5cm was employed for brick molding. The mold was lubricated with oil, and the saturated mixture was filled in thirds, compacted using a 2-ton arbor press, and leveled with a trowel and manual pressure. Subsequently, the bricks were left to rest for 3-5 minutes in the sun before being demolded and air-dried. This procedure is delineated in Figure 23 and elaborated upon in Appendix A.

Figure 23: summarized procedure for brick compaction

Six bricks of each mixture type were manufactured, with three subjected to compressive strength testing in the direction of a 20cm x 10cm face, and three in the direction of a 10cm x 5cm face (Figure 24). Strength and stiffnesses are in Tables 3 & 4; stress-strain plots available in Appendix A.

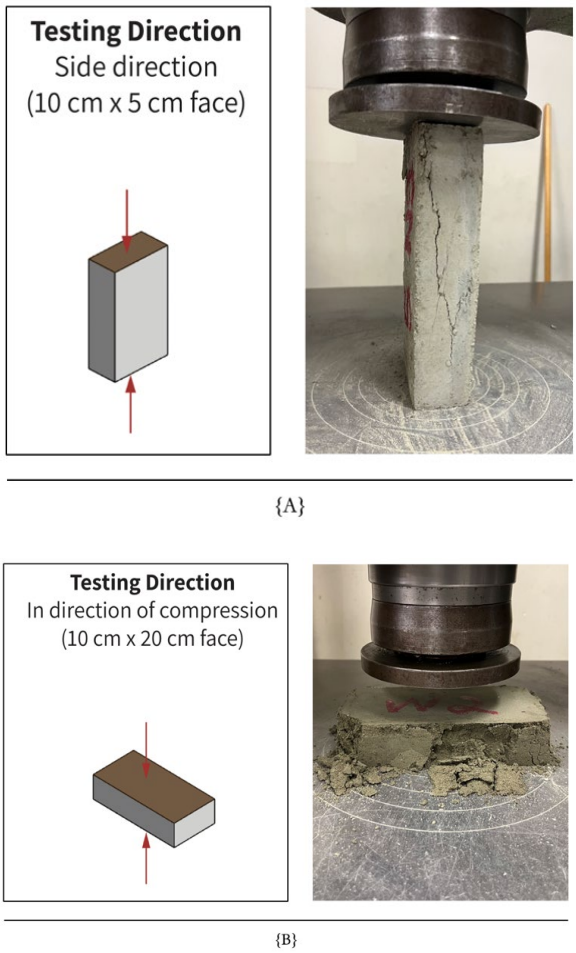

Figure 24: Testing direction for compressive strength of CSEBs

Table 3: Boston CSEB 14 Day Ultimate Strength and Stiffness – Compressed Direction

	Sample 1		Sample 2		Sample 3		**AVERAGE**		
	σ [MPa]	MOE [MPa]	σ [MPa]	MOE [MPa]	σ [MPa]	MOE [MPa]	**σ [MPa]**	**MOE [MPa]**	**ϱ [g/cm³]**
3G	5.2	72	4.6	69	7.4	93	**5.8**	**78**	**2.0**
3NG	11.3	105	11.4	93	11.1	97	**11.2**	**98**	**2.0**
5G	5.9	115	8.4	95	8.1	84	**7.5**	**98**	**2.1**
5NG	9.2	110	14.5	128	14.5	115	**12.7**	**118**	**2.0**

Table 4: Boston CSEB 14 Day Ultimate Strength and Stiffness – Tall Direction

	Sample 1		Sample 2		Sample 3		**AVERAGE**		
	σ [MPa]	MOE [MPa]	σ [MPa]	MOE [MPa]	σ [MPa]	MOE [MPa]	**σ [MPa]**	**MOE [MPa]**	**ϱ [g/cm3]**
3G	1.51	364	1.0	116	1.7	281	**1.4**	**254**	**2.0**
3NG	4.0	677	2.4	811	2.2	782	**2.3**	**757**	**2.0**
5G	2.1	427	2.0	330	1.7	289	**1.6**	**349**	**2.0**
5NG	4.2	1270	3.3	642	4.3	1113	**4.0**	**1008**	**2.0**

{A} {B}

Figure 25: (a) 500 3NG bricks during left to air dry; (b) brick during 24-hour soak before compressive testing

Mix design 3NG was chosen for the prototype due to its superior cement-to-strength ratio. Furthermore, the strength outcomes in the vertical direction were considered negligible due to the influence of the slender aspect ratio. Five hundred bricks of mix design 3NG were produced for the prototype. Following literature recommendations, curing was deemed complete after 30 days (Auroville Earth Institute, 2020). Consequently, spot tests were conducted on three dry bricks at 50 days, along with three additional bricks soaked for 24 hours (Denoted as "Wet") before undergoing crushing tests. Results are outlined in Tables 5 & 6, with stress-strain plots provided in Appendix A.

Table 5: 3NG 50 Day Dry Ultimate Strength and Stiffness – Compressed Direction

	Sample 1		Sample 2		Sample 3		**AVERAGE**		
	σ [MPa]	MOE [MPa]	σ [MPa]	MOE [MPa]	σ [MPa]	MOE [MPa]	**σ [MPa]**	**MOE [MPa]**	**ϱ [g/cm3]**
3NG	9.3	126	9.1	111	11.5	155	**10**	**131**	**1.9**

Table 6: 3NG 50 Day Wet Ultimate Strength and Stiffness – Compressed Direction

	Sample 1		Sample 2		Sample 3		**AVERAGE**			
	σ [MPa]	MOE [MPa]	σ [MPa]	MOE [MPa]	σ [MPa]	MOE [MPa]	**σ [MPa]**	**MOE [MPa]**	**ϱ [g/cm3]**	**Absorption [%]**
3NG	5.4	90	5.1	100	5.1	98	**5.2**	**96**	**2.0**	**6.4**

3.1.2. Retesting Bricks and Brick Prisms

In addition, several 3NG bricks were evaluated after eight months. Alongside individual brick assessments, brick prisms were subjected to testing and constructed per ASTM C104 2021 standards. They comprised three bricks with two mortar layers (Figure 26-A). Two types of mortar were investigated: a 1:3 cement-sand mixture and a mud mortar featuring a ratio of 1:4.5:11 for cement, Boston blue clay, and sand, respectively. Results are delineated in Tables 7 & 8, while stress-strain plots can be found in Appendix A.

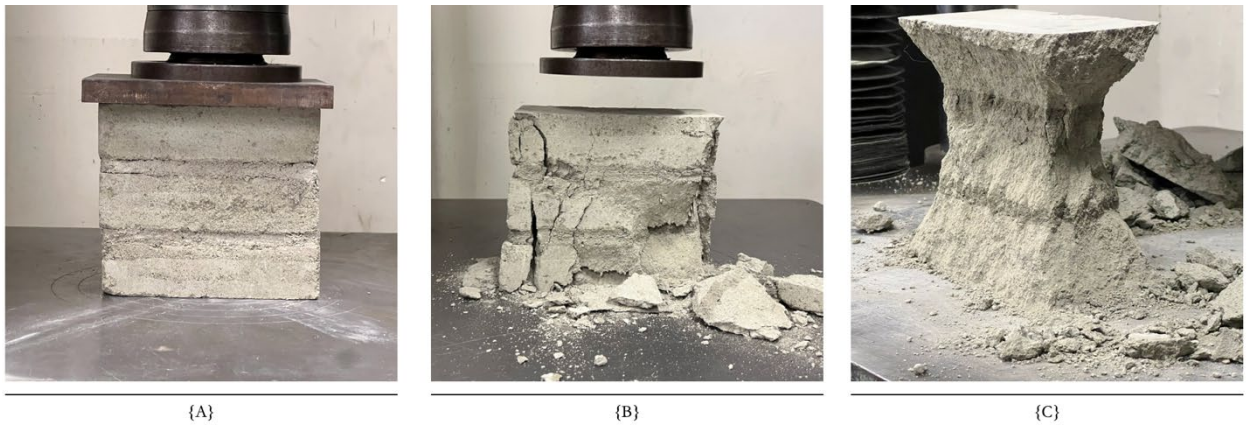

Figure 26: (a) Cement prism post 30-day curing; (b) crushed prism; (c) crushed prism highlighting 45 degree typical shear failure

Table 7: 3NG 8 Month Dry Ultimate Strength and Stiffness - Compressed Direction

	Sample 1		Sample 2		Sample 3		**AVERAGE**		
	σ [MPa]	MOE [MPa]	σ [MPa]	MOE [MPa]	σ [MPa]	MOE [MPa]	**σ [MPa]**	**MOE [MPa]**	**ϱ [g/cm3]**
3NG	6.1	73	9.0	144	7.3	72	**7.5**	**96**	**1.9**

Table 8: 3NG Prism Ultimate Strength and Stiffness - Compressed Direction

	Sample 1		Sample 2		Sample 3		**AVERAGE**	
	σ [MPa]	MOE [MPa]	σ [MPa]	MOE [MPa]	σ [MPa]	MOE [MPa]	**σ [MPa]**	**MOE [MPa]**
3NG Prism Cement Mortar	1.95	168	2.1	138	1.1	89	**1.71**	**132**
3NG Prism Mud Mortar	1.9	94	2.6	136	1.9	87	**2.1**	**106**

3.2. CSEBs in Ethiopia

3.2.1. Soil Selection & Brick Production

In contrast to the production process of Compressed Stabilized Earth Blocks (CSEBs) in Boston, where an artificial soil was created by blending Boston blue clay and sand, soil from two construction sites in Ethiopia was utilized. A soil characterization test was conducted on samples obtained from two distinct regions within the capital city of Addis Ababa, Ethiopia, as depicted in Figure 27. The soil characterization of these samples was conducted per BS 1337 Part 1-2 standards, with the results detailed in Table 9; A comprehensive sieve analysis is available in Appendix A.

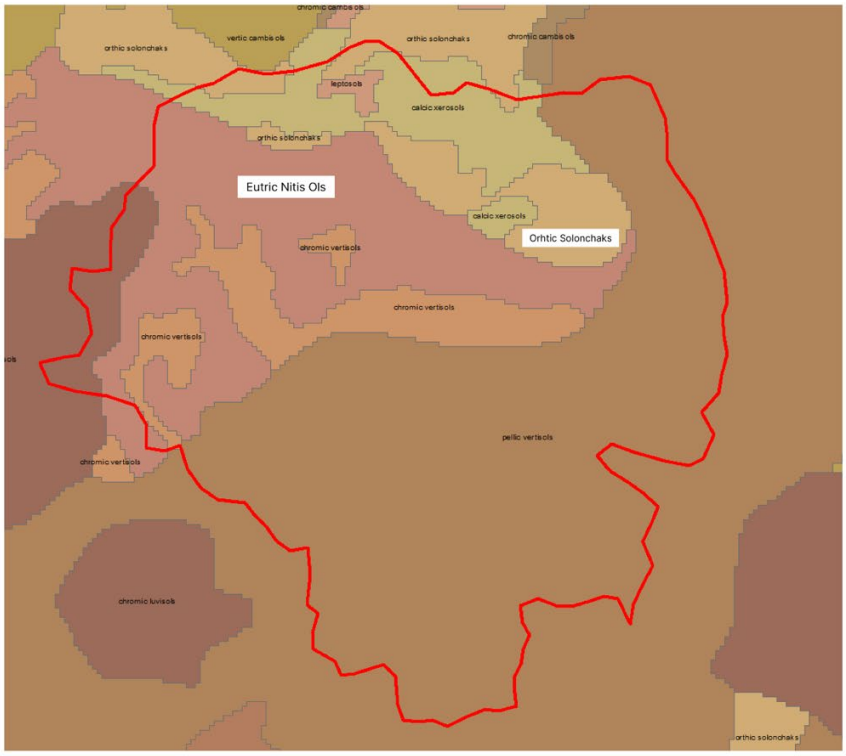

{A}

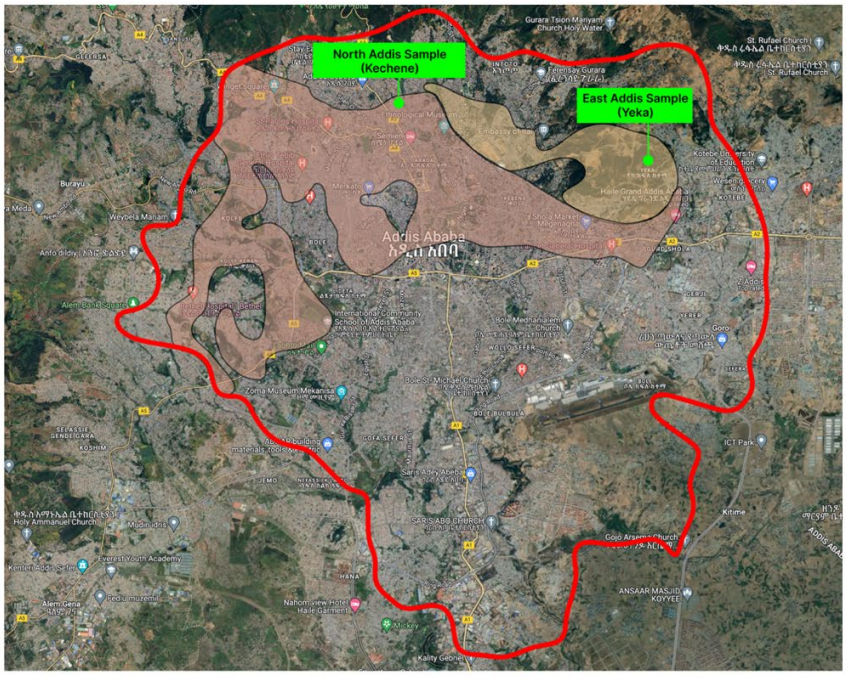

{B}

Figure 27: (a) Soil map of Addis, Ababa [Ethiopia Ministry of Agriculture (MOA)]; (b) soil sample locations
Table 9: Ethiopia Soil Characterization

Soil Type	Sand	Silt	Clay
North Addis	21%	60%	19%
East Addis	17%	67%	16%
Augmented North Addis	50%	37%	13%
Augmented East Addis	50%	40%	10%

Following characterization, both soil batches underwent sieving using a 9.5 mm sieve. Literature suggests that ideal soil for CSEBs should contain around 30-50 % sand content (Auroville Earth Institute, 2020). Therefore, to achieve a target sand content of 50%, for both soil types, the existing mass of dry sand in each batch was first determined by assessing its moisture content. Additional construction-grade sand was then added, measured by mass, to augment the soil's sand composition. The augmented compositions are detailed in Table 9.

{A}

{B}

Figure 28: (a) Sieving soils in Ethiopia through 9.5mm sieve; (b) adding additional sand to each soil type.

Similarly to the practices in Boston, four mix designs were explored (Table 10). However, unlike the mix designs utilized for Boston CSEBs, none of the mix designs for the Ethiopian context incorporated gravel. This decision was informed by the lower strengths observed in Boston bricks when using gravel mixes (Table 3). Instead, the four mix variations in Ethiopia varied in soil type (East and North) and the degree of cement stabilization, either 3% or 7%.

Table 10: Ethiopia CSEB Mix Designs

Mix Name	Sand	Silt	Clay	Cement
North 3% (N3)	48.5%	35.9%	12.6%	3%
East 3% (E3)	48.5%	38.8%	9.7%	3%
North 7% (N7)	46.5%	34.4%	12.1%	7%
East 7% (E7)	46.5%	37.2%	9.3%	7%

Following the preparation of dry mixes, the brick production process in Ethiopia closely resembled that outlined for those made in Boston (as described in 3.1.1), with two notable alterations. Firstly, due to the unavailability of arbor presses in Ethiopia, bricks were pressed using a hydraulic press at a pressure of 4 MPa. Secondly, owing to the higher compaction pressure, the procedure deviated from filling and compressing the molds in a series of layers; instead, the molds were filled and pressed in a single operation.

{A} {B}

Figure 29: (a) Compaction of bricks using hydraulic press; (b) additional steel "lip" made to over fill mold to be pressed in one pass.

As outlined in section 3.1.2, brick prisms were tested in Ethiopia, mirroring the methodology employed for the Boston CSEBs. Similarly, two types of mortar were examined for each brick type. For the cement mortar, a 1:3 cement-sand mix was utilized for both brick types. Regarding the mud mortar, a ratio of 1:10:4 (cement-sand-soil) was applied for the 3% bricks, while a ratio of 2:10:3 (cement-sand-soil) was used for the 7% bricks. Results for these tests are presented in Table 15.

{A} {B}

Figure 30: (a) Construction of prism; (b) prisms during air drying period.

3.2.2. Brick Material Properties

Twelve bricks were produced for each mixture type, of which three underwent testing for dry compressive strength in the direction of a 20cm x 10cm face (Figure 24). Additionally, three more bricks from each mixture type were subjected to testing after being soaked for 24 hours. These tests were conducted at 14 and 30 days to observe the strength progression during the curing process. Similarly, six prisms were manufactured for each mixture type, three with mud mortar and three with cement mortar. The results of these tests are presented in Tables 11-14. A significant limitation in the data presented is that the testing apparatus did not measure strain, thus precluding the brick and prism stiffness calculation.

{A} {B}

Figure 31: (a) Bricks during 24-hour soak; (b) bricks dissolving during 24-hour soak

Table 11: Ethiopia CSEB 14 Day Dry Ultimate Strength – Compressed Direction

	Sample 1	Sample 2	Sample 3	**AVERAGE**	
	σ [MPa]	σ [MPa]	σ [MPa]	**σ [MPa]**	**ϱ [g/cm³]**
N3	3.6	3.8	4.8	**4.0**	**1.5**
E3	4.2	5.9	3.3	**4.4**	**1.6**
N7	5.1	4.7	5.6	**5.1**	**1.5**
E7	4.8	5.1	5.6	**5.2**	**1.6**

Table 12: Ethiopia CSEB 14 Day Wet Ultimate Strength – Compressed Direction

	Sample 1	Sample 2	Sample 3	**AVERAGE**		
	σ [MPa]	σ [MPa]	σ [MPa]	**σ [MPa]**	**ϱ [g/cm³]**	**Absorption [%]**
N3	-	-	-	**-**	**1.5**	**-**
E3	-	-	-	**-**	**1.6**	**-**
N7	1.5	1.6	1.7	**1.6**	**1.5**	**21**
E7	2.9	2.2	2.5	**2.5**	**1.6**	**16**
*Blank boxes represent samples that dissolved while soaking						

Table 13: Ethiopia CSEB 30 Day Dry Ultimate Strength – Compressed Direction

	Sample 1	Sample 2	Sample 3	**AVERAGE**	
	σ [MPa]	σ [MPa]	σ [MPa]	**σ [MPa]**	**ϱ [g/cm³]**
N3	3.9	5.2	4.1	**4.4**	**1.5**
E3	4.1	4.4	3.6	**4.0**	**1.6**
N7	4.6	4.3	4.1	**4.3**	**1.5**
E7	5.2	4.4	6.6	**5.4**	**1.6**

Table 14: Ethiopia CSEB 30 Day Wet Ultimate Strength – Compressed Direction

	Sample 1	Sample 2	Sample 3	**AVERAGE**		
	σ [MPa]	σ [MPa]	σ [MPa]	**σ [MPa]**	**ϱ [g/cm³]**	**Absorption [%]**
N3	-	-	-	**-**	**1.5**	**-**
E3	0.9	0.9	0.7	**0.9**	**1.6**	**5**
N7	6.0	4.1	2.8	**4.3**	**1.5**	**3**
E7	3.9	4.1	5.4	**4.5**	**1.6**	**1**
*Blank boxes represent samples that dissolved while soaking						

Table 15: Ethiopia CSEB Prism Ultimate Strength - Compressed Direction

	Sample 1	Sample 2	Sample 3	AVERAGE
	σ [MPa]	σ [MPa]	σ [MPa]	σ [MPa]
N3 Prism Cement Mortar	1.00	1.35	-	**1.2**
E3 Prism Cement Mortar	1.0	0.7	0.6	**0.7**
N7 Prism Cement Mortar	1.4	1.2	1.2	**1.2**
E7 Prism Cement Mortar	1.5	0.8	1.3	**1.2**
N3 Prism Mud Mortar	1.2	0.9	1.1	**1.0**
E3 Prism Mud Mortar	1.3	-	-	**1.3**
N7 Prism Mud Mortar	1.4	1.2	1.2	**1.2**
E7 Prism Mud Mortar	1.6	1.6	-	**1.6**
*Blank boxes represent samples that were damaged before testing				

3.3. Discussion

This chapter underscores the viability of compressed stabilized earth bricks (CSEBs) by confirming comparable compressive strengths in existing literature (Murmu & Patel, 2018). Figure 19 from Chapter 2 demonstrates that all floor typologies can span distances typical of mid-rise buildings while maintaining low maximum working stresses. Notably, even at shallow aspect ratios of span/20, a 5-meter span earthen floor of any typology exhibits maximum stresses around 2.5 MPa, decreasing to 1.25 MPa at span/10. The results presented herein showcase the production of CSEBs in Boston and Ethiopia, attaining strengths exceeding 5 MPa. These results underscore the potential of CSEBs as cost-effective, low-carbon masonry materials for vaulted floor systems across various regions.

However, a concern requiring further investigation is the significant reduction in compressive strength observed in prisms compared to individual bricks in both Addis Abab, Ethiopia and Boston. Possible explanations include geometrically unfavorable aspect ratios of the testing prisms, or weaker shear strength of the bricks, which may lead to lower failure stresses not evident at the individual brick scale. These hypotheses warrant detailed material testing beyond the scope of this thesis.

Furthermore, the considerable disparity in strength between CSEBs produced in Ethiopia and those in Boston, along with their heightened vulnerability when soaked, necessitates further inquiry. One plausible explanation may be Ethiopian soil's higher silt and lower clay content, resulting in reduced compaction ability and increased water permeability. Future investigations should explore different soil compositions by augmenting the clay percentage to levels more akin to those of Boston CSEBs.

Additionally, the labor-intensive and time-consuming nature of CSEB production, taking between one and one-half hours per five bricks in both Ethiopia and Boston, raises concerns regarding scalability. Given the extensive masonry required for the proposed floor systems, further research into optimizing the manufacturing process of CSEBs and achieving consistency at scale is imperative.

In summary, this chapter contributes to understanding CSEBs' potential as sustainable masonry materials for vaulted floor systems. Yet, unresolved questions regarding prism strength discrepancies, soil composition effects, and production scalability underscore the need for continued research in these areas to realize CSEBs' full potential in construction practices.

4. Earthen Masonry Barrel Vaulted Floor Prototype

Much of the existing literature on earthen masonry vaulted floor systems is limited to theoretical calculations such as those presented in Chapter 2, and (Gaitan, 2021). The work described in this chapter looks to validate the theoretical feasibility of these proposed systems by load testing a 3-meter scale prototype of one of the proposed floor in accordance with International Building Code loads.

4.1. Methodology

4.1.1. General Design

The prototype, as shown in Figures 32 and 33, is 3 meters in span, 1.5 meters in depth, and has a 5 cm thick primary barrel vault with a span-to-rise ratio of 1/20 giving a primary vault depth of 15 cm. It has 10 cm thick stiffening walls spaced at roughly 50 cm and an apex rise of 2.5 cm. For the sake of simplicity, the finishing surface was chosen to be 2 cm thick plywood piece spanning stiffening walls without attachment, giving the vault floor a total depth of 27 cm (including mortar layers). The entire vault sandwiched between two steel angles which rest on concrete hollow blocks which elevate the vault in the air for ease of construction but have no structural attachment to the steel angles nor vault. The vault thrust was managed by connected steel ties at the two center stiffening walls. The primary vault and the stiffening walls were constructed with a 3% CSEB with an ultimate strength of 11 MPa as described in Section 3.1.1.

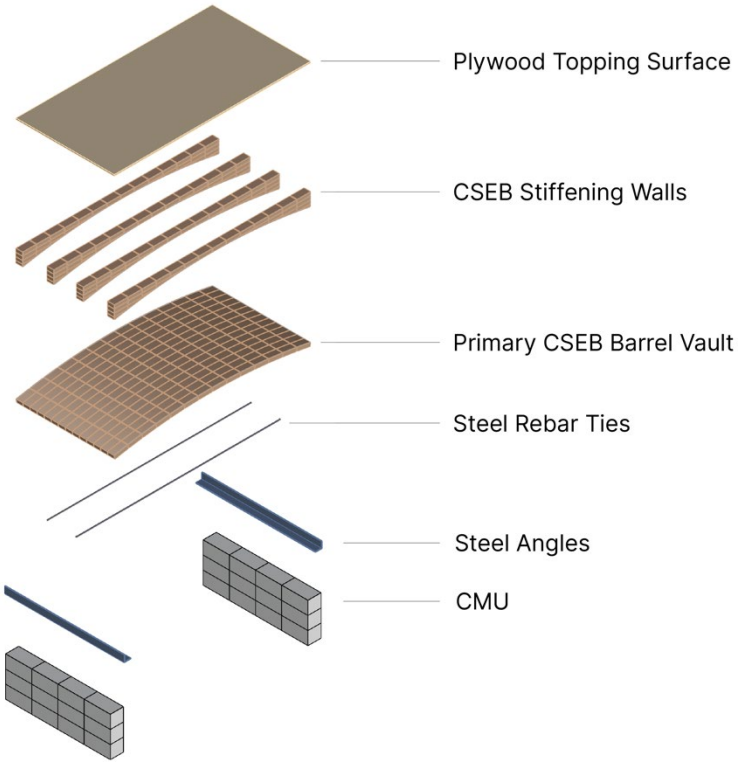

Figure 32: Exploded axonometric drawing of prototype

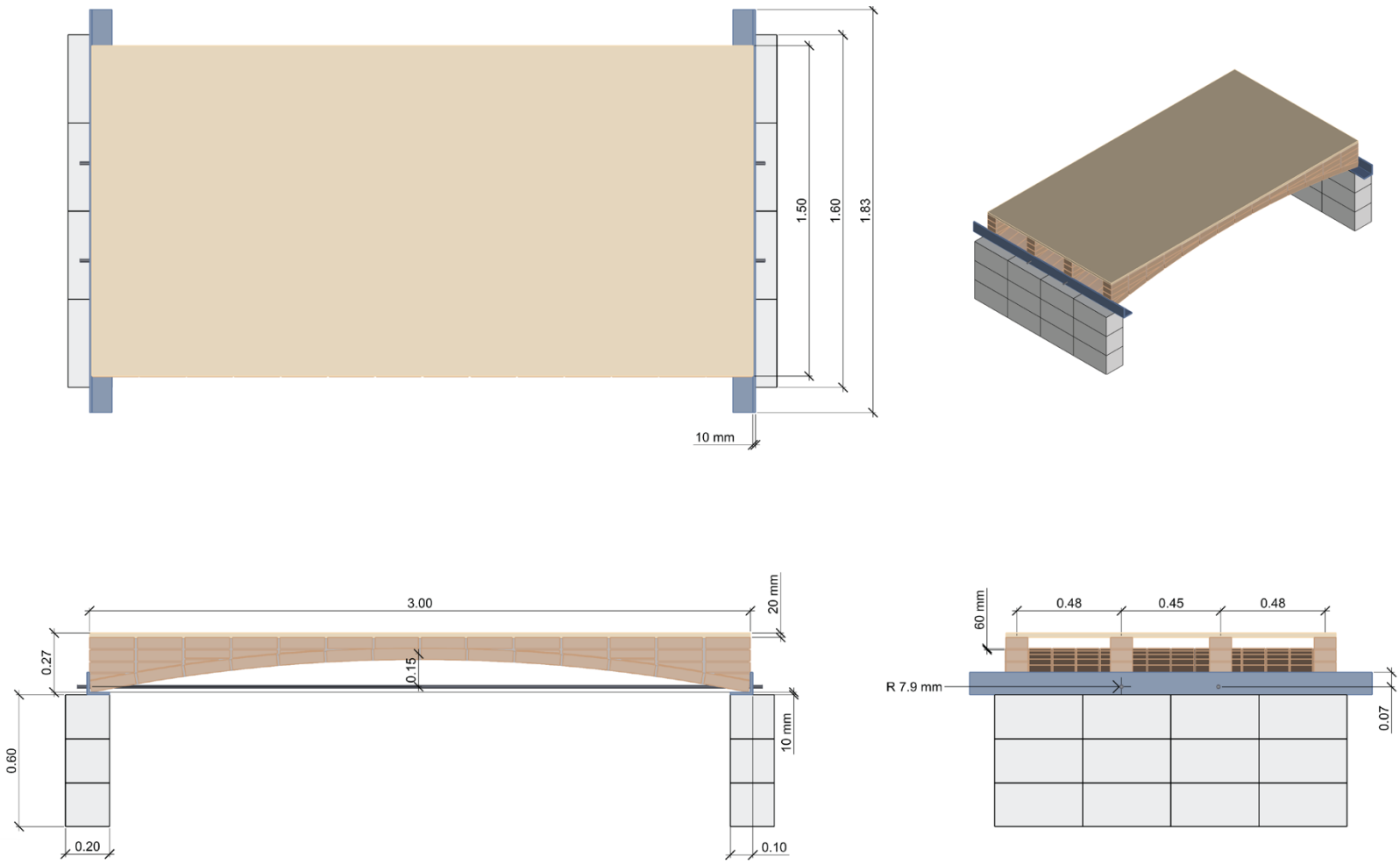

Figure 33: Technical drawing of prototype [m]

4.1.2. Preliminary Structural Analysis

4.1.2.1. 2D Analysis

Following the procedures outlined in Section 2.1.2, a 2D equilibrium analysis was conducted on the prototype. It underwent testing under an unfactored live load of 2 kN/m2, both in symmetrical and asymmetrical configurations, and an unfactored double live load of 4 kN/m2, again in symmetrical and asymmetrical setups. Despite its demonstrated higher capacity, as illustrated in Figure 19, the prototype was tested under these lower loads due to limitations of the available testing equipment, which did not permit testing at the 7.5 kN/m2 building code load derived in Chapter 2. The asymmetrical cases represent a more complex loading scenario that is more likely to induce stability failures. Using the same assumptions in Section 2.1.2, that loads are transferred vertically, parabolic shape of the primary barrel vault, and linearly projected loads, the forces in the vault are computed as a three-hinge arch under combined symmetric and asymmetrical loading:

$$\text{Thrust} = \frac{L^2}{16y}[2q_{Dead} + q_{Live}] \quad (3)$$

$$\text{Vertical}_{No\ Live\ Load\ Side} = \frac{q_{Dead}L}{2} + \frac{q_{Live}L}{8} \quad (4)$$

$$\text{Vertical}_{Live\ Load\ Side} = \frac{q_{Dead}L}{2} + \frac{3q_{Live}L}{8} \quad (5)$$

In addition to checking maximum working stress, a 2D thrust network diagram is drawn for each vault to demonstrate the thrust line fits within the primary vault during asymmetrical loading. This confirms stability per Heyman's Safe theorem, akin to the example of Guastavino in Figure 7-B. An abbreviated calculations for the most critical load scenario for stability, asymmetrical load at 4 kN/m^2, is presented in Figure 34. Detailed worked solutions for all load cases in Appendix B.

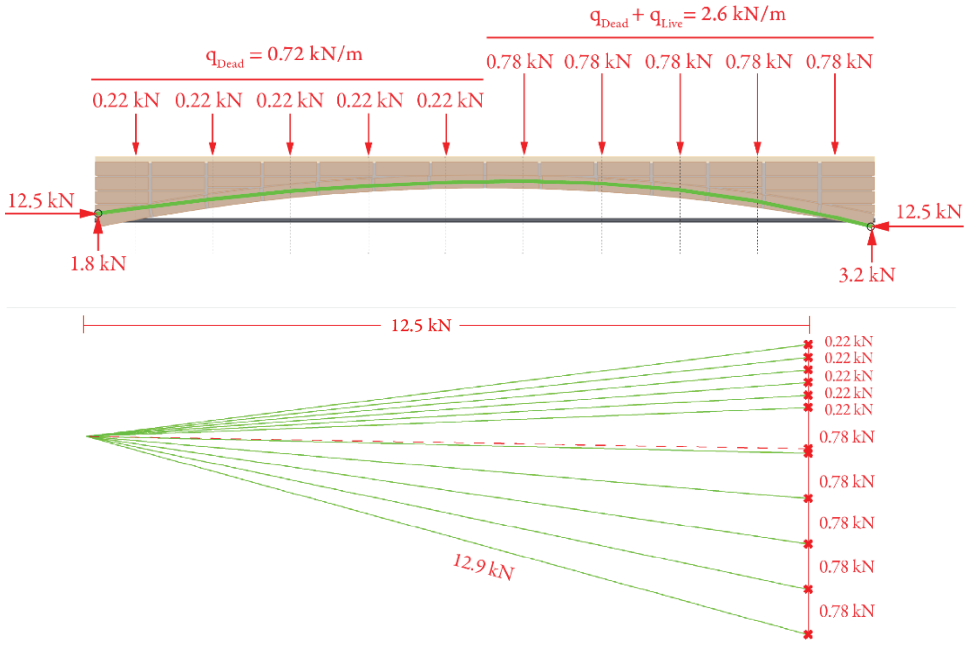

Figure 34: Forces and thrust line in prototype under 4 kN/m^2 asymmetric live load

Under all load cases, calculations showed that the working stresses remained well under the strength of the brick, Table 16, as well as maintaining the thrust line withing solely the primary barrel vault assuming conservatively the stiffening walls only transfer forces vertically from the plywood.

Table 16: Max Working Stresses in Prototype Vault Under Various Load Cases

Load Case	Max Working Stress	Utilization of Dry CSEB (10 MPa)	Factored Utilization of Dry CSEB (3.33 MPa)
2 kN/m² Symmetrical	0.54 MPa	5.4%	16.2%
2 kN/m² Asymmetrical	0.39 MPa	3.9%	11.7%
4kN/m² Symmetrical	0.85 MPa	8.5%	25.5%
4 kN/m² Asymmetrical	0.55 MPa	5.5%	16.5%

One additional concern was analyzing the stress concentration near the support ties for the highest stress case: 4kN/m² symmetrical. Each tie takes half the entire vault's thrust and two localized stress blocks were analyzed the first being the tributary width of a single stiffening wall (Figure 35-A) and the second more conservative being the width of two bricks (Figure 35-B). Both gave safe results as shown in Table 17.

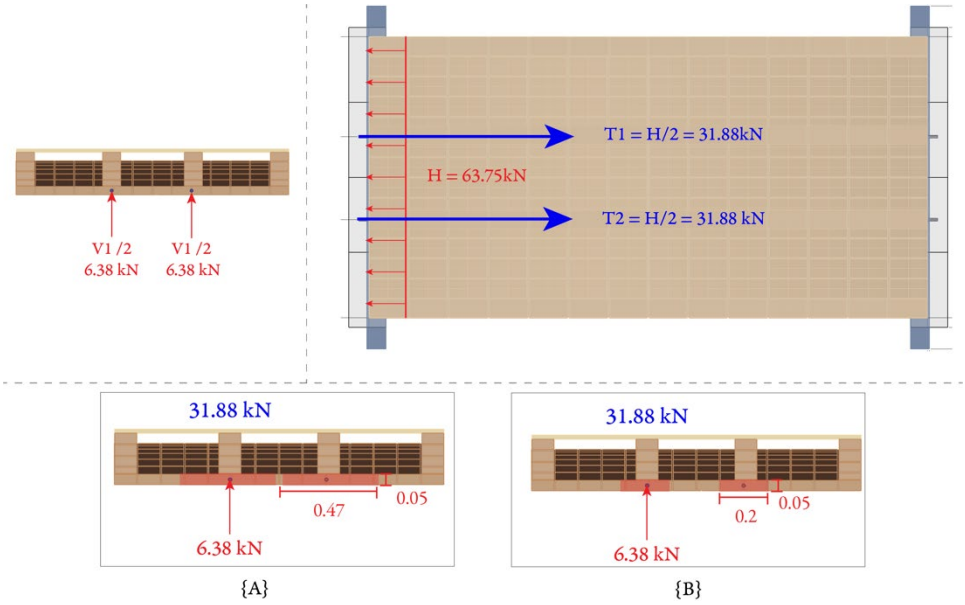

Figure 35: Stress concentration analysis; thrust and reaction forces solved in Appendix B - "Sizing Steel Tie"

Table 17: Critical Stress Based on Stress Block

Stress Block	Stress Block Area	Utilization of Dry CSEB (10 MPa)	Factored Utilization of Dry CSEB (3.33 MPa)
Tributary Bay	1.38	13.8%	41.4%
2x Brick Width	3.25	32.5%	97.5%

Following this verification, the rebar ties were sized at 15.8 mm (5/8") diameter for the highest stress case, 4 kN/m² symmetrically. Furthermore, the bending capacity of the steel angles was verified as adequate given that the vault thrust against the angle for 0.5m on either side before resolving the thrust at the tie (Figure 33). Detailed calculations for both are found in Appendix B.

4.1.2.2. 3D Analysis

The 2D analysis was complemented with a 3D equilibrium thrust network analysis utilizing the Thrust Network Optimization (TNO) plugin by BRG (Maia Avelino, 2023). The first verification involved the symmetric loading case of 4 kN/m^2. The loading grid utilized is depicted in figure 36. Notably, slight discrepancies exist between the grid and stiffening wall locations (delineated by dashed blue lines in Figure 37) compared to the 2D analysis. This variance arises from the prototype's as built dimensions, which measured 1.55 meters long, causing the stiffening walls to shift from their anticipated positions. Similar to the 2D analysis the thrust line is limited to the primary barrel vault.

TNO operates differently from the 2D analysis, as it considers load paths beyond just the rib locations. Consequently, it distributes the self-weight of the vault across all nodes, visualized as green dots in Figure 36. The red dots indicate points where the combined loads (rib load, plywood, self-weight, and live loads) are applied, while the two orange dots at the ends represent small partial loads from the nearby tributary area near the supports. Load values corresponding to the most critical stiffening wall on the grid are labeled. It's noteworthy that the summed point load value closely aligns with the 2D analysis, and the final results find a better minimum thrust solution.

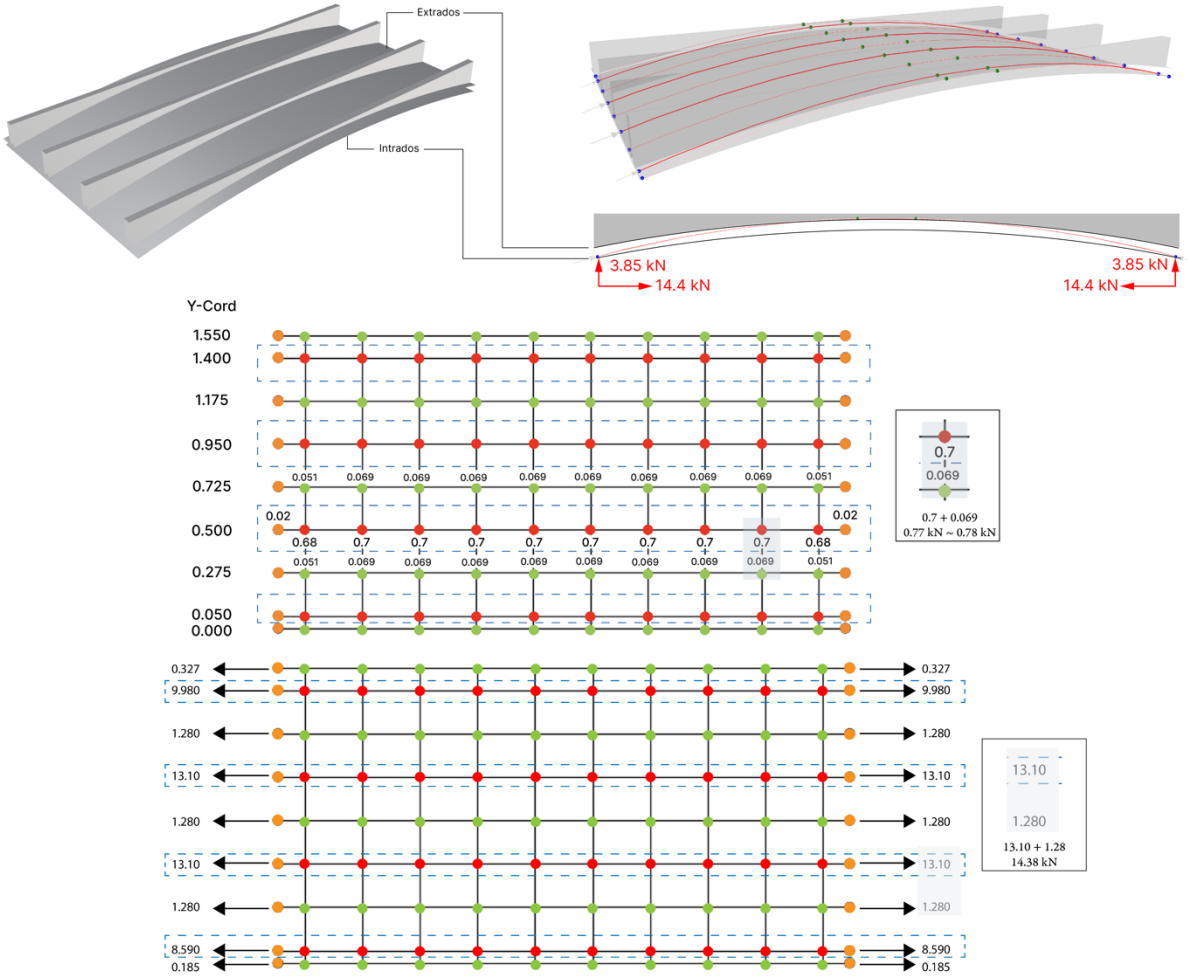

Figure 36: TNO analysis for 4 kN/m2 symmetrically loaded

The same analysis was done for the asymmetrical case, shown in Figure 37, and again the analysis found a lower thrust solution than the 2D solution shown in Figure 34. The blue dots represent the points in the stiffening wall where only the rib load, and self-weight is applied, the remaining colors represent the same as the previous example.

A caveat about the 3D analysis is that the single curvature barrel vault is mostly a 2-D problem, and as a result the reductions in thrust found by a 3D analysis will be minor. Were the vault to be doubly curved and supported on four sides the reductions between 2D and 3D analysis would be greater.

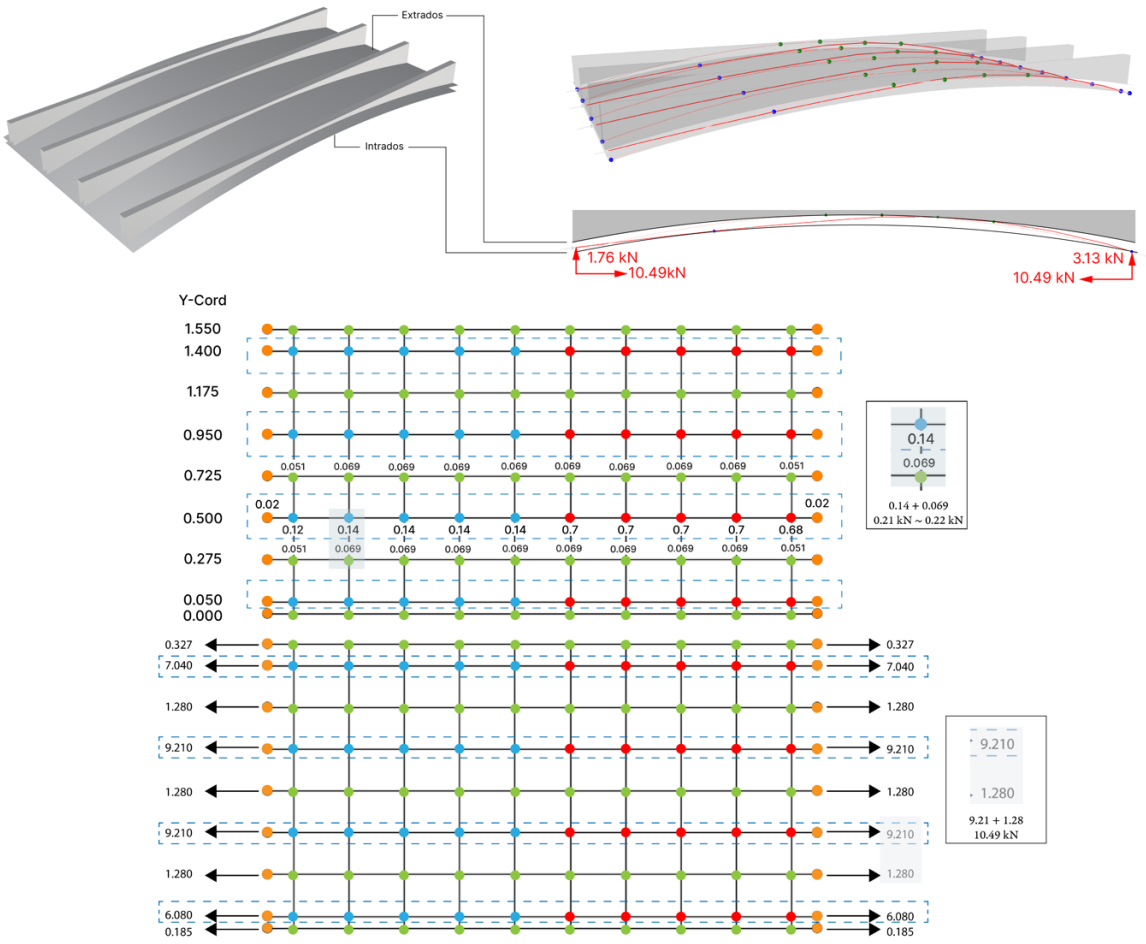

Figure 37: Figure 36: TNO analysis for 4 kN/m2 asymmetrically loaded

4.2. Testing Results

The figures below show the completed vault, as described earlier after construction, the vault was 5 centimeters longer than anticipated, however the stiffening walls ware adjusted to maintain the 1.5-meter depth. For loading, the prototype was loaded with 20-liter buckets of water were spread out on the vault, each bucket being 0.185 kN in load. The loading sequence was as followed:

1. 2 kN/m² asymmetrically; 25 buckets over half vault
2. 2 kN/m² symmetrically; 50 buckets over half vault

3. 2 kN/m² symmetrically + 1.25 kN point load at center; 50 buckets over entire vault + two people standing at center.
4. 4 kN/m² asymmetrically; 50 buckets over half vault
5. Premature failure reached before 4 kN/m² symmetrically.

The prototype withstood symmetrical and asymmetrical loads at 2 kN/m^2 for a sustained period. When the two human point loads were added, there was a significant deflection without elastic recovery, discussed in 4.3, however it remained stable. The vault stood for roughly 7 minutes after being loaded at 4 kN/m^2 asymmetrically, but slowly deforming under the continued stress before ultimately collapsing. The collapse was unexpected given the analysis on the undeformed geometry shown in Section 4.1; the premature failure is expanded on in Section 4.3.

Figure 38: Completed vault floor prototype perspective view

Figure 39: Completed vault floor prototype elevation view

Figure 40: Completed vaulted floor prototype with author walking on top

Figure 41: Twenty-five buckets being filled with water during 2 kN/m2 asymmetrical loading

Figure 42: 2 kN/m2 symmetric load case with 1.25 kN point load at center

Figure 43: Fifty buckets full of water on half of vault during 4 kN/m2 asymmetrical loading

Figure 44: Vault at moment of collapse showcasing three bar hinge mechanism

4.3. Collapse Analysis

4.3.1. Deformations

A clear observation while testing is that the prototype had unexpected deformations. Heyman's theory for masonry analysis which was used for both 2D and 3D analysis assumes that the masonry is infinitely rigid so shape remains constant (Heyman, 1995). Furthermore, preliminary analysis assumed that supports are fixed, while the steel angles were tied together preventing them from sliding, they experienced slight rotations (in the scale of mm) under loading. While settlements of this order are usually negligible the shallow aspect ratio at span/20 makes the design highly sensitive to any support sliding.

While the horizontal displacements were not recorded, using snapshots from slowed down footage the vertical displacement at the center and quarter point of the vault were able to be calculated; detailed calculations can be found in Appendix B. Using this information, the analysis framework shown in Figure 45 was used to calculate the deformed shape of the vault; the deformed span and aspect ratios are tabulated in Table 18 and shown in Figure 46.

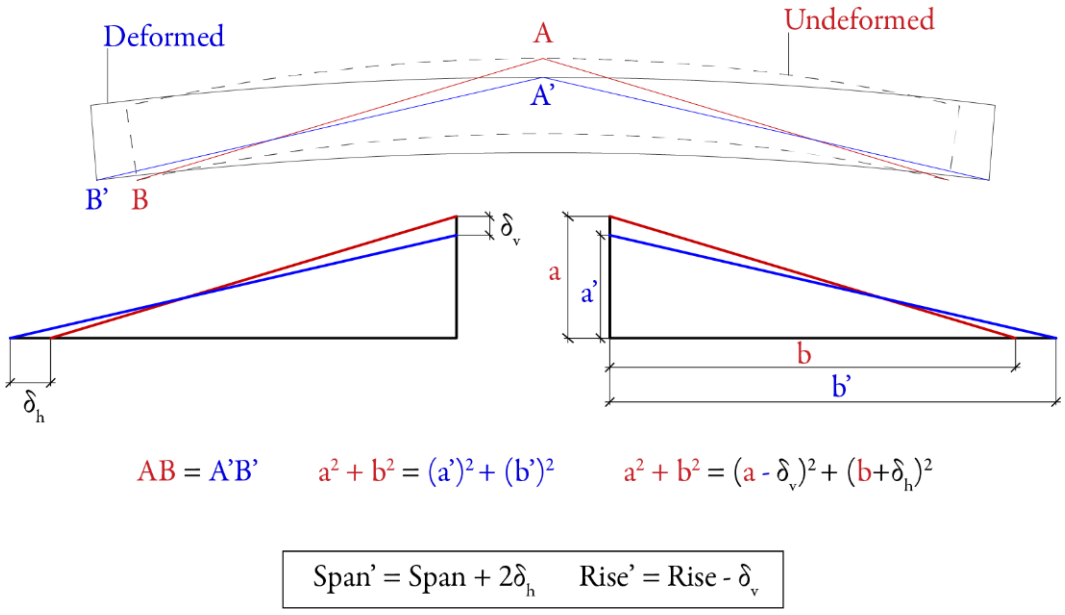

Figure 45: Analysis approach for calculating deformed geometry of vault

Table 18: Deformations of Prototype Compared to Original Sate During Loading

Load Case	a [m]	b [m]	δv [cm]	δh [mm]	Span [m]	Span' [m]	Rise [m]	Rise' [m]	Span'/ Rise'
2 kN/m² Asym.	1.5	0.15	-	-	3	3	0.15	0.15	20
2 kN/m² Sym.	1.5	0.15	0.9	0.9	3	3.002	0.15	0.141	21.3
2 kN/m² Sym. and 1.25 kN Point Load	1.5	0.15	2.5	2.3	3	3.005	0.15	0.125	24
4 kN/m² Asym. @ Failure	1.5	0.15	3.8	3.3	3	3.007	0.15	0.112	26.8

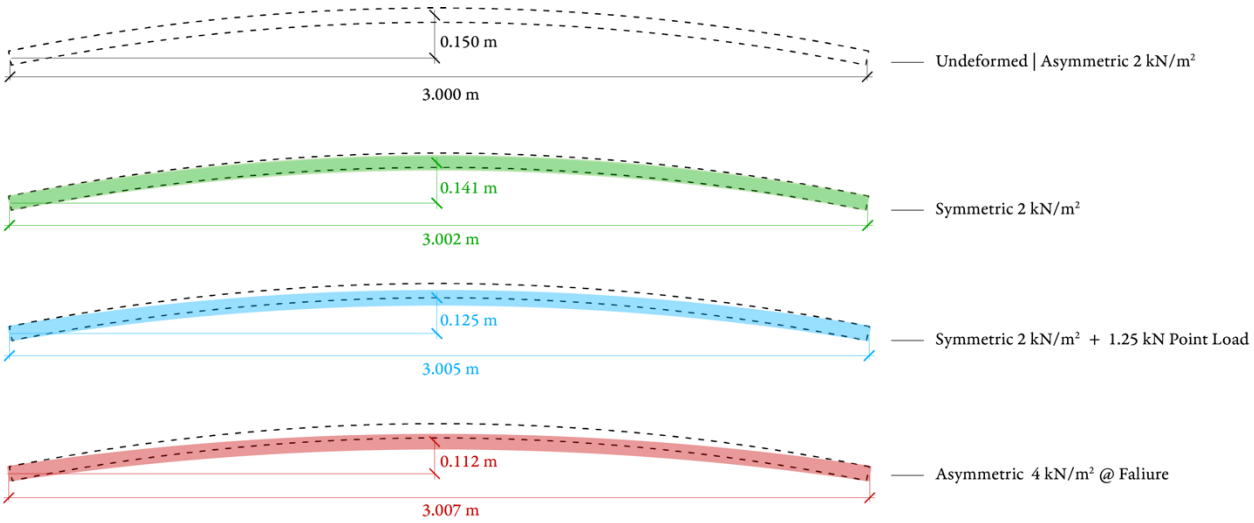

Figure 46: Deformed geometries of prototype during loading

4.3.2. 2D Analysis Revisited

The prototype was reanalyzed, using 2D equilibrium as done Section 4.1.2.1, for the 4kn/m^2 asymmetric load using the ultimate deflected geometry which is 3.8 cm shallower than the initial vault (red geometry in Figure 46) to see if it explained the vault failure. The first pass of calculations, Figure 47, showed that even in the deformed state that it could maintain stability; full calculation in Appendix B.

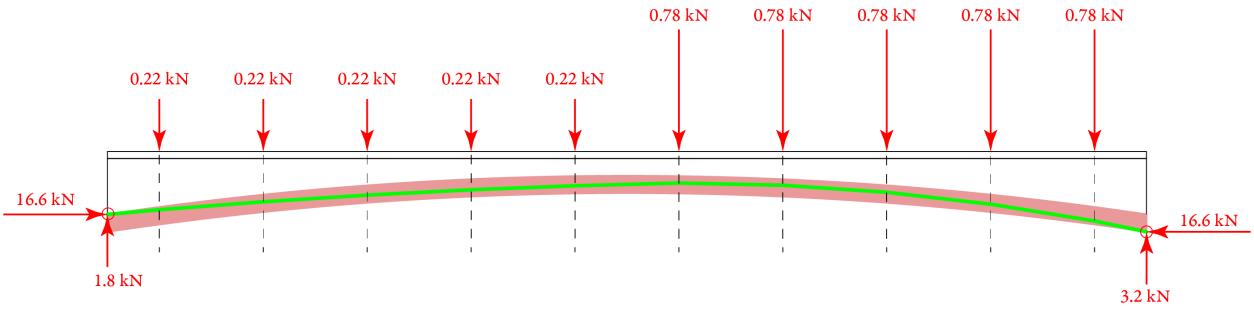

Figure 47: Forces and thrust line in 0.47 cm strip of deformed prototype under 4 kN/m^2 asymmetric live load

This result is adequate for a first pass; however, it is not accurate because the hinge is allowed to form right at the edge of the vault which is allowed under limit analysis because it assumes that masonry is significantly stronger than the stresses in the vault allowing for an extremely small stress block hence a hinge at the edge (Heyman, 1995). For this very shallow prototype because CSEBs are a weaker masonry unit they cannot be treated as infinitely strong. Given this consideration, the previous analysis is redone assuming stress blocks of 1 mm, 1 cm, 2 cm, 2.5 cm height by 47 cm in depth - the tributary depth of a stiffening wall. An optimization loop is used to find the minimum thrust solution for each. The resulting stresses and thrusts are shown in Figure 48.

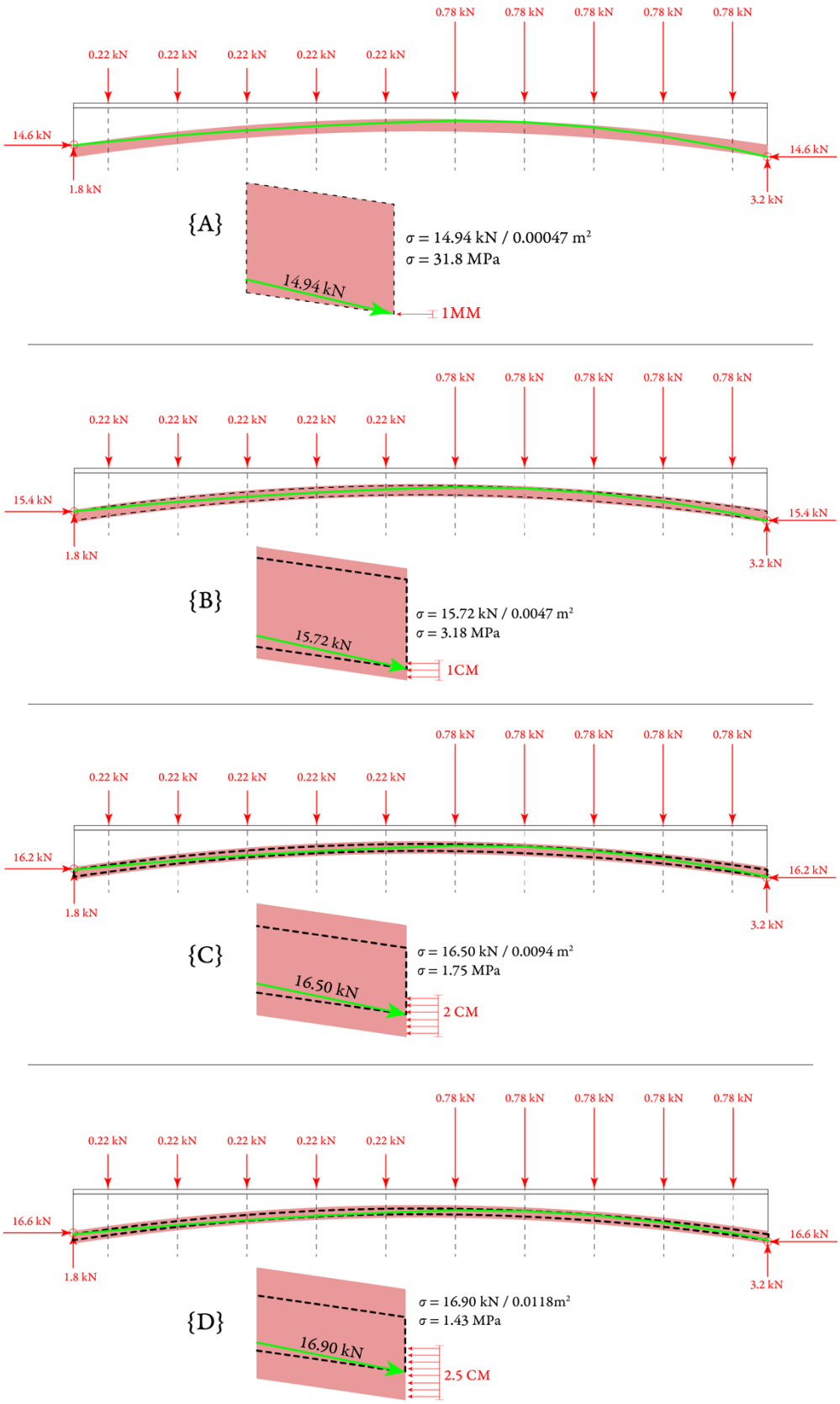

Figure 48: Limit analysis of a 0.47 cm wide strip of deformed prototype.

4.3.3. Explanation for Failure

These results lead to the conclusion that even in its deformed state the vault should have stayed stable so long as the strength of the masonry was 1.43 MPa or greater. This is in contradiction to what was observed during testing, as the vault did collapse in response to the vault's deformations. This contradiction is what prompted the experiments in Chapter 3, Section 3.1.2 as it was hypothesized that the bricks must have been weaker than expected or the confined masonry was weaker than an individual brick. The retested bricks had an average strength of 8 MPa which did not resolve the contradiction. The prism however shed some light on the findings; the average strength of the mud mortar prisms was 2.1 MPa which is near the limit of 1.43 MPa (Figure 48-D).

When observing the failure of the vault it is important to note that the vault did not fail suddenly, but rather it deformed slowly over seven minutes continually getting shallower until its ultimate collapse. The main question in explaining the vaults failure is what caused this continued deformation which can be attributed to three main factors: tie elongation, and shortening of the vault due to elastic shrinkage, and local crushing of the mortar joints.

The continued flattening of the vault is first increased as a result of support settlement due to the lengthening of the steel tie. If the collapse point is revisited assuming the vault had a strength of 2.1MPa, Figure 48-C represents the closets stable equilibrium state of the deformed vault. The thrust in each tie at that point would be 25.9 kN which is calculated by taking the thrust at that point and multiplying by 1.5/0.47, to represent the full vault and not one tributary bay, then dividing by two because each tie takes half. The elongation of the 3 meter steel tie at this point would be:

$$\Delta L = \frac{PL}{AE} = \frac{25.8\ kN * 3000\ mm}{0.000196\ m^2 * 200{,}000{,}000\ kPa} = 1.97\ mm$$

Rearanging the equation in Figure 45, and inputing half the elongation as **δh** the corresponding vertical deflection of 1.9 cm can be calculated as shown in Table 19. The vault at this point has deflected a total of 5.2 cm from the original design, but a stable solution still exists (Figure 50).

Table 19: Deformations of Already Deformed Vault Due to Tie Lengthening

Load Case	a [m]	b [m]	δv [cm]	δh [mm]	Span [m]	Span' [m]	Rise [m]	Rise' [m]	Span'/ Rise'
4 kN/m² Asym. Deformed Geo.	1.507	0.112	1.4	0.985	3.007	3.009	0.112	0.098	30.7

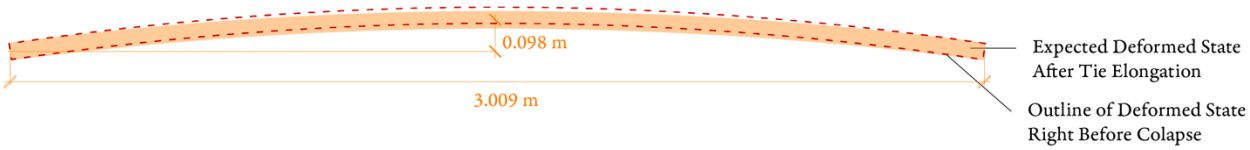

Figure 49: Deformed shape of prototype after tie elongation

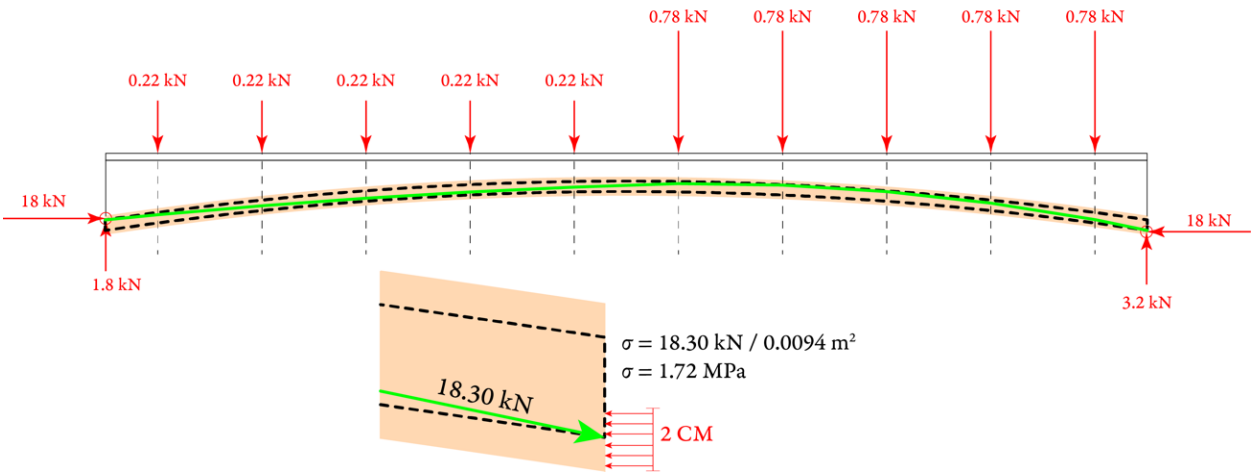

Figure 50: Stresses in prototype after tie elongation

In addition to tie elongation, the flattening of the vault is furthered as a result of elastic shortening. The original analysis in Figure 45 dictates that the length of AB = A'B' which physically represents that the deformation of the vault is caused by support settlement because the length of the vault remains constant. This is based on the limit analysis assumption that masonry is infinitely stiff, so the compressive shrinkage of the masonry is negligible. However in the case of CSEBs it is known that it they are not stiff material in comparison to masonry as shown by the stress strain plot in Figure 51.

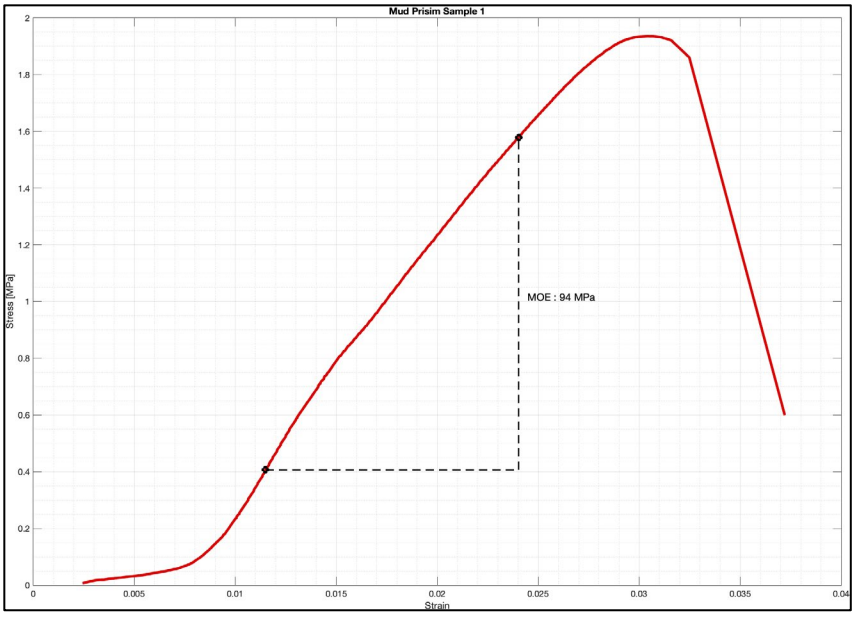

Figure 51: Stress - Strain curve of Mud Prism 3

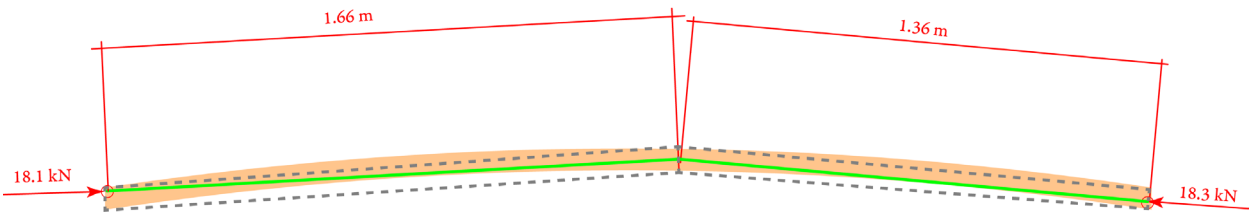

Figure 52: Simplified 2 bar representation of deformed vault

Knowing this, the vault in Figure 49 is reanalyzed, simplifying it into two bars as shown in Figure 52 that have cross sections equal to the depth of the vault (0.05 m) and a depth equal to a tributary bay (0.47 m). The shrinkage of each bar can be calculated using the modulus of elasticity from Figure 51:

$$\Delta L_{right} = \frac{PL_{right}}{AE} = \frac{18.3\ kN * 1360\ mm}{0.0235\ m^2 * 94{,}000\ kPa} = 11.4\ mm$$

$$\Delta L_{Left} = \frac{PL_{Left}}{AE} = \frac{18.1\ kN * 1660\ mm}{0.0235\ m^2 * 94{,}000\ kPa} = 13.6\ mm$$

The two values are added to conclude that the vault length shortens by a total of 25 mm. If the combined length of the two bars is taken as an estimate of the curve length of the centerline of the vault, the deformed vault for the same span of 3.009 meters, the vault would need to deflect an additional 1.6 cm, meaning the vault has shrunk a total of 6.8 cm from the original design increasing the span to rise ratio to span/36.5 from span/20.

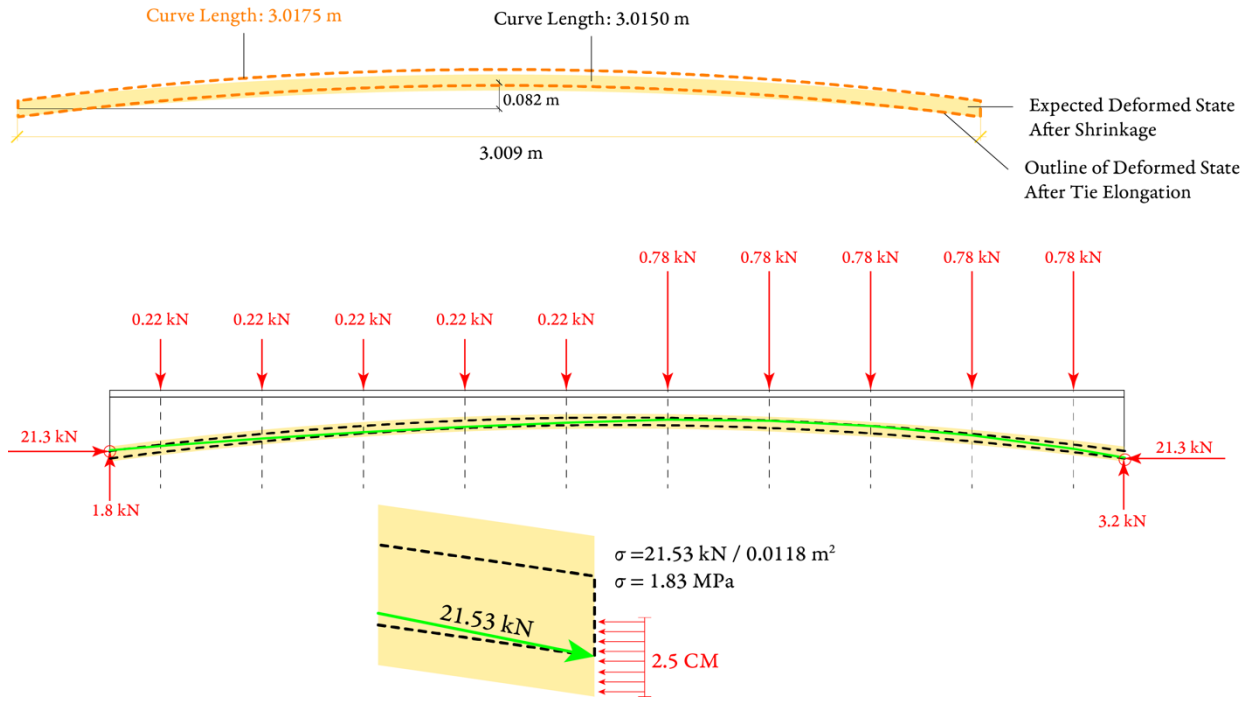

Figure 53: Analysis of deformed vault to meet shrinkage requirements

Table 20: Summary of Elastic Vault Deformations

Load Case	a [m]	b [m]	δv [cm]	δh [mm]	Span [m]	Span' [m]	Rise [m]	Rise' [m]	Span'/ Rise'
2 kN/m² Asym.	1.5	0.15	0.0	0.0	3	3	0.15	0.15	20
2 kN/m² Sym.	1.5	0.15	0.9	0.9	3	3.002	0.15	0.141	21.3
2 kN/m² Sym. + 1.25 kN Point Load	1.5	0.15	2.5	2.3	3	3.005	0.15	0.125	24
4 kN/m² Asym.	1.5	0.15	3.8	3.3	3	3.007	0.15	0.112	26.8
4 kN/m² Asym. Tie Elongation	1.507	0.112	5.2	0.985	3.007	3.009	0.112	0.098	30.7
4 kN/m² Asym. Elastic Shrinkage	-	-	6.8	-	-	3.009	0.098	0.082	36.5

The combination of support settlements and vault deformations explains the slow and shallow flattening of the vault. Given the maximum stress is 1.83 MPa at the end of this deformation, Figure 53, which puts it near or in the plastic deformation region of the brick prisms shown in Figure 51, the vault's failure makes sense. Already close to or at failure, the breaking point of the vault can be attributed to local joint failures. While the individual bricks were 8 MPa and the prisms were 2.1 MPa, the mud mortar, which was not tested, could have been weaker. As a result, it is possible that the mortar experienced more crushing (to create a larger stress block) than an adjacent brick. This greater localized crushing at the mortar joints allows the bricks to rotate locally, making the vault even shallower. The deformation due to local rotations and the fact that the mortar was crushed first could not be calculated. However, this failure behavior is furthered greatly because the hinges at failure formed precisely at the mortar locations, not in the bricks, as seen in Figure 44.

4.4. Discussion

The testing and results carried out in this chapter expanded upon the limited existing literature of the physical feasibility of vaulted earthen floor systems. Specifically, it was able to show that the theoretical earthen floor systems such as those discussed in (Gaitan, 2021) and described in Chapter 2, with shallow aspect ratios span/20, can safely hold an unfactored building code live load of $2kN/m^2$ symmetrically and asymmetrically.

While taking a big step in confirming the structural feasibility of earthen vaulted floor systems, the work presented in this chapter has also brought to light critical areas for further research. One point made clear by the large deformations observed is that while Heyman's rules for limit analysis of masonry vaults are a good starting point for analysis, further research on the deformation behavior of earthen vaults is needed to understand and predict the real-world behavior of these systems.

Another area that requires further research is an investigation in the true strength of the composite masonry mortar matrix used in the vaults. Without understanding what the strength of the two are in composite calculation and explaining the structural capacity of the floor systems will be a challenge.

A closing lesson from this prototype is the importance of construction details as well as robust testing equipment. With respect to construction, Table 18 highlights that the 3.8 cm vertical deflection of the vault at center can be attributed to a mere 6.6 mm horizontal settlement in the supports. In this case the angles were tied but not bolted down thus unintentionally giving them the room to slightly rotate and potentially have provided the 6 mm horizontal displacement that caused such drastic vertical deflections at center. With respect to testing much of the collapse analysis was pieced together using video footage, in the future using emended sensors, string gauges on the ties, and targeted camera work will allow for a much more improved understanding of the internal forces in the vault as well as how it is failing over time.

This chapter has advanced our understanding of vaulted earthen floor systems' structural feasibility, confirming their ability to withstand building code live loads. However, it highlights the need for further research into the nonlinear, both geometric and material, behavior of earthen vaults and the true strength of composite masonry mortar matrix. Additionally, it underscores the importance of meticulous construction details and improved testing methodologies to better understand these systems' behavior. This chapter lays the groundwork for future investigations of building more prototypes with the ultimate goal of a working prototype carrying a full factored residential load of 7 to 8 kN/m^2.

5. Case Study: Cost & Carbon Savings

A void in the current scholarly discourse pertains to quantifying the embodied carbon and cost efficiencies of earthen barrel-vaulted floor systems compared to conventional concrete flat slabs. This chapter endeavors to bridge this gap through a case study examining the cost and embodied carbon implications of two vaulted earthen floor designs vis-à-vis a flat slab within a recently completed 15-story building in Addis Ababa, Ethiopia.

5.1. Context

5.1.1. Integrated Housing Development Programme

Ethiopia is an apt context for a case study on the feasibility of earthen vaulted floor systems due to the substantial demand for affordable housing. In 2006, in alignment with the United Nations' Millennium Development Goals to furnish adequate shelter for the economically disadvantaged, the UN, in conjunction with the Ethiopian government, established the Integrated Housing Development Programme (IHDP). This initiative aimed to construct 400,000 subsidized government housing units, with 175,000 units earmarked for the capital, Addis Ababa, between 2006 and 2010 These housing units were intended to be provided to citizens solely at the construction cost, without any land payment (Alemu, 2021; UN Habitat, 2010).

The IHDP delineated three housing schemes: 10/90, 20/80, and 40/60. The 10/90 condominiums encompass low-rise single or two buildings, predominantly featuring studio apartments. The 20/80 condominiums comprise mid-rise 11-story structures, primarily housing one and two-bedroom units, with 10% of the space (ground floor units) allocated for commercial purposes. The 40/60 condominiums constitute 13-story buildings, with two and three-bedroom units being the predominant apartment sizes, alongside an increased commercial space of 20%.

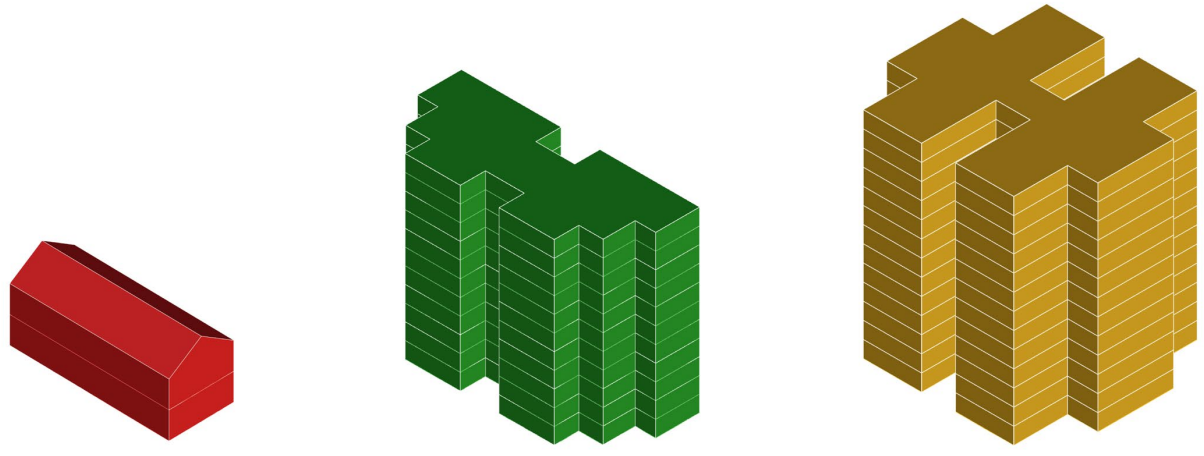

Figure 54: a) 10/90 condominium; (b) 20/80 condominium; (c) 40/60 condominium

Figure 55: Finished 40/60 condominiums on outskirts of Addis Ababa

Figure 56: 40/60 condominiums under construction on outskirts of Addis Ababa [Charlie Rosser, 2017]

The condo allocation mechanism proposed by the IHDP entails a lottery system wherein citizens can register to be allocated a government-sponsored condo. Upon selection, individuals are matched with an apartment based on their income and family size. For instance, recipients of apartments in the 10/90 condo (targeting the lowest income group) must make a 10% down payment, with the government-owned Commercial Bank of Ethiopia (CBE) extending a 20-year mortgage for the remaining 90%. Similar structures apply to the 20/80 and 40/60 condos, which are tailored to low-middle and middle-income households. Condominium ownership is transferred only upon the winner's ability to pay down payment, with provisions for savings over specified periods (3, 7, and 5 years, respectively) for those unable to meet the initial payment (Keller & Mukudi-Omwami, 2017).

5.1.2. Shortcomings of Integrated Housing Development Programme

The IHDP, although successful to an extent, has faced challenges in meeting its ambitious targets. As of 2019, the government had constructed and transferred 380,000 housing units to citizens, falling short of the planned 400,000 units and nearly a decade behind schedule (Sendin, 2015). Moreover, rapid urban population growth has exacerbated the housing deficit, necessitating an estimated 1.2 million additional housing units, predominantly low-cost options, between 2013 and 2023. However, the IHDP's annual production capacity of approximately 25,000-35,000 units is insufficient to meet the escalating demand (Sendin, 2015).

The exorbitant costs associated with construction materials pose a primary impediment to the IHDP's ability to deliver subsidized housing at the required pace (UN Habitat, 2010). IHDP condominiums employ concrete frame structures with concrete flat slabs and hollow block walls, predominantly relying on imported materials (Figure 52). Consequently, the government's financial constraints on importing the necessary volume of materials have hindered the expansion of subsidized housing, exacerbating the housing deficit.

Beyond limiting the production rate of the housing units, high construction prices have also made it difficult for low-income residents to afford the subsidized units. For reference one study in 2017 estimated that the 10/90 and 20/80 condos can have monthly loan payments ranging from 3,000 – 8,000 birr a month based on size (Keller & Mukudi-Omwami, 2017). A 2023 study estimated the price of a one-bedroom IHDP condo has reached 1.25 million Ethiopian Birr roughly $23,000, meaning the monthly loan payments have likely increased as well (Centre for Affordable Housing Finance, 2023). These prices are too expensive for low-income individuals; given a level 1 federal employee (for example a gate guard) in 2019 had a base salary of 1,100 birr and even a level 10 worker (a mid-level office worker) has a base pay of 5,300 birr a month (F.D.R. of Ethiopia, 2023).

In response to this, it is common practice for individuals who win the lottery but do not have the down payment ready or don't have the income to make the monthly loan payments to 1) illegally sell their condominium spot to someone who can afford it or 2) add walls inside their already small condo to rent a portion to someone (UN Habitat, 2010). This in effect has made the units overpopulated bringing on other issue of health and safety or in the worst case made the housing units inaccessible to the very people it sought to help.

The persisting housing demand and the ongoing challenges confronting the IHDP underscore the relevance of Ethiopia as a context for evaluating the feasibility of earthen vaulted floor systems. Adoption of these systems holds the potential to reduce structural costs, thereby facilitating the construction of more affordable housing units.

5.2. Methodology

5.2.1. Floor Designs

The floor designs are tailored for a 5x8 meter column grid spacing (40 m^2), reflecting Ethiopia's typical slab span in the 10/90 and 20/80 mid-rise condo buildings (Alemu, 2021; Deribe, 2024). The flat two-way concrete slab used in this comparison, provided by (Deribe, 2024), comes from a recently built 15 story building which while not a government sponsored condo has a similar design. This comparative slab, presented in Figure 57, is made from C35 concrete, is 17 cm thick with a reinforcement ratio of approximately 0.7%.

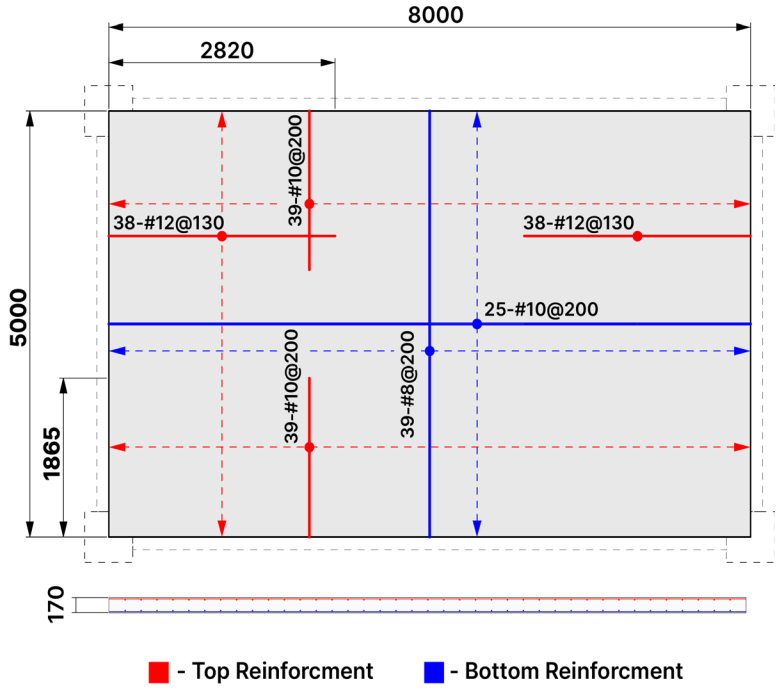

Figure 57: As built two-way flat slab details (mm)

The first earthen slab (EFV1), Figure 58, is a dense rib type, as defined in 2.1.1, with a 5-meter span, 8-meter depth, and a span/20 shallowness ratio. The total thickness, including the tile finishing surface, is 37 cm. For this design a 2.5 cm thick ceramic tile finishing surface is proposed; if the density of the tile is taken at 2000 kg/m^3 a finishing surface load is 0.49 kN/m^2 is reached which is in line with the assumptions set out in 2.1.1.

The second earthen slab (EFV2), Figure 59, is a sparse rib type, as defined in 2.1.1, with a 5-meter span, 8-meter depth, and a span/20 shallowness ratio. The total thickness, including the tile finishing surface, is 42 cm. The finish, called out at the bottom of Figure 59 and similar to the composite deck in Figure 4-B, consists of a 1 mm thick corrugated steel deck and a 3.5 cm thick light weight C25 concrete slab, resulting in a total finishing thickness of 7 cm. If the density of the concrete and steel is taken at 1400 kg/m^3 and 1400 kg/m^3 respectively, a finishing surface load of about 0.91 kN/m^2 is reached which is in line with the assumptions set out in 2.1.1.

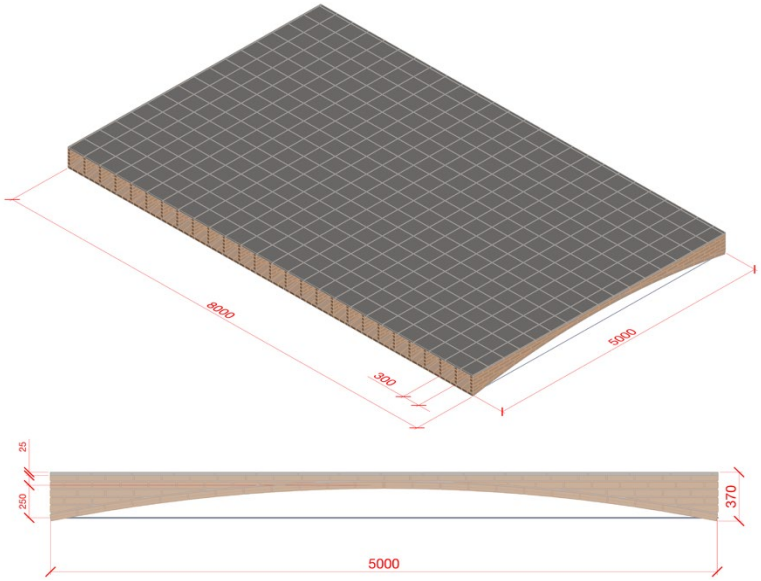

Figure 58: Earthen Vaulted Floor Design 1 (mm)

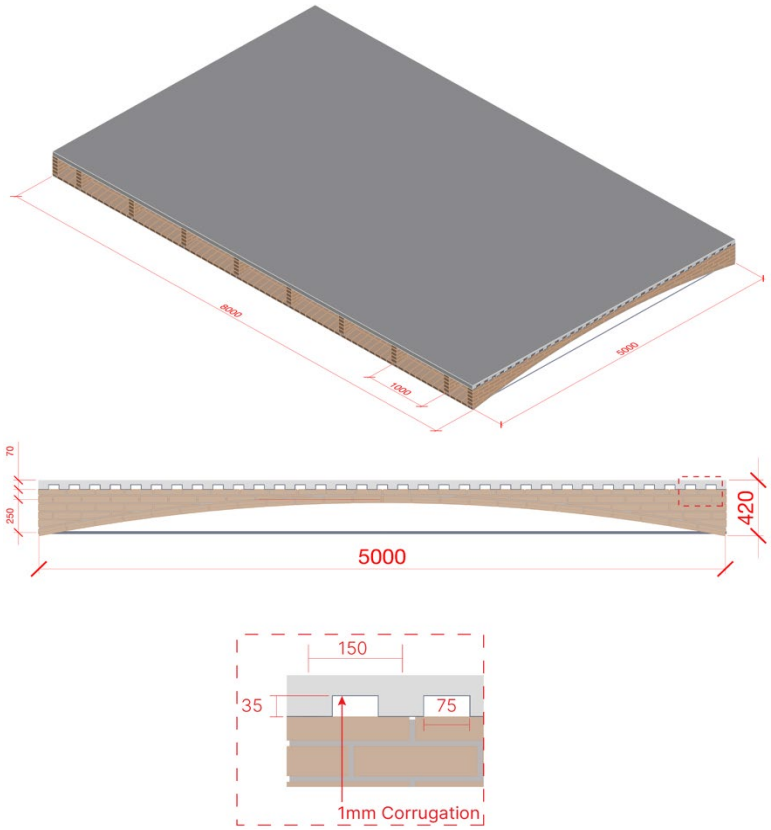

Figure 59: Earthen Vaulted Floor Design 2 (mm)

5.2.2. Embodied Carbon Coefficients and Material Costs

Table 21 represents A1-A3 embodied carbon coefficients (ECC) of building materials in kg_{CO2e}/unit. To obtain values that most closely relate to Ethiopia, the Rwanda Embodied Carbon Calculator (RwECC), a collaborative effort by the MASS Design Group, ARUP, and The University of Rwanda, was the source (MASS Design Group, 2023). The Inventory of Carbon & Energy database (ICE) is used for any unavailable values (Hammond et al., 2019). With respect to CSEB choice, Chapter 3 showed that 3% and 7% cement stabilized bricks with a strength of 5+ MPa could be achieved in Ethiopia thus the value in Table 21 which is for a 5% brick in Rwanda is deemed a fair estimate of ECC for the CSEBs used in the proposed designs.

Table 21: Embodied Carbon Coefficients

Material	Density [kg/m3]	ECC [kg_{CO2e}]	Source
C35 Concrete	2400	339 / m^3	RwECC
LW C25 Concrete	1400	270 / m^3	RwECC
1:3 Mortar	1800	0.2 / kg	RwECC
Steel Corrugation	7850	1.44 / kg	ICE
Steel Tie (Rebar)	7850	1.2 / kg	RwECC
5% Cement CSEB	2000	0.041 / kg	RwECC
Clay Tile	2000	0.22 / kg	RwECC

The material and labor costs presented in Table 22 were obtained through an interview with a local engineer (Deribe, 2024) and data collected from CSEBs testing in Ethiopia. Formwork costs are conservatively taken to be the same cost for both vaults and concrete slabs. Regarding masonry labor, the local rate for masonry work is \$2/m^2. However, due to the increased complexity of vault construction, this is assumed to increase to \$6/m^2. Lastly due to variation from project to project, concrete labor costs are not given per square meter but rather estimated to constitutes 35% of the total structural material cost; this which was derived from an interview the author had with an engineer's audit of 15 recently constructed buildings (Deribe, 2024).

Table 22: Cost of Material and Labor

Material / Labor	USD	Unit
C35 Concrete	\$241	m^3
LW C25 Concrete	\$185	m^3
1:3 Mortar	\$139	m^3
Steel Corrugation	\$31	m^2
Steel Tie (Rebar)	\$2	kg
5% Cement CSEB	\$93	m^3
Clay Tile	\$8	m^2
Formwork*	\$30	m^2
Masonry Labor*	\$6	m^2
Concrete Labor*	35%	%

For each design a 3D model of the floor system was made, and the total volumes and masses were recorded and multiplied by the ECC to get the total embodied carbon and cost.

5.3. Results

Figures 60 shows that both earthen vaulted floor design cases have significant reductions in cost. EFV1 showed a 62% reduction in cost while EFV2 showed a 42% reduction in cost. Some notable points include that in the case of EFV2 46% of the total cost of the floor system is in the finishing surface alone with 35% of that being the steel corrugation. Thus, while having fewer stiffening walls does cut the cost of masonry labor by nearly a quarter, the premium for the corrugation is not worth it. Comparing the two vaulted structures to the slab the key savings comes from the reduction of concrete and rebar which in the slab sum to $81/m^2$ which is already more than the entire EFV1 and nearly equal to the entire cost of EFV2.

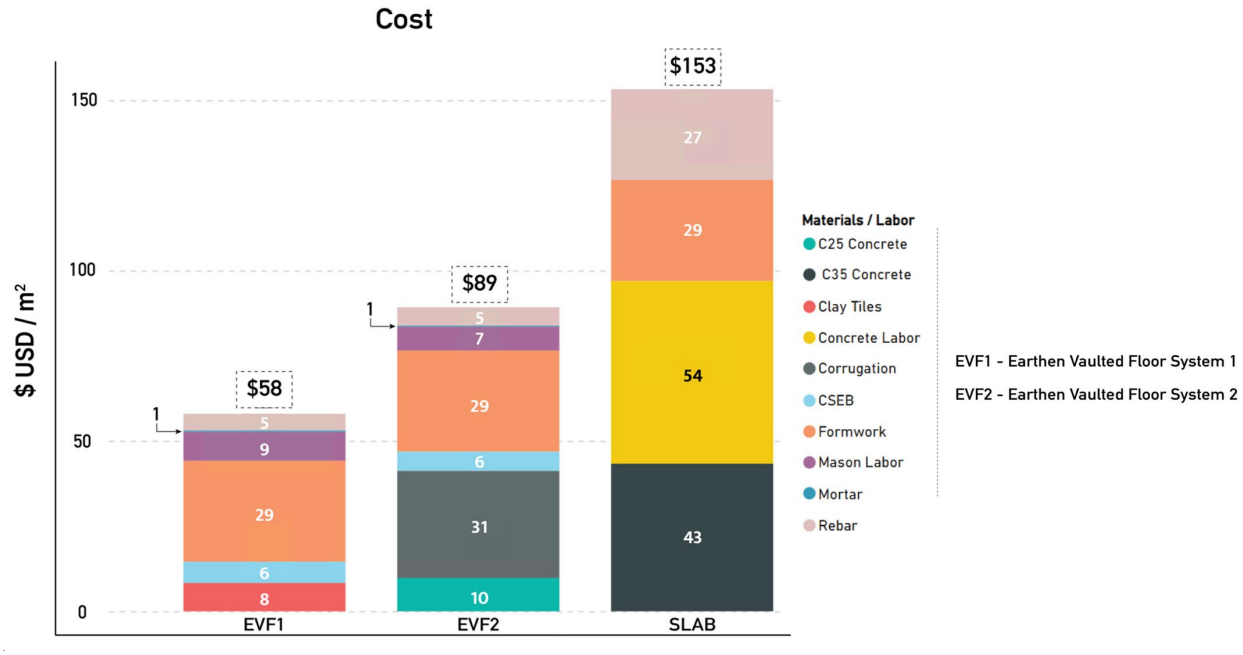

Figure 60: Cost per m² breakdown of case study floor systems

Table 23: Cost per m² Breakdown of Case Study Floor Systems by Percentage of Total

	Percent of Total Cost		
Material / Labor	EVF1	EVF2	SLAB
C35 Concrete	-	-	28.1
LW C25 Concrete	-	11.2	-
1:3 Mortar	1.7	1.1	-
Steel Corrugation	-	34.8	-
Steel Tie (Rebar)	8.6	5.6	17.6
5% Cement CSEB	10.3	6.7	-
Clay Tile	13.8	-	-
Formwork*	50.0	32.6	19.0
Masonry Labor*	15.5	7.9	-
Concrete Labor*	-	-	35.2

As is the case with cost, Figures 61 shows that with respect to embodied carbon that both earthen vaulted floor design cases have significant reductions in cost. EFV1 showed a 74% reduction in embodied carbon while EFV2 showed a 50% reduction. As anticipated the concrete and the rebar in the slab make up its entire carbon footprint with the concrete alone being more than the two earthen designs in their entirety. Comparing EVF1 to EVF2, again the composite finishing surface of EVF2 comes at a premium making up 75% of the design embodied carbon, and its additional 18 kg_{CO2e}/m^2 make it three times more carbon intensive than the clay tiles used in EVF1.

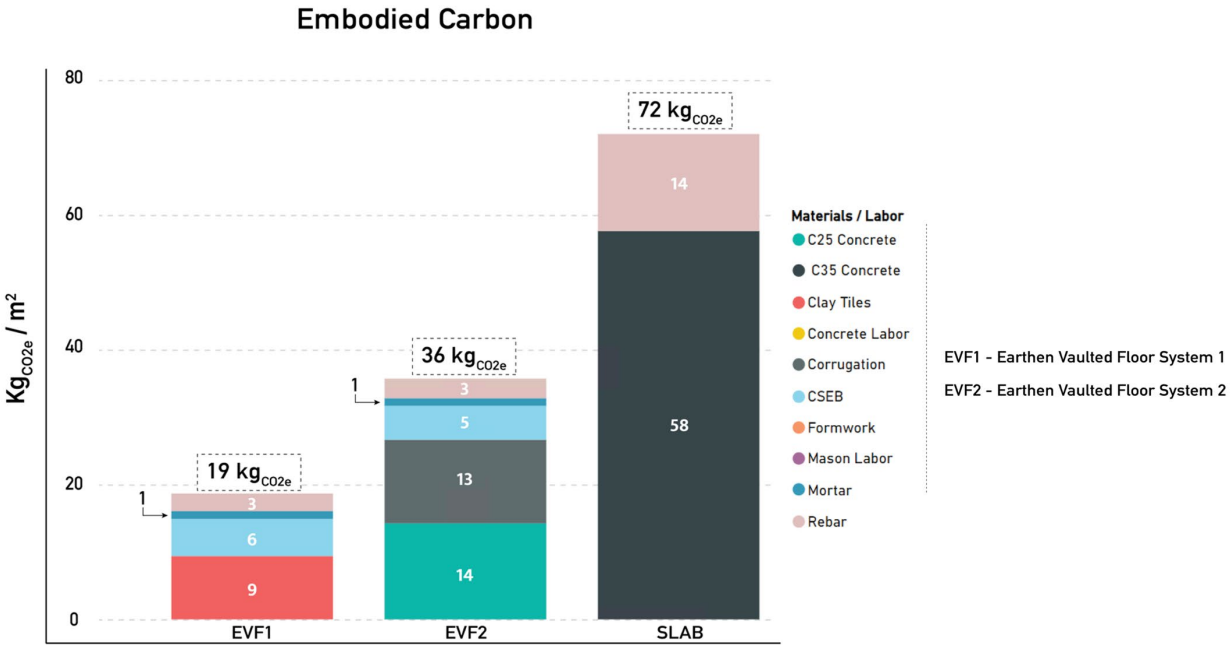

Figure 61: Embodied carbon per m² breakdown of case study floor systems

Table 24: Embodied Carbon per m² Breakdown of Case Study Floor Systems by Percentage of Total

	Percent of Total Cost		
Material / Labor	EVF1	EVF2	SLAB
C35 Concrete	-	-	81.0
LW C25 Concrete	-	38.9	-
1:3 Mortar	5.2	2.7	-
Steel Corrugation	-	36.2	-
Steel Tie (Rebar)	15.8	8.3	19.0
5% Cement CSEB	31.6	13.9	-
Clay Tile	47.3	-	-
Formwork*	-	-	-
Masonry Labor*	-	-	-
Concrete Labor*	-	-	-

Looking at the weight of the three systems both earthen typologies are similar to one another, both being less than half the mass of the slab (42% and 47%). This in itself is impressive, yet the notable reduction in weight is even more compelling considering that as a result of reduction at the floor level, the size and mass of columns and foundations can be reduced, providing even further savings in embodied carbon and cost.

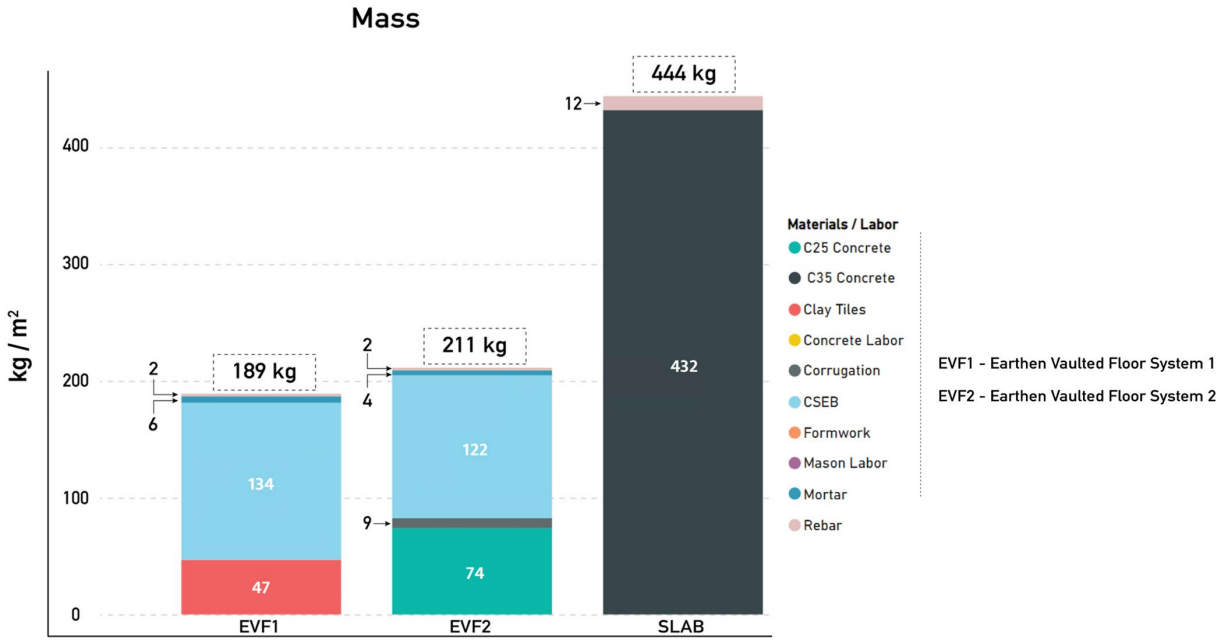

Figure 62: Weight per m² breakdown of case study floor systems

Table 25: Weight per m² Breakdown of Case Study Floor Systems by Percentage of Total

	Percent of Total Cost		
Material / Labor	EVF1	EVF2	SLAB
C35 Concrete	-	-	97.3
LW C25 Concrete	-	35.1	-
1:3 Mortar	3.2	1.9	-
Steel Corrugation	-	4.3	-
Steel Tie (Rebar)	1.1	1	2.7
5% Cement CSEB	70.9	57.8	-
Clay Tile	24.9	-	-
Formwork*	-	-	-
Masonry Labor*	-	-	-
Concrete Labor*	-	-	-

5.4. Discussion

The present chapter addresses a notable void in the scientific literature by quantifying the embodied carbon and cost savings associated with earthen barrel-vaulted floor systems compared to traditional concrete flat slabs. Through a detailed case study involving two earthen vaulted floor systems and employing prevailing market rates for materials and labor costs, the investigation demonstrates that earthen vaulted floor systems can offer cost savings of up to 62% compared to a comparable slab. This finding underscores the economic feasibility and favorability of these floor typologies. Furthermore, the study reveals significant environmental benefits, with carbon savings reaching as high as 74%, thus highlighting the system's positive environmental impact.

While the initial findings of this study are promising, it is imperative to acknowledge the limitations inherent in this case study. A primary constraint lies in the reliance on estimated values for the costs and embodied carbon of materials and labor, which are often adaptations from related sources and may not reflect precise figures. For instance, the assumption that masonry labor for vaulted structures is three times more expensive than for walls may not hold universally, potentially impacting the accuracy of the results. Similarly, lacking a pre-existing market for CSEB in Ethiopia necessitated deriving pricing assumptions based on traditional fired clay bricks and the production of CSEBs outlined in Chapter 3. However, the actual cost of CSEBs at scale remains uncertain and warrants further investigation for precise estimation. Hence, future research endeavors should prioritize refining this case study by constructing a full-scale prototype, tracking actual costs in Ethiopia, and conducting additional case studies in other LEDC contexts to understand potential variations in cost savings.

An additional constraint of this case study is its restricted focus on analyzing floor systems solely at the floor level. To enhance the comprehensiveness of the findings, it would be advantageous to redesign an entire 20/80 or 40/60 condominium, encompassing various floor typologies, from the foundation upwards. Such an approach would provide a holistic understanding of different floor designs' potential carbon, cost, and weight savings. One example of second-order effects is that while using the vaulted floor might reduce mass at the floor level by 50%, it might require more complex columns that increase their reinforcement or mass so that the total savings might be less than 50%.

In summary, this chapter illuminates the viability of earthen barrel-vaulted floor systems compared to traditional concrete flat slabs. However, it acknowledges limitations such as reliance on estimated costs and the absence of an established market for Compressed Stabilized Earth Blocks (CSEBs) in Ethiopia. Future research should refine methodologies and explore broader structural implications to provide more accurate economic and environmental benefits assessments, thus aiding sustainable construction practices and addressing affordable housing challenges.

6. Conclusion

6.1. Summary of Contributions

This thesis addresses three critical questions regarding low-cost, low-carbon earthen vaulted floor systems:

1. What is the spanning capacity of unreinforced earthen vaulted floor systems under typical loads?
2. Are unreinforced earthen vaulted floor systems structurally viable in full-scale testing?
3. What are an unreinforced earthen vaulted floor's cost and carbon savings compared to a concrete flat slab?

Regarding the first point, Chapter Two demonstrated that various earthen floor typologies can span typical residential floor spans while maintaining stresses below 6 MPa at a 10-meter span and 2.5 MPa at a 5-meter span. These findings validate the system's potential, highlighting stress levels consistent with low-cost and low-strength masonry units such as compressed earth bricks. This chapter also contributes that for safety that a span to rise ratio of L/10 is most adequate when using earthen bricks in LEDC contexts.

Concerning the second research question, Chapter Three introduced a construction technique for producing Compressed Stabilized Earth Blocks (CSEBs). Furthermore, it showed that CSEBs with strengths suitable for constructing the proposed floor system can be produced in different contexts, achieving strengths of 5 MPa in Addis Ababa, Ethiopia, and over 10 MPa in Boston. Chapter Four validated the theoretical framework for earthen vaulted floor systems by constructing and testing a large-scale prototype, demonstrating its capacity to hold up to building code live loads of 2 kN/m2 symmetrically and asymmetrically.

Addressing the last research question, the case study in Chapter Five illustrated that earthen vaulted floor systems are more affordable and carbon-efficient in Ethiopia, with potential cost savings of up to 62% and carbon reductions of up to 74% compared to a concrete flat slab. This underscores the suitability of the proposed system for use in Least Economically Developed Countries (LEDCs).

6.2. Limitations and Future Work

Regarding the theoretical framework, despite promising results, this thesis acknowledges several limitations. The analysis only considers uniform loading conditions, overlooking potential instability issues, which are often the primary failure modes in vaulted structures. Future analyses should incorporate asymmetrical loading, as demonstrated in the prototype in Chapter Four. Additionally, seismic behavior needs further exploration.

Regarding CSEB production and physical validation of the floor system, there is a need for deeper exploration into understanding the strength of CSEBs when laid into a prism and vault, as shown by the significant reduction in CSEB strengths when tested individually versus as part of a prism. Furthermore, the material and geometric nonlinear behavior of earthen vaults requires study to validate the theoretical framework up to a factored building code load of 7 kN/m2.

Lastly, the case study's reliance on estimated costs and embodied carbon values introduces uncertainties, emphasizing the need for further refinement through real-world case studies and market analysis. Additionally, case studies need to be expanded to include the entire building structure, which would provide a more comprehensive understanding of carbon and cost impacts.

6.3. Closing Remarks

The findings of this thesis underscore the potential of earthen barrel-vaulted floor systems as a sustainable and cost-effective solution to housing challenges in LEDCs, holding significant implications for the construction industry. These innovations can transform building practices by offering a cost-effective and environmentally sustainable alternative to conventional floor systems, facilitating the rapid and affordable construction of housing infrastructure in urban areas. This addresses the urgent demand for affordable housing options for the projected 2.5 billion additional urban residents by 2050 while contributing to inclusive and environmentally conscious urban development aligned with global sustainability objectives. Through continued research and implementation efforts, earthen barrel-vaulted floor systems can pave the way for a more equitable and sustainable future for urban populations worldwide.

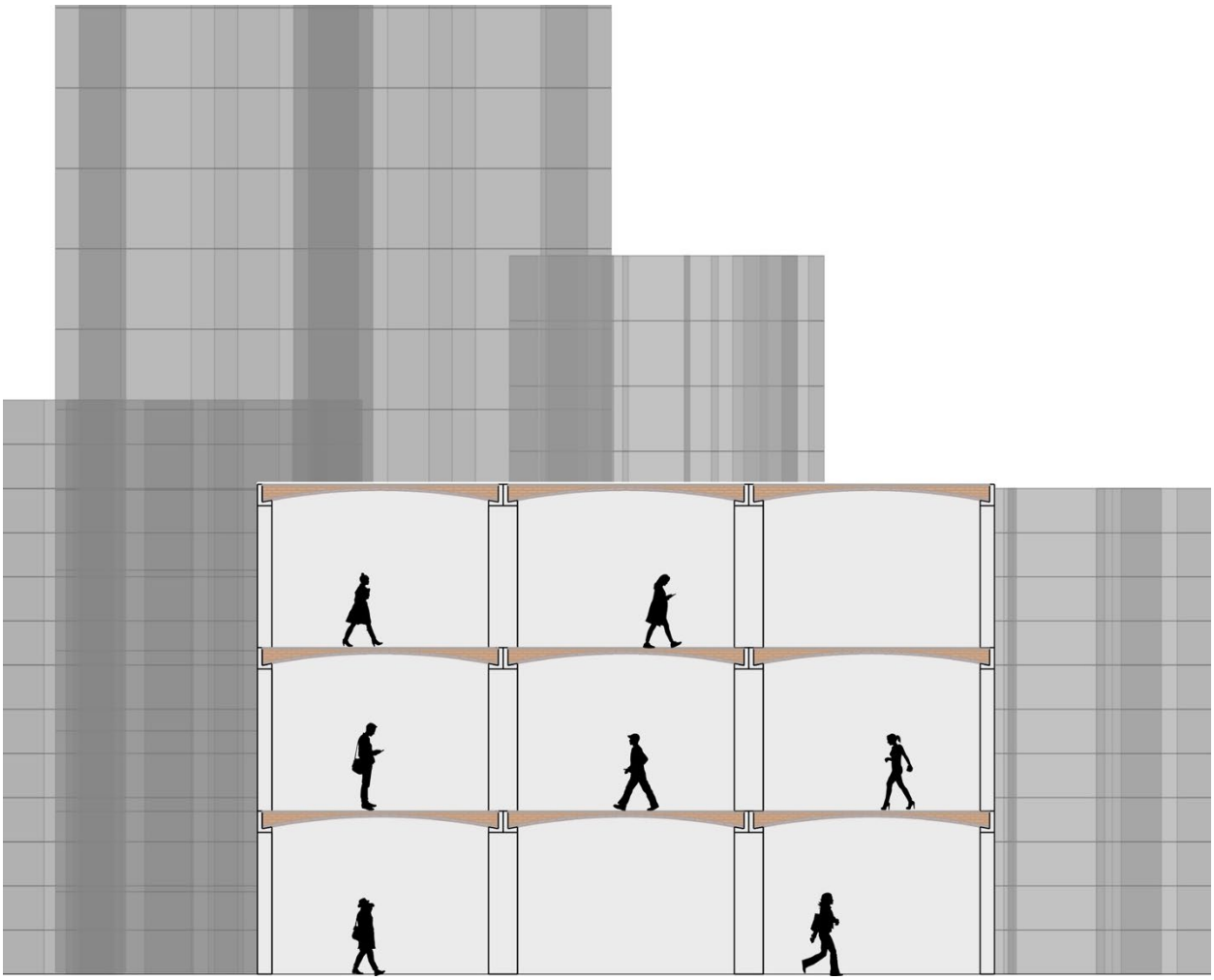

Bibliography

Abdel Gelil Mohamed, N., & Abo Eldardaa Mahmoud, I. (2023). Cost-effectiveness and affordability evaluation of a residential prototype built with compressed earth bricks, hybrid roofs and palm midribs. Frontiers in Built Environment, 9, 1058782

Alemu, K. D. (2021). Assessment of housing demand and feasibility of establishing real estate business in Ethiopia. Journal of Land Management and Appraisal, 8(2), 28–38. https://doi.org/10.5897/JLMA2021.0024

Architecture 2030. All Rights Reserved. Data Source: IEA (2022), Buildings, IEA, Paris

Auroville Earth Institute., (2020). "Compressed Stabilized Earth Block." Accessed January 15, 2021. http://www.earth-auroville.com/compressed_stabilised_earth_block_en.php.

Bah, Eh.M., Faye, I., Geh, Z.F. (2018). The Construction Cost Conundrum in Africa. In: Housing Market Dynamics in Africa. Palgrave Macmillan, London.

Bailey, C. G. (2003). Efficient arrangement of reinforcement for membrane behaviour of composite floor slabs in fire conditions. Journal of Constructional Steel Research, 59(7), 931–949. https://doi.org/10.1016/S0143-974X(02)00116-5

Centre for Affordable Housing Finance (2023). Housing Finance in Africa Yearbook: 14th Edition – 2023. https://housingfinanceafrica.org/resources/yearbook

Deribe, Y. (2024, January 15). State of Construction in Addis Ababa, Ethiopia. personal.

De Wolf, Catherine & Ramage, Michael & Ochsendorf, John. (2016). Low Carbon Vaulted Masonry Structures. Journal of the IASS. 57. 10.20898/j.iass.2016.190.854.

Federal Democratic Republic of Ethiopia. (2019, October 2). Federal civil servants position rating, grading and salary scale council of ministers. Federal Negarit Gazette.

Gaitan, S. (2021). Vaulted Earthen Floor Systems for Low-Cost Housing Construction [Thesis, Massachusetts Institute of Technology]. https://dspace.mit.edu/handle/1721.1/139007

Guastavino, R. (1893). Essay on the theory and history of cohesive construction.

Hammond, G., Jones, C., Lowrie, E. F., & Tse, P. (2019). Embodied carbon. The inventory of carbon and energy (ICE). Version (3.0).

Hawkins, W. J. (2020). Thin-shell Concrete Floors for Sustainable Buildings. https://doi.org/10.17863/CAM.45976

Heyman, Jacques. (1995). The Stone Skeleton: Structural Engineering of Masonry Architecture.

Hoornweg, D., & Pope, K. (2017). Population predictions for the world's largest cities in the 21st century. Environment and Urbanization, 29(1), 195-216.

Huberman, N., Pearlmutter, D., Gal, E., and Meir, I.A., "Optimizing structural roof form for life-cycle energy efficiency," Energy Build., vol. 104, no. Supplement C, pp. 336–349, Oct. 2015.

International Code Council (ICC). International Building Code. Falls Church, Va. :ICC, 2021.

Ismail, M. A. (2023). Reshaping concrete: Empowering development through low-carbon structural design. Massachusetts Institute of Technology.

Keller, E. J., & Mukudi-Omwami, E. (2017). Rapid urban expansion and the challenge of pro-poor housing in Addis Ababa, Ethiopia. Africa Review, 9(2), 173–185. https://doi.org/10.1080/09744053.2017.1329809

Kilroy, A. (2024, March 22). How much does it cost to build a house in 2023?. Quicken Loans. https://www.quickenloans.com/learn/how-much-does-it-cost-to-build-a-house

Kitchin, J. (2021). Deriving embodied carbon factors from scratch. Structural Engineer,99(7),18-20.

Leone, F., Macchiavello, R., & Reed, T. (2021). The Falling Price of Cement in Africa. The World Bank. https://doi.org/10.1596/1813-9450-9706

Liew, A., López, D. L., Van Mele, T., & Block, P. (2017). Design, fabrication and testing of a prototype, thin-vaulted, unreinforced concrete floor. Engineering Structures, 137, 323–335. https://doi.org/10.1016/j.engstruct.2017.01.075

Maia Avelino R., (2023). 'Thrust Network Optimisation for the Assessment of Vaulted Masonry Structures', Ph.D. thesis, ETH Zurich, Zurich,.

Meikle, Jim. (2011). "A New Approach to International Construction Price Comparisons." 5th Technical Advisory Group Meeting. Worldbank ICP.

Murmu, A. L., & Patel, A. (2018). Towards sustainable bricks production: An overview. Construction and Building Materials, 165, 112–125.

Niazi, Z., Khanna, P., Gupta, S., and Sirohi, R. (2020) Stabilized Compressed Earth Block (SCEB) - Production and Construction Guide. New Delhi: Development Alternatives.

Ochsendorf, J. (2010). Guastavino Vaulting: The Art of Structural Tile. Princeton Arch. Press.

Ranaudo, F., Van Mele, T., & Block, P. (2021). A low-carbon, funicular concrete floor system: Design and engineering of the HiLo floors. 2016–2024. https://doi.org/10.2749/ghent.2021.2016

Report of the Intergovernmental Panel on Climate Change (IPCC), (2018).

Sendin, P. (2015). Addis Ababa's Ambitious Housing Programme to Half Slum Areas. Not Only About Architecture: Art, Land, Climate. Retrieved March 31, 2024, from https://www.patriciasendin.com/2015/04/addis-ababa-ambitious-housing-programme.html

Sory, L. Y. K. (2023). Physics-based Estimates of Structural Material Quantities for Urban-level Embodied Carbon Assessment in Buildings [Thesis, Massachusetts Institute of Technology].

United Nations, Department of Economic and Social Affairs (UN-DESA), Population Division (2019). World Population Prospects 2019: Highlights. ST/ESA/SER.A/423

Weber, Ramon and Mueller, Caitlin and Reinhart, Christoph, Building for Zero, The Grand Challenge of Architecture without Carbon (October 8, 2021).

World Bank Open Data. (2024). World Bank Open Data.

World Bank. (2011). International Comparison

Appendix A – CSEBs

Procedure for Making CSEB

Legend

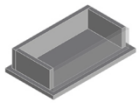

Brick Mold

Tampening Plate

Arbor Press

Rubber Mallet

Metal Scrapper

Brush

Layer 1

1 - Fill brick mold 1/2 to 3/4 of the way full with soil mixture.

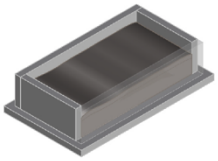

2 - Move the plate to one side and apply pressure to the center of the plate using the arbor press. Move plate to opposite side and repeat. Move plate to the center and repreat once more.

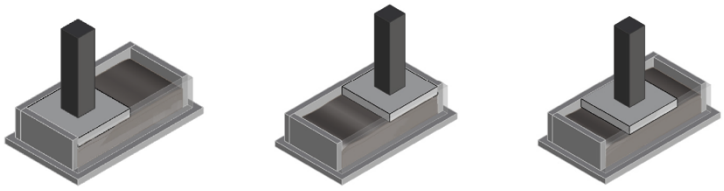

3 - Move plate to left side and apply pressure to top left corner, bottom left corner, and center of right edge of plate using the abor press. Move the plate to the oppsoite side and apply pressure at the top right corner, bottomright corner, and center of left edge of plate.

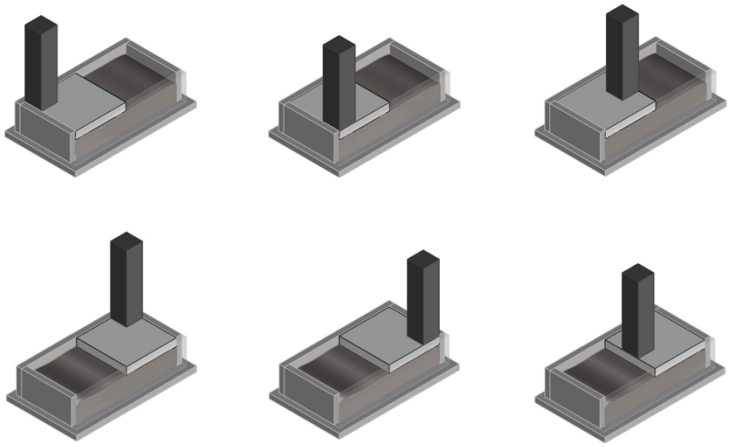

4 - Wet newly compacted surface. Then apply three holes in the center of the brick using a stick or similar object like a scredriver or pencil.

Layer 2

1 - Fill brick mold 3/4 to just under the top of the way full with soil mixture.

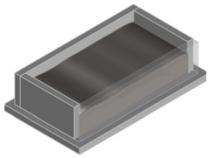

2 - Move the plate to one side and apply pressure to the center of the plate using the arbor press. Move plate to opposite side and repeat. Move plate to the center and repreat once more.

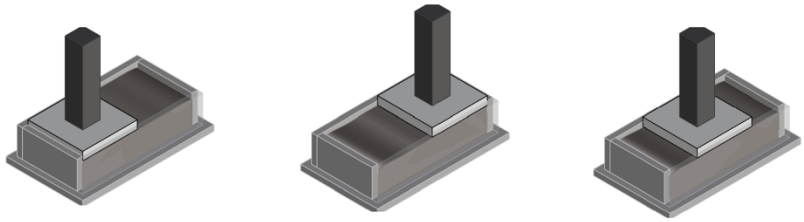

3 - Move plate to left side and apply pressure to top left corner, bottom left corner, and center of right edge of plate using the abor press. Move the plate to the oppsoite side and apply pressure at the top right corner, bottomright corner, and center of left edge of plate.

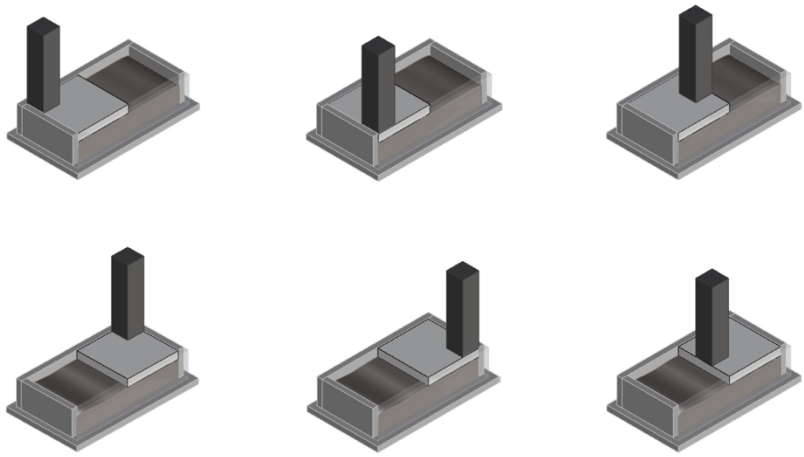

4 - Wet newly compacted surface. Then apply four holes inset from the corner of the the brick using a stick or similar object like a scredriver or pencil.

Layer 3

1 - Fill brick mold past the top making a mound above the top of the mold.

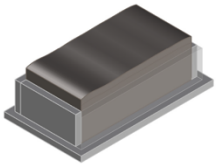

2 - Move the plate to one side and apply pressure to the center of the plate using the arbor press. Move plate to opposite side and repeat. Move plate to the center and repreat once more.

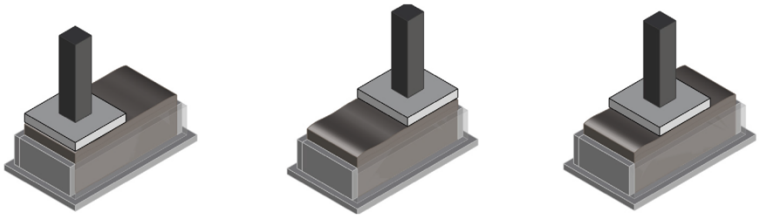

3- The mound should still be present above the top of the mold, but now more compacted.

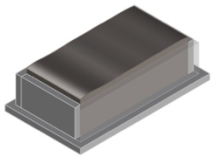

4- Move the plate each corner so that half the plate is hanging off the mold (see image below) and hit the center of the plate with a mallet. Do the same at each side of the center of the brick as well.

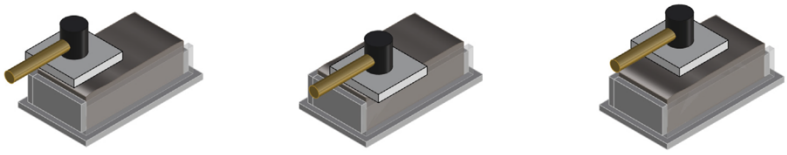

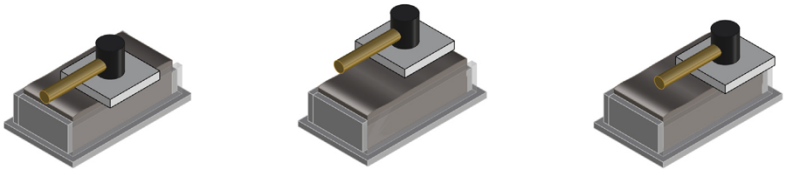

5- A thin, flat, and level mound should be present protruding slightly above the surface of the mold.

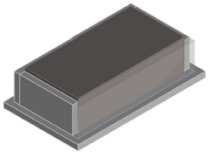

6- Using the metal scraper, gently scrape off and level the thin mound leaving the brick flush with the top of the mold.

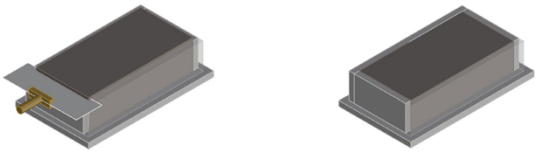

7- Lightly brush the surface of the brick with water. Once wet, using a consdierable amount of pressure, use your finger and palms to rub the surface of brick smooth using circular motions.

8 - Let the brick rest for 2-5 minutes and then demold.

Boston CSEB 14 Day Stress Strain Plots - Compression Direction

3% Gravel

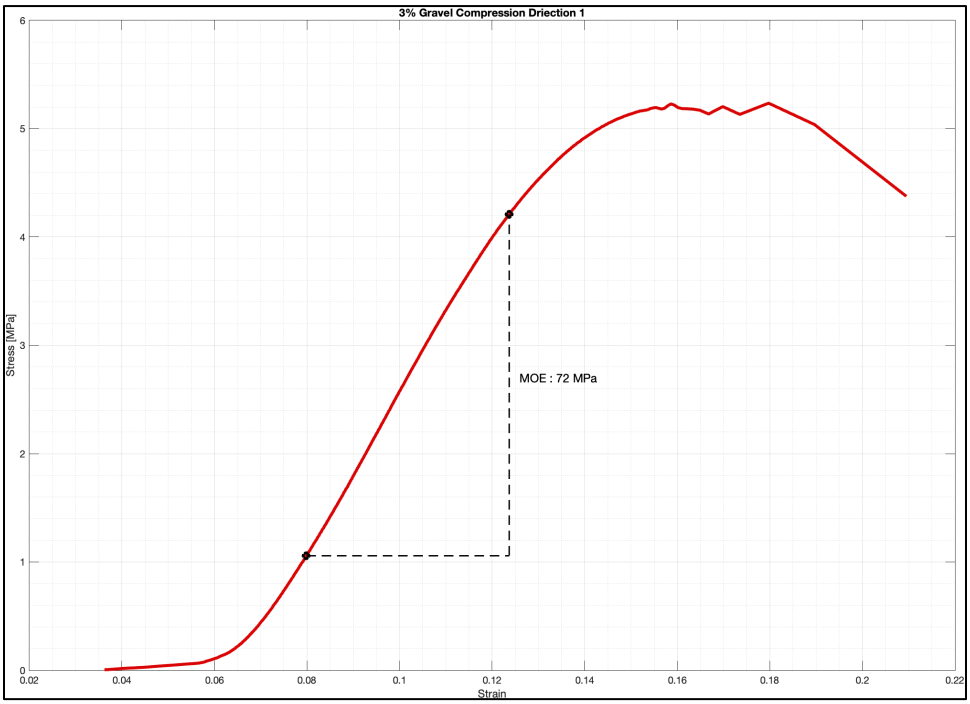

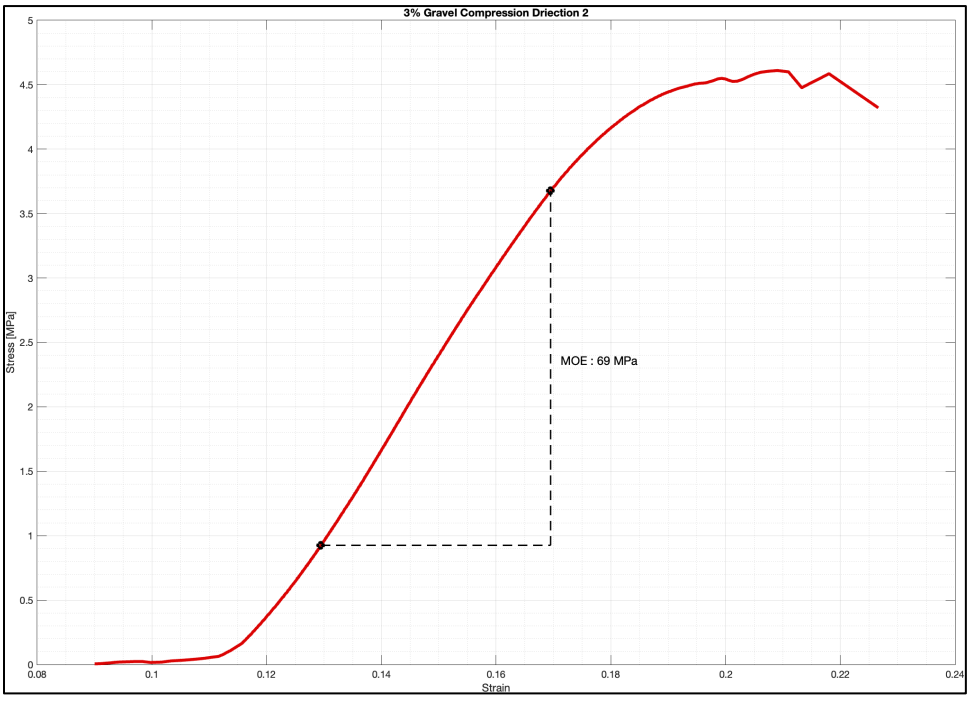

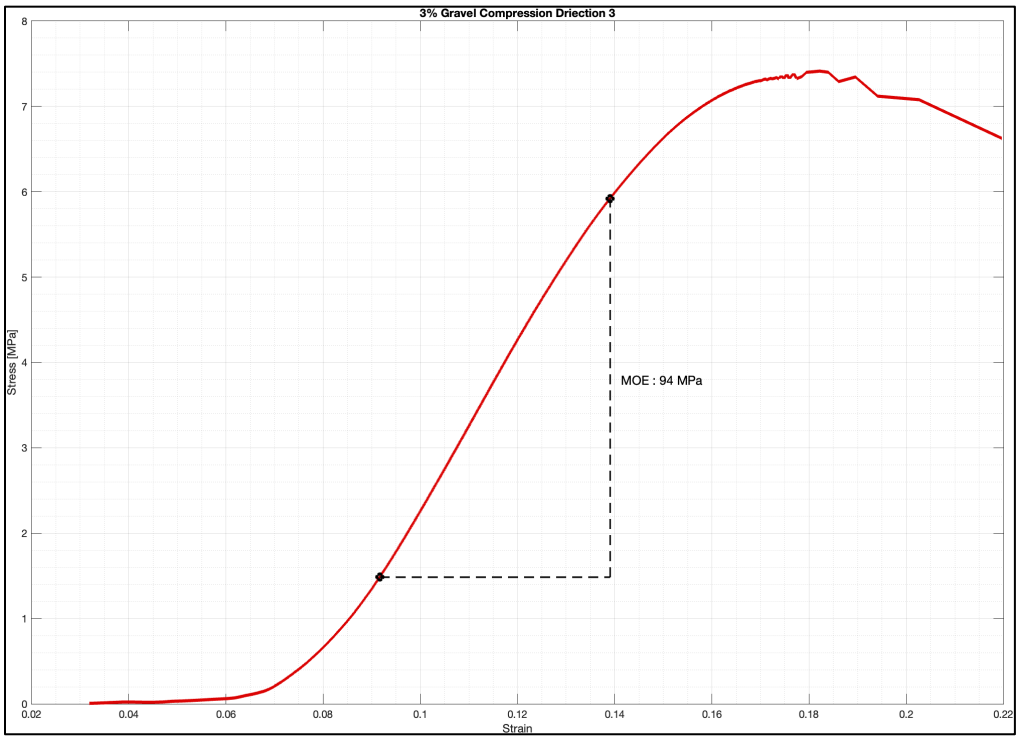
3% Gravel Compression Driection 3
Stress [MPa]
Strain
MOE : 94 MPa
0
1
2
3
4
5
6
7
8
0.02
0.04
0.06
0.08
0.1
0.12
0.14
0.16
0.18
0.2
0.22

3% No Gravel

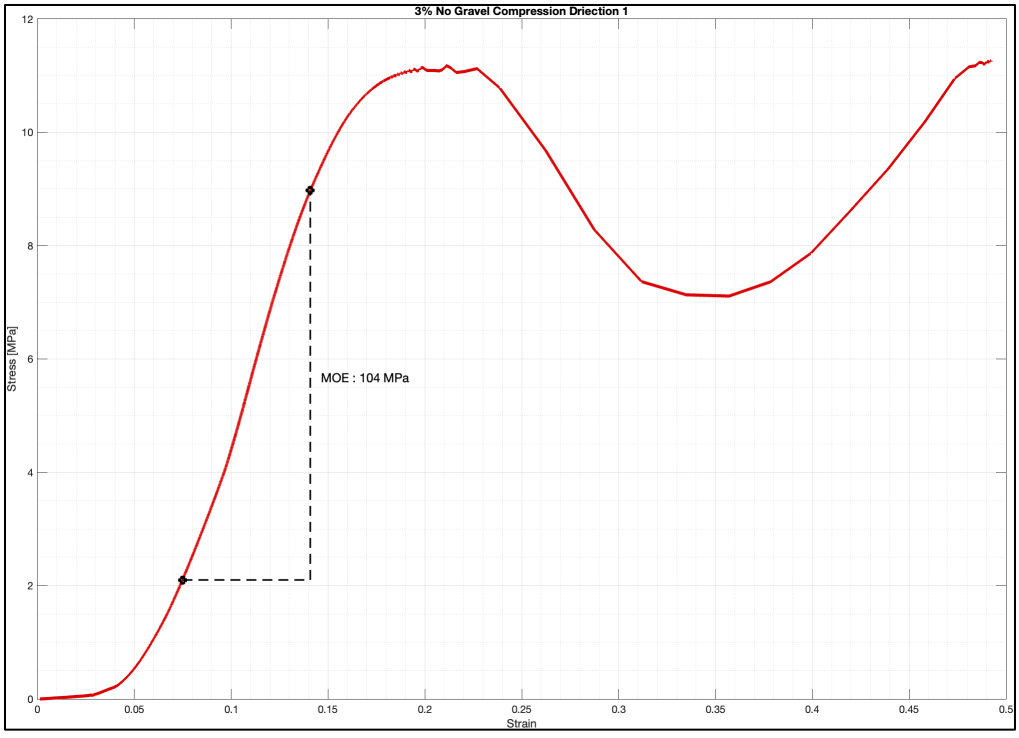
3% No Gravel Compression Driection 1
Stress [MPa]
Strain
MOE : 104 MPa
0
2
4
6
8
10
12
0
0.05
0.1
0.15
0.2
0.25
0.3
0.35
0.4
0.45
0.5

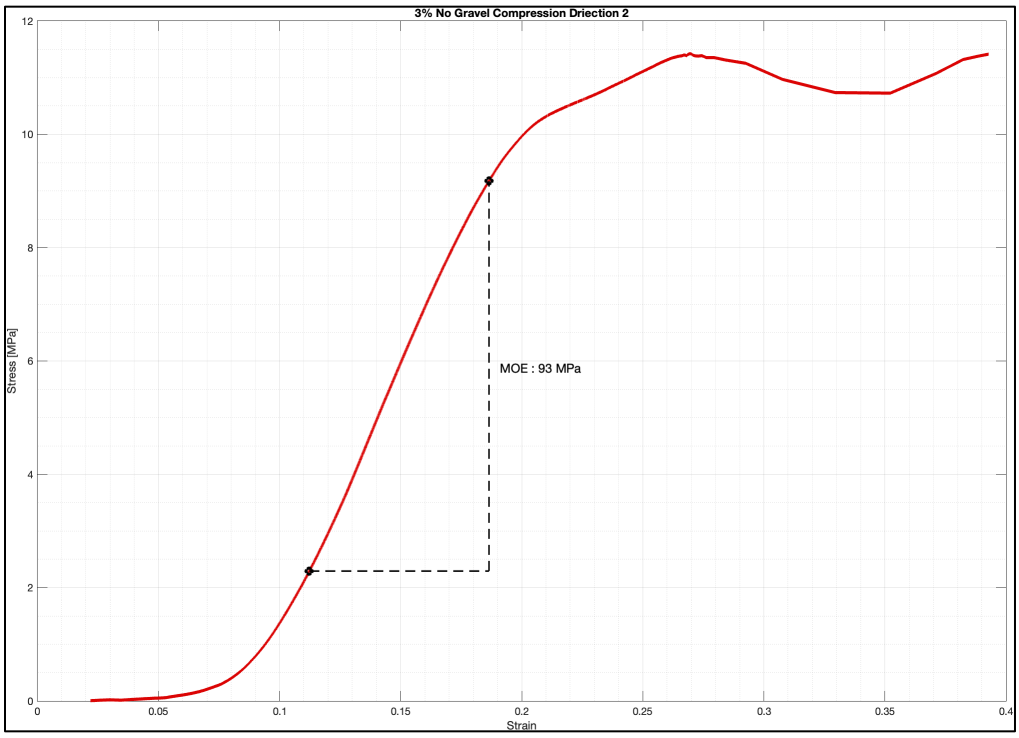
3% No Gravel Compression Driection 2
Stress [MPa]
Strain
MOE : 93 MPa
0
2
4
6
8
10
12
0
0.05
0.1
0.15
0.2
0.25
0.3
0.35
0.4

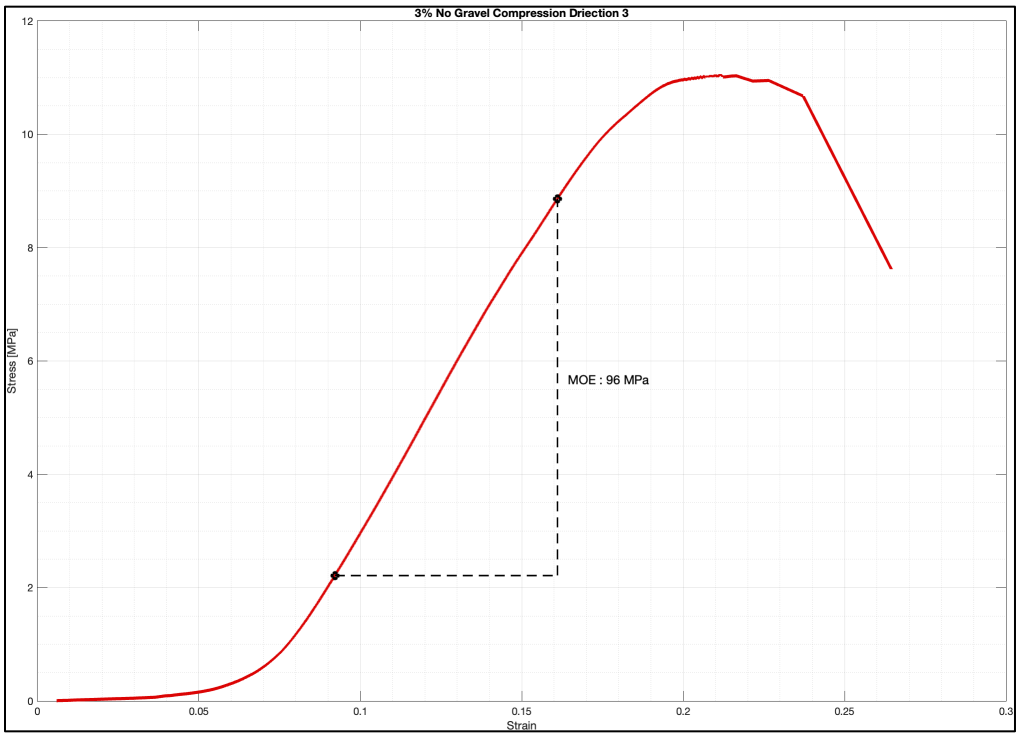
3% No Gravel Compression Driection 3
Stress [MPa]
Strain
MOE : 96 MPa
0
2
4
6
8
10
12
0
0.05
0.1
0.15
0.2
0.25
0.3

5% Gravel

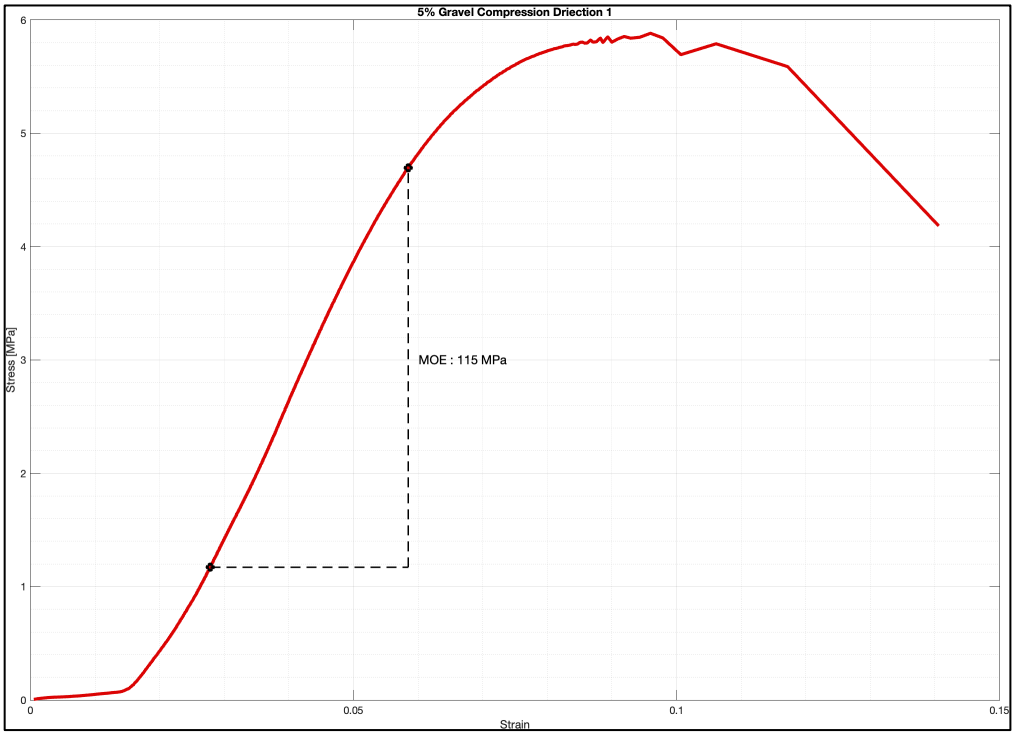
5% Gravel Compression Driection 1
Stress [MPa]
Strain
MOE : 115 MPa
0
1
2
3
4
5
6
0
0.05
0.1
0.15

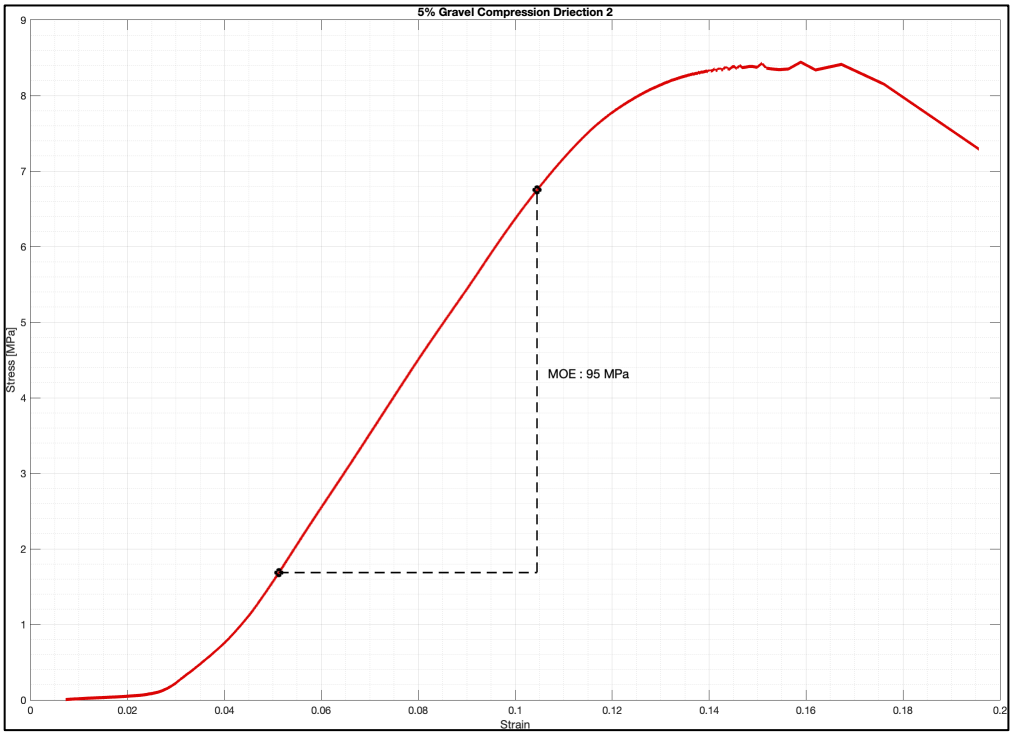
5% Gravel Compression Driection 2
Stress [MPa]
Strain
MOE : 95 MPa
0
1
2
3
4
5
6
7
8
9
0
0.02
0.04
0.06
0.08
0.1
0.12
0.14
0.16
0.18
0.2

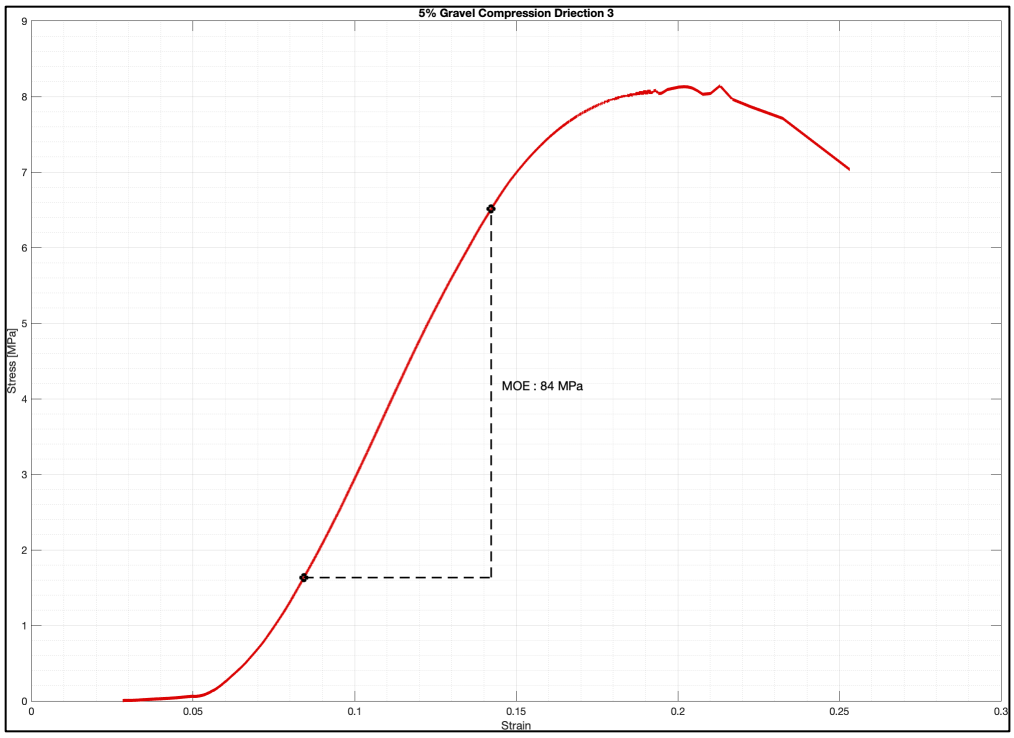
5% Gravel Compression Driection 3
Stress [MPa]
Strain
MOE : 84 MPa
0
1
2
3
4
5
6
7
8
9
0
0.05
0.1
0.15
0.2
0.25
0.3

5% No Gravel

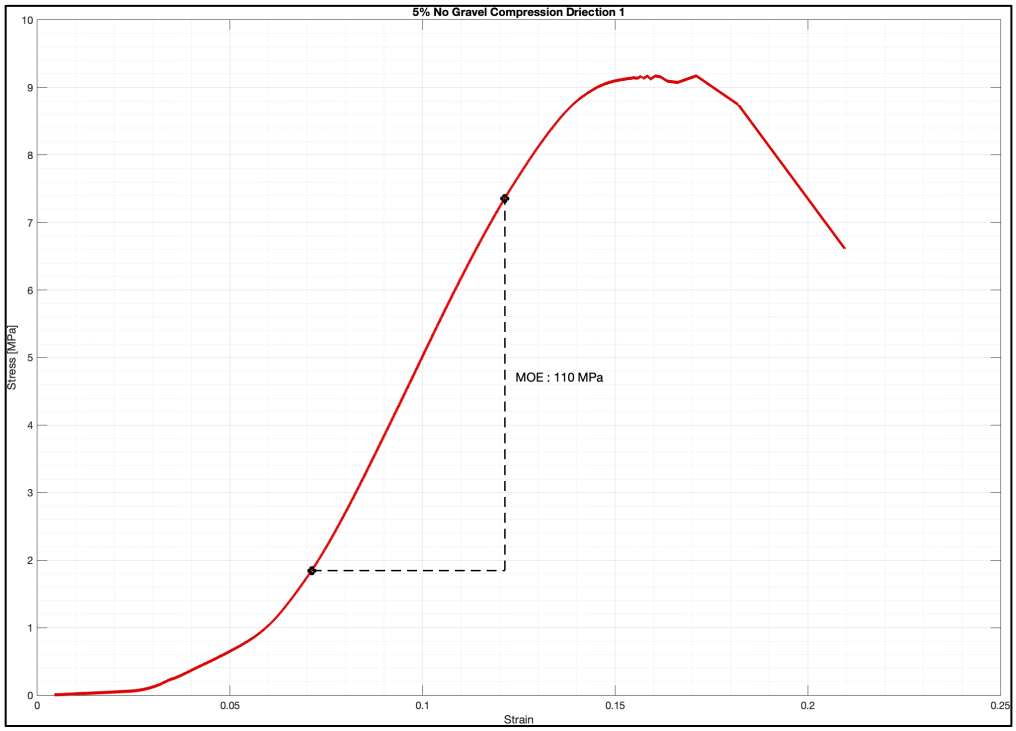
5% No Gravel Compression Driection 1
Stress [MPa]
Strain
MOE : 110 MPa
0
1
2
3
4
5
6
7
8
9
10
0
0.05
0.1
0.15
0.2
0.25

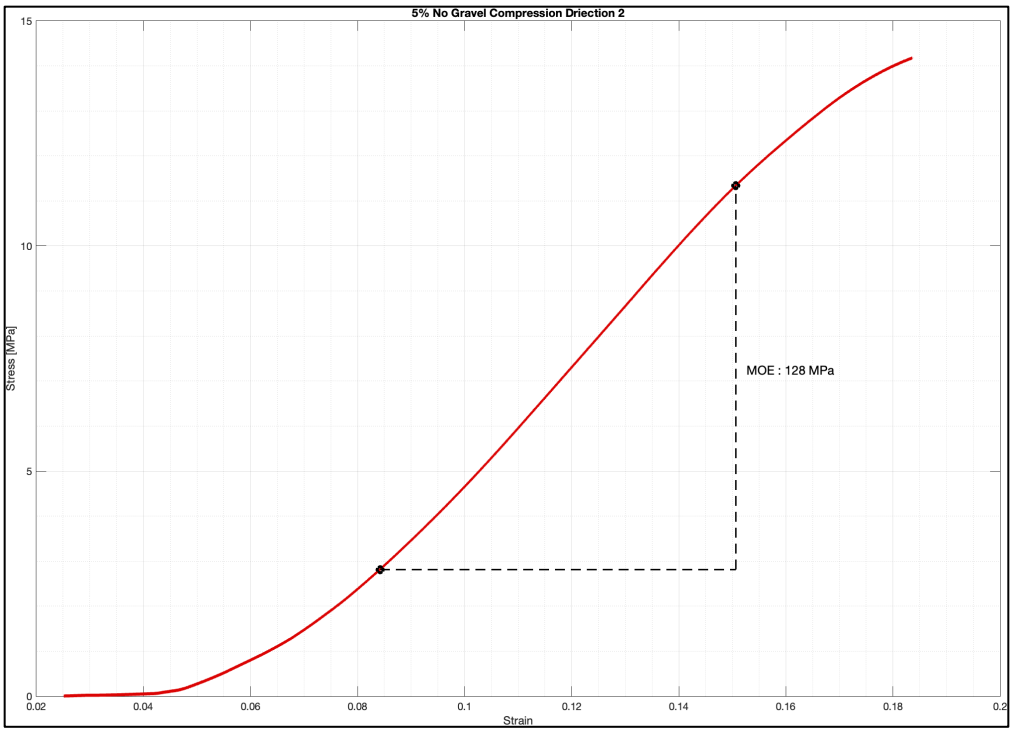
5% No Gravel Compression Driection 2
Stress [MPa]
Strain
MOE : 128 MPa
0
5
10
15
0.02
0.04
0.06
0.08
0.1
0.12
0.14
0.16
0.18
0.2

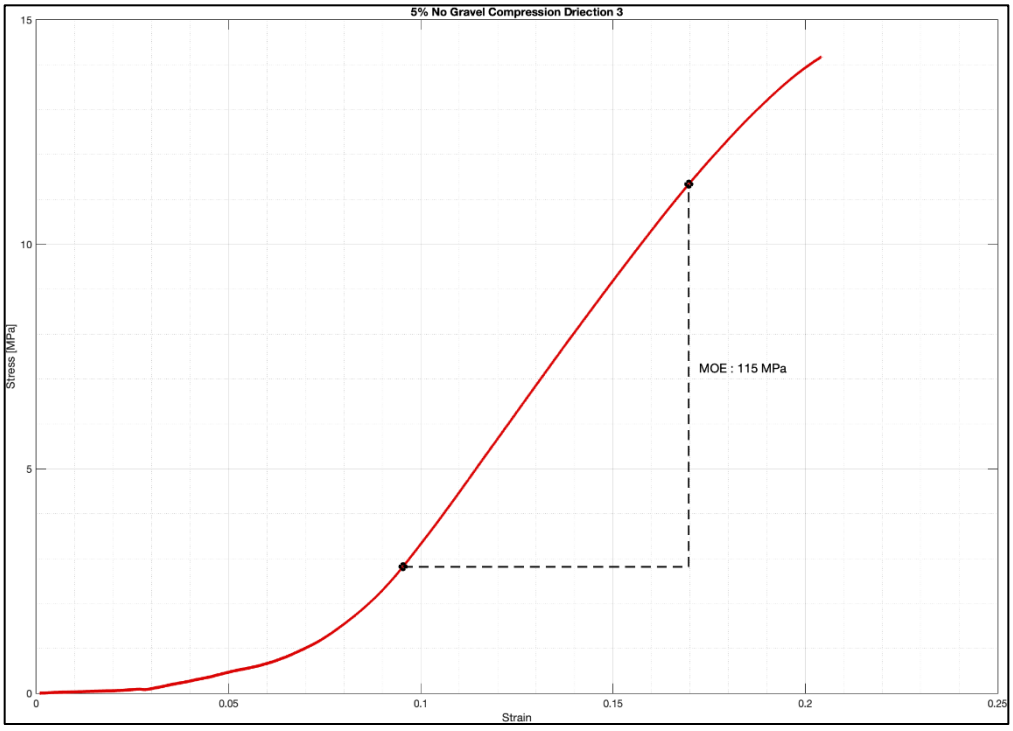
5% No Gravel Compression Driection 3
Stress [MPa]
Strain
MOE : 115 MPa
0
5
10
15
0
0.05
0.1
0.15
0.2
0.25

Boston CSEB 14 Day Stress Strain Plots - Tall Direction

3% Gravel

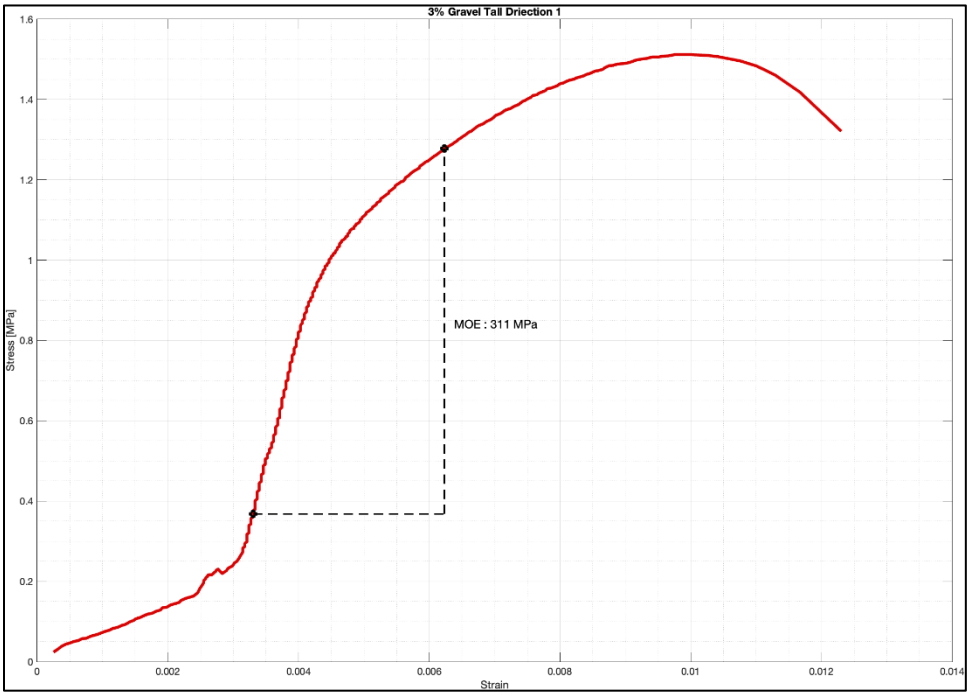

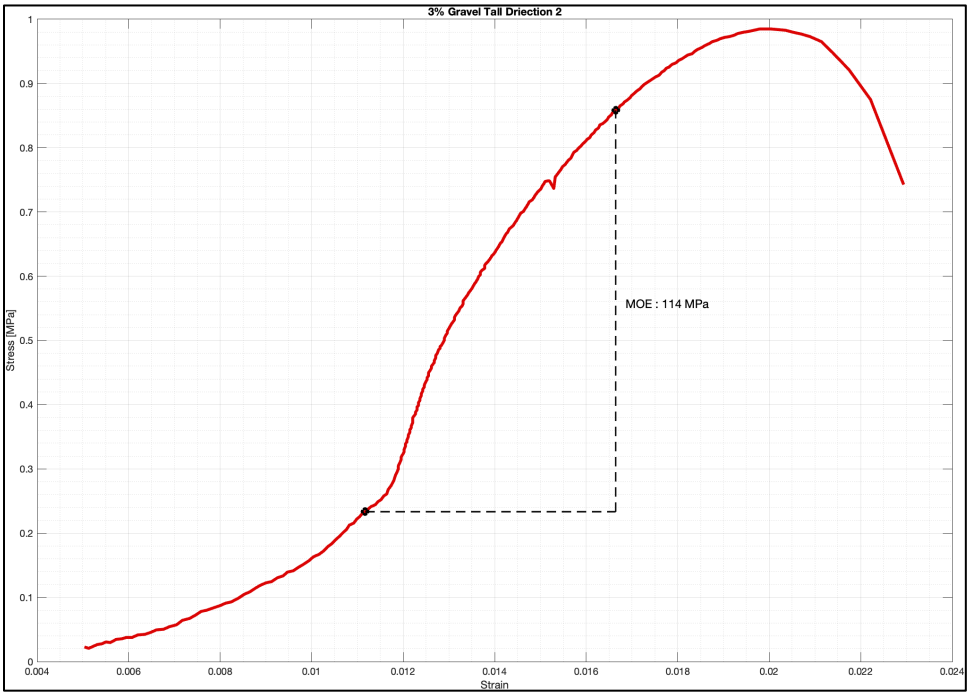

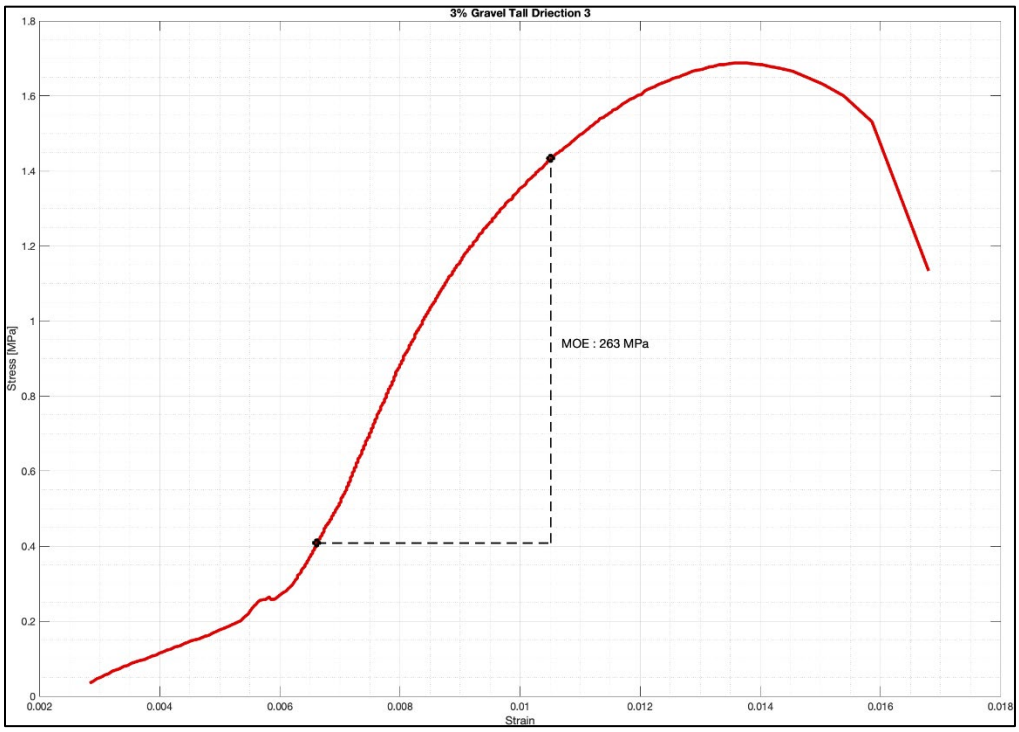
3% Gravel Tall Driection 3
Stress [MPa]
Strain
MOE : 263 MPa
0
0.2
0.4
0.6
0.8
1
1.2
1.4
1.6
1.8
0.002
0.004
0.006
0.008
0.01
0.012
0.014
0.016
0.018

3% No Gravel

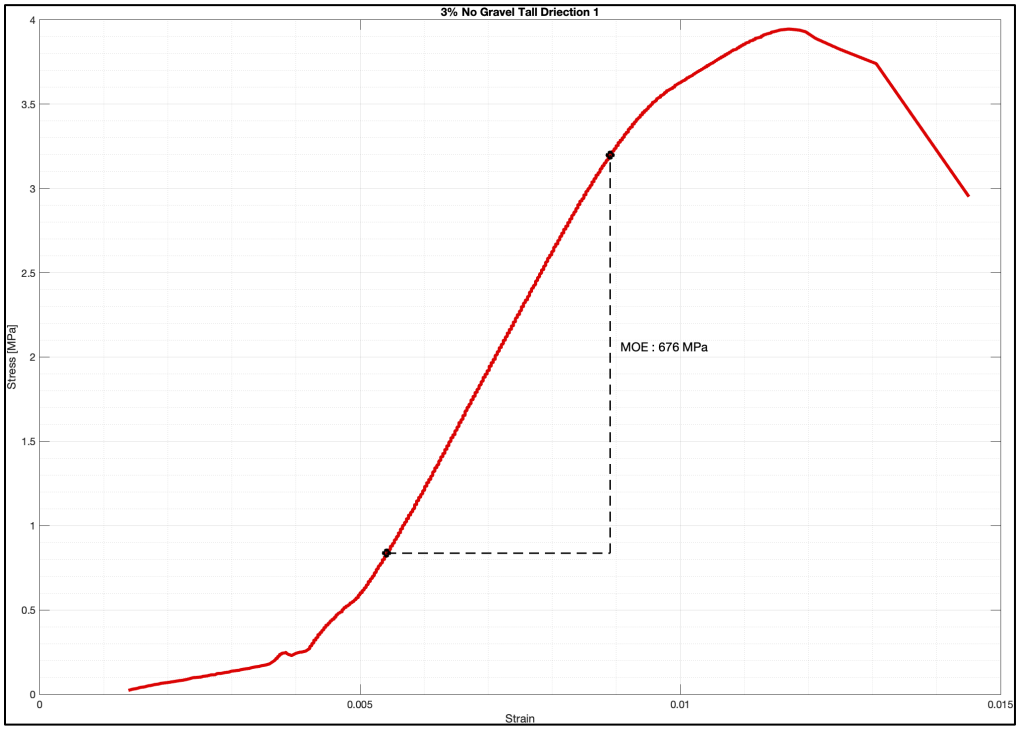
3% No Gravel Tall Driection 1
Stress [MPa]
Strain
MOE : 676 MPa
0
0.5
1
1.5
2
2.5
3
3.5
4
0
0.005
0.01
0.015

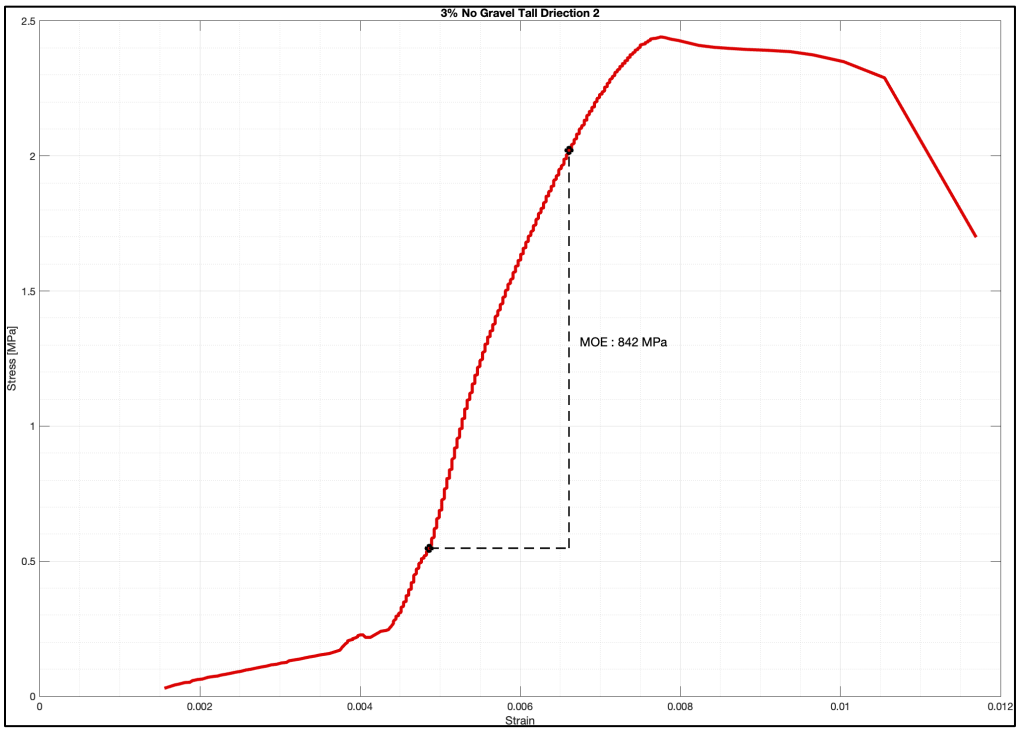
3% No Gravel Tall Driection 2
Stress [MPa]
Strain
MOE : 842 MPa
0
0.5
1
1.5
2
2.5
0.002
0.004
0.006
0.008
0.01
0.012

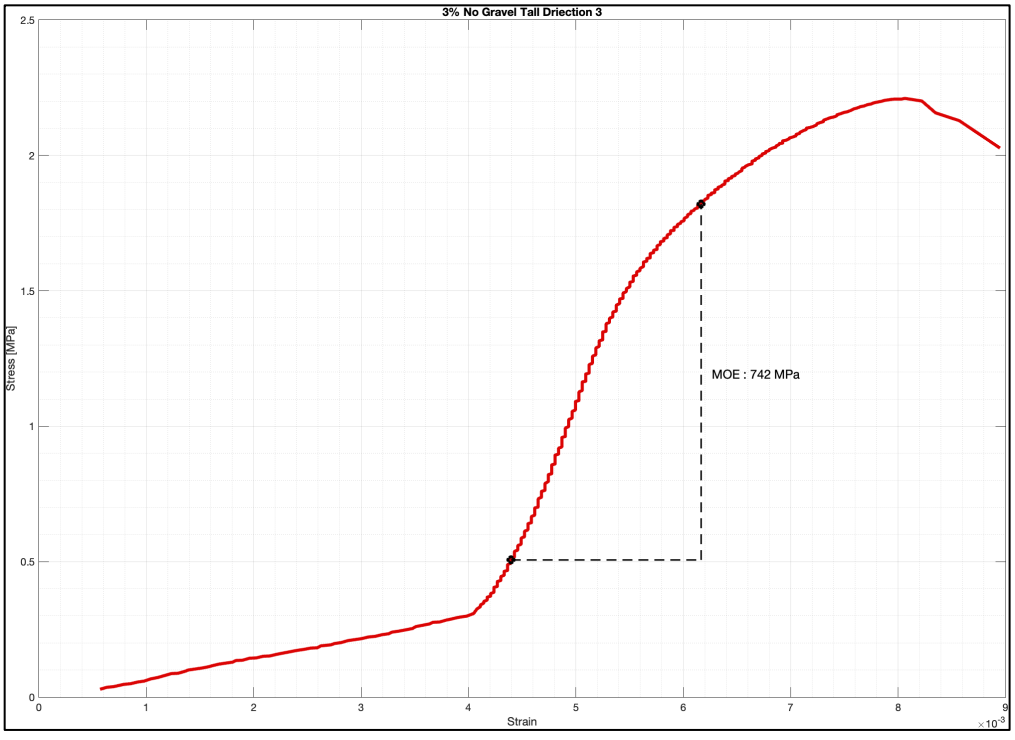
3% No Gravel Tall Driection 3
Stress [MPa]
Strain
MOE : 742 MPa
0
0.5
1
1.5
2
2.5
1
2
3
4
5
6
7
8
9

5% Gravel

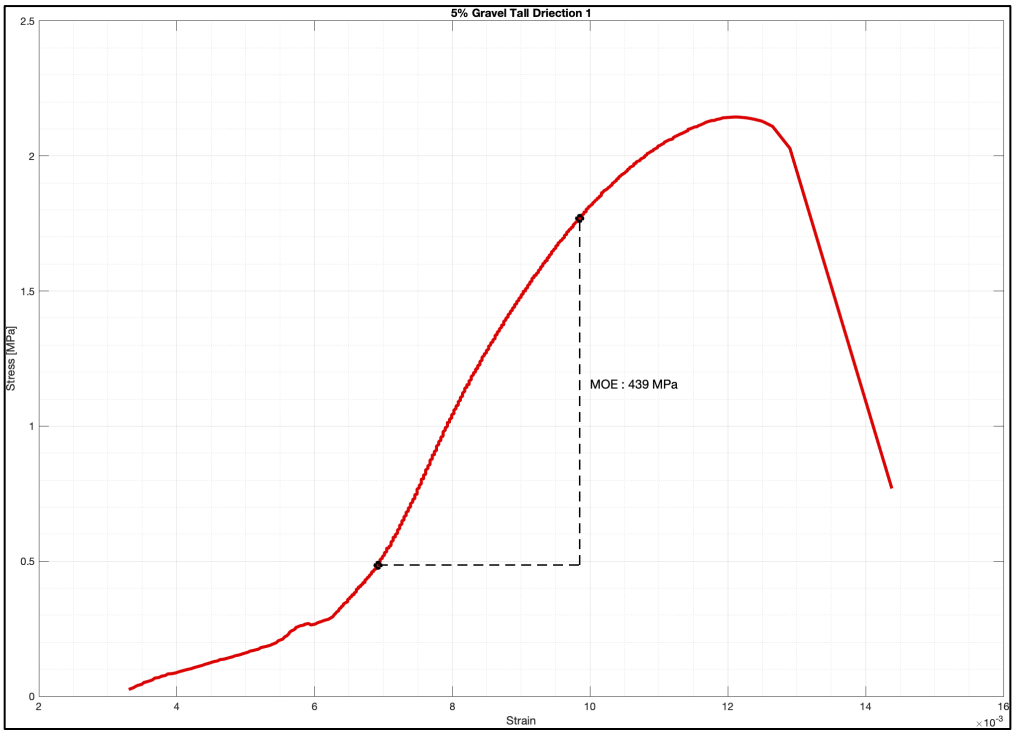
5% Gravel Tall Driection 1
Stress [MPa]
Strain
×10^-3
MOE : 439 MPa
0
0.5
1
1.5
2
2.5
2
4
6
8
10
12
14
16

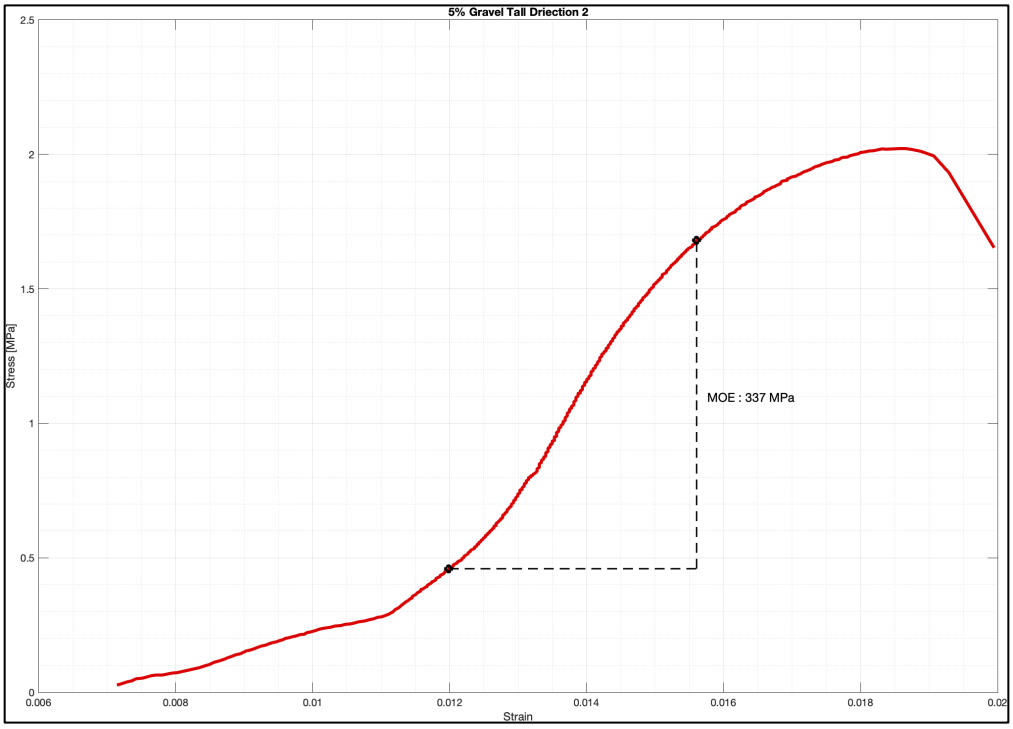
5% Gravel Tall Driection 2
Stress [MPa]
Strain
MOE : 337 MPa
0
0.5
1
1.5
2
2.5
0.006
0.008
0.01
0.012
0.014
0.016
0.018
0.02

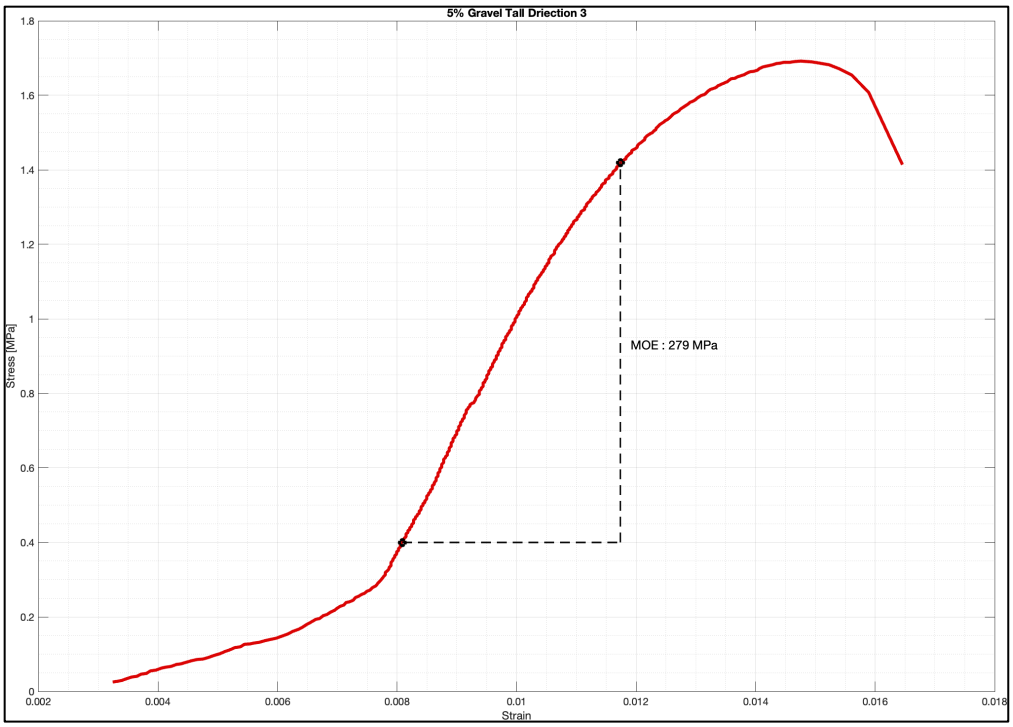
5% Gravel Tall Driection 3
Stress [MPa]
Strain
MOE : 279 MPa
0
0.2
0.4
0.6
0.8
1
1.2
1.4
1.6
1.8
0.002
0.004
0.006
0.008
0.01
0.012
0.014
0.016
0.018

5% No Gravel

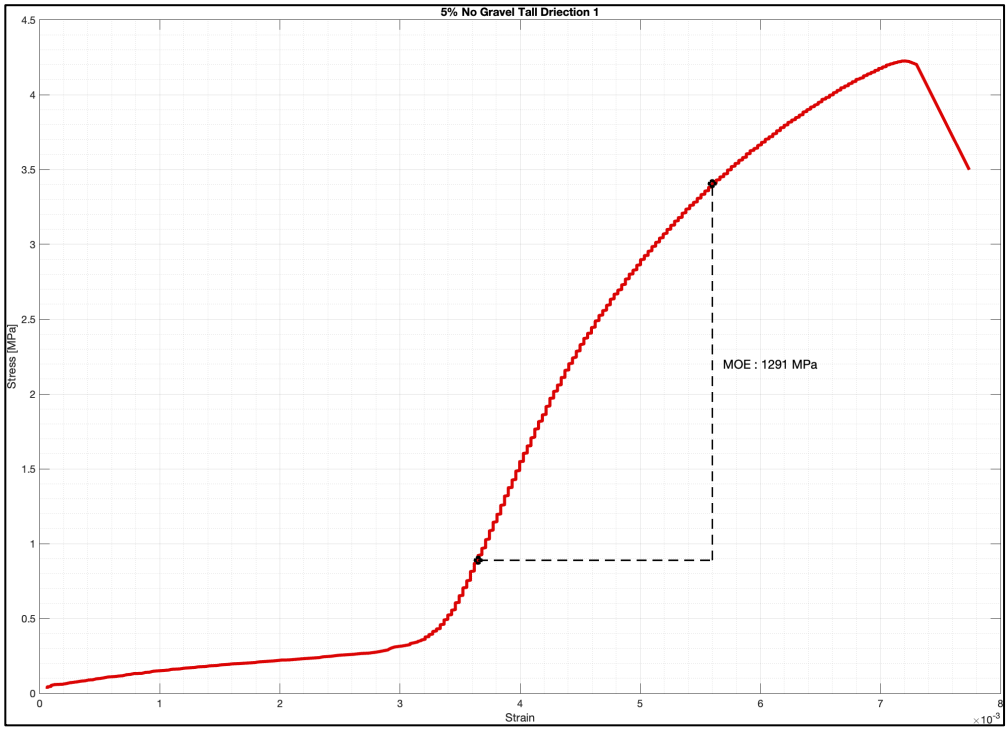
5% No Gravel Tall Driection 1
Stress [MPa]
Strain
MOE : 1291 MPa
0
0.5
1
1.5
2
2.5
3
3.5
4
4.5
0
1
2
3
4
5
6
7
8
×10-3

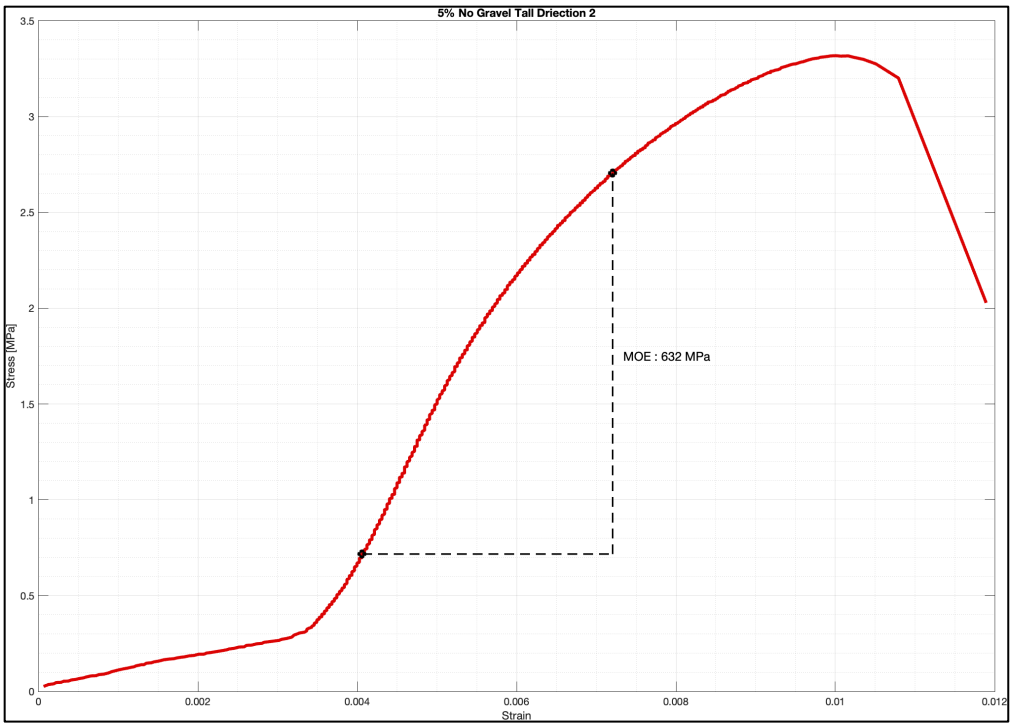
5% No Gravel Tall Driection 2
Stress [MPa]
Strain
MOE : 632 MPa
0
0.5
1
1.5
2
2.5
3
3.5
0.002
0.004
0.006
0.008
0.01
0.012

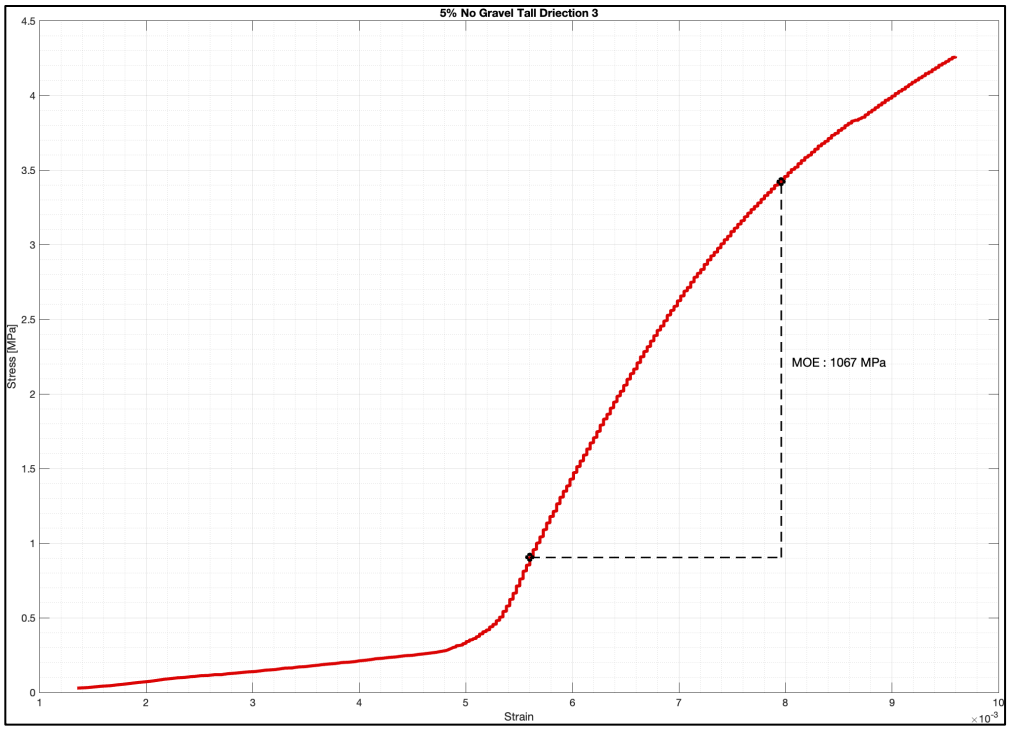
5% No Gravel Tall Driection 3
Stress [MPa]
Strain
MOE : 1067 MPa
0
0.5
1
1.5
2
2.5
3
3.5
4
4.5
1
2
3
4
5
6
7
8
9
10
×10-3

Boston 3NG CSEB 50 Day Stress Strain Plots

Dry Bricks

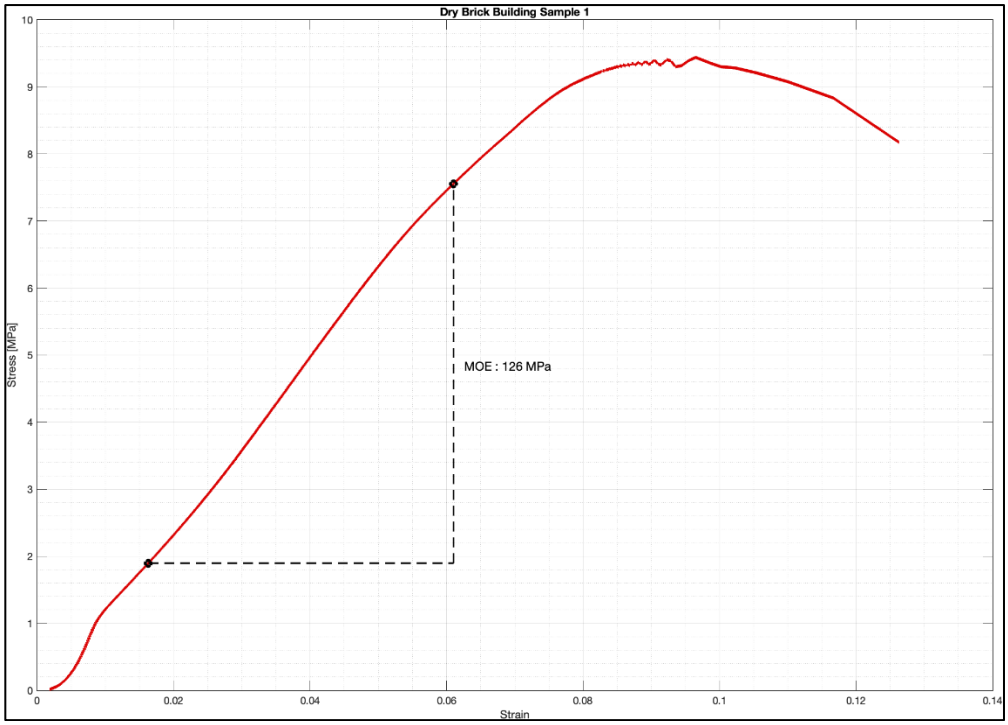

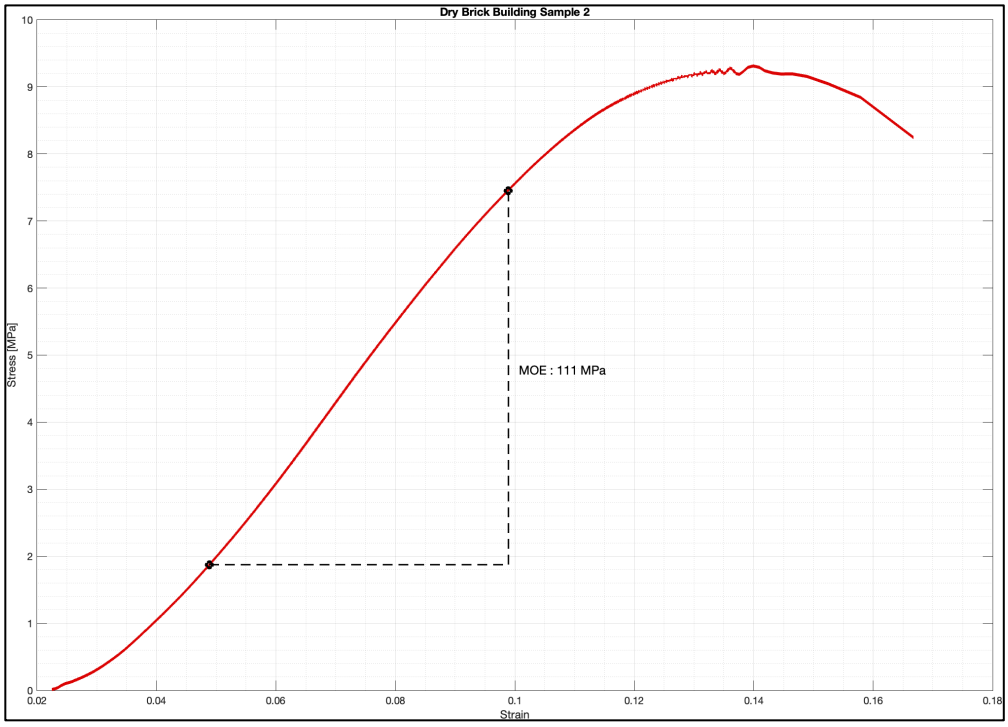

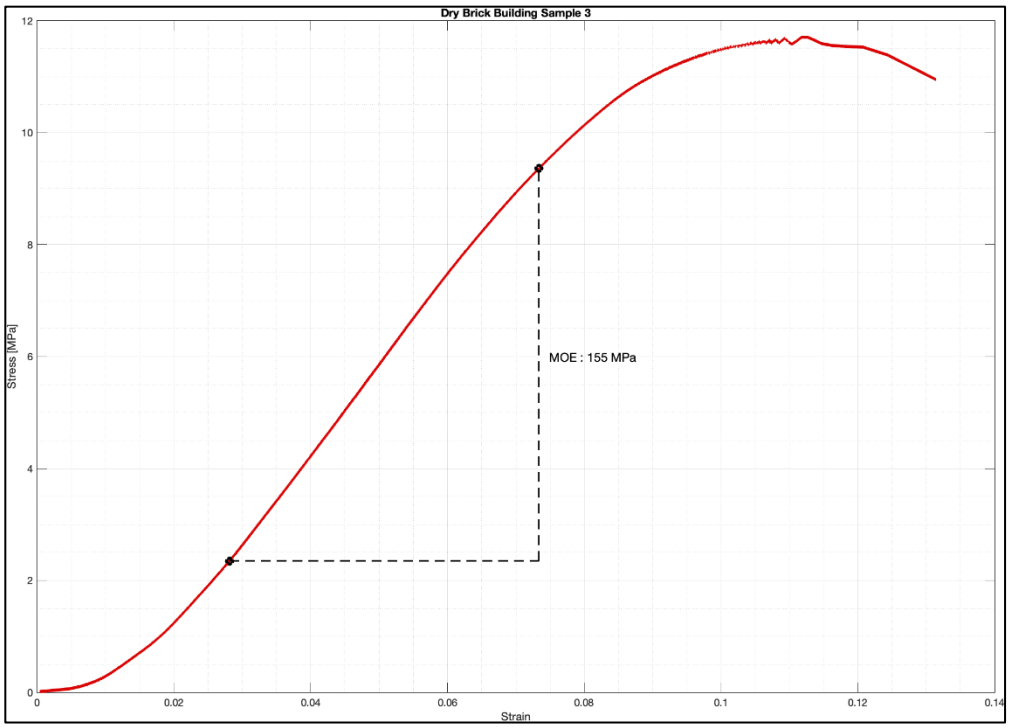
Dry Brick Building Sample 3
Stress [MPa]
Strain
MOE : 155 MPa
0
2
4
6
8
10
12
0
0.02
0.04
0.06
0.08
0.1
0.12
0.14

Wet Bricks

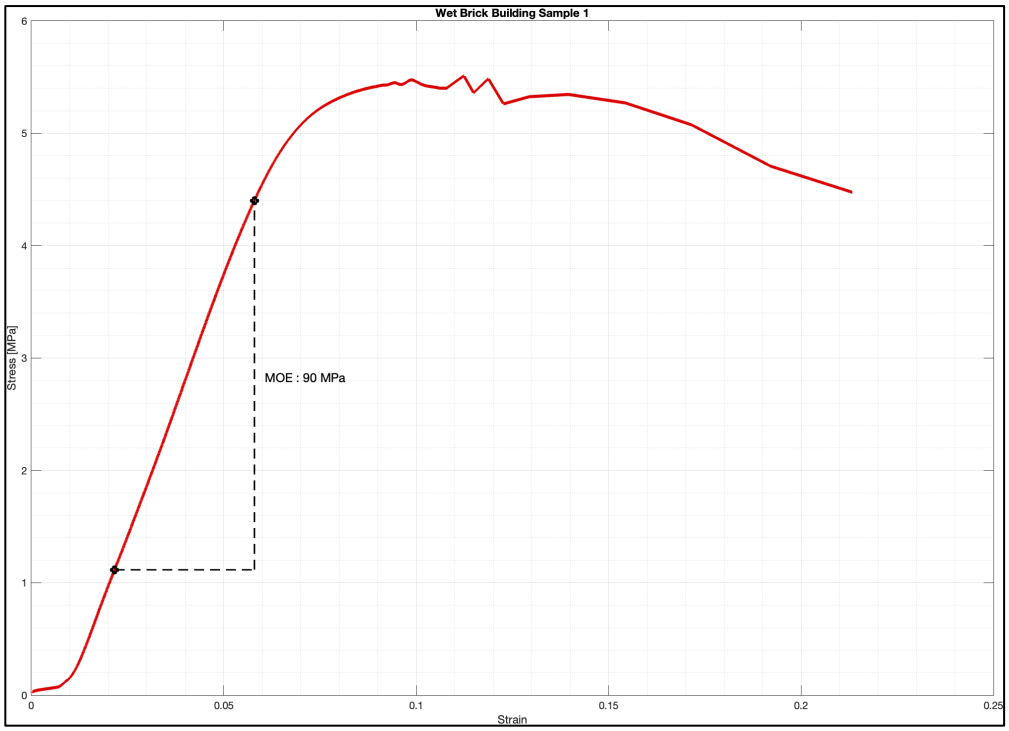
Wet Brick Building Sample 1
Stress [MPa]
Strain
MOE : 90 MPa
0
1
2
3
4
5
6
0
0.05
0.1
0.15
0.2
0.25

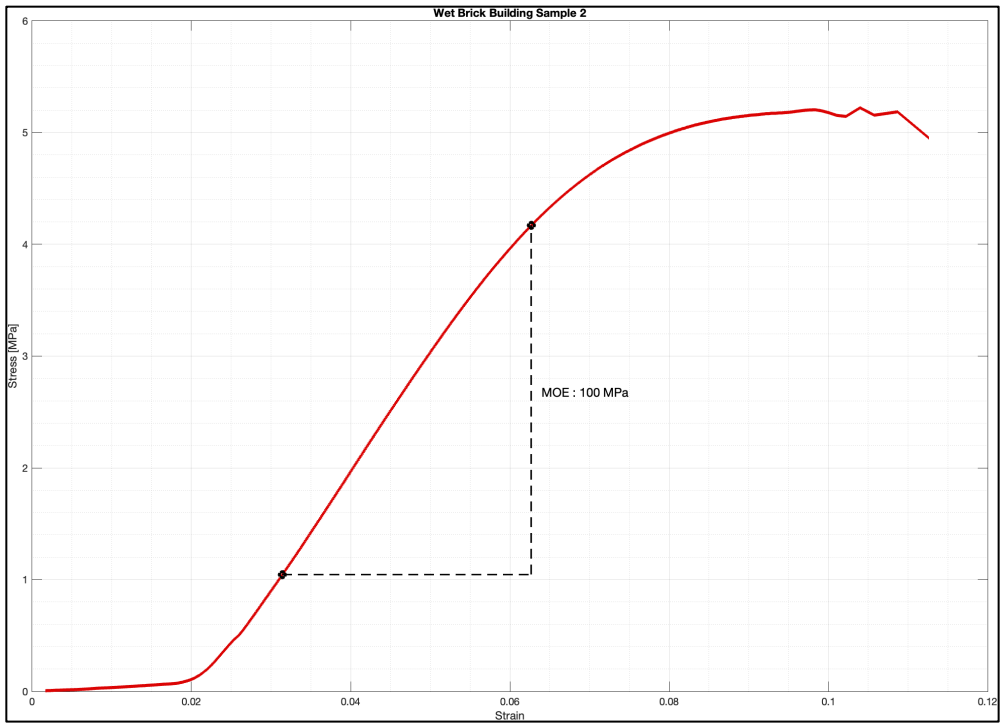
Wet Brick Building Sample 2
Stress [MPa]
Strain
MOE : 100 MPa
0
1
2
3
4
5
6
0
0.02
0.04
0.06
0.08
0.1
0.12

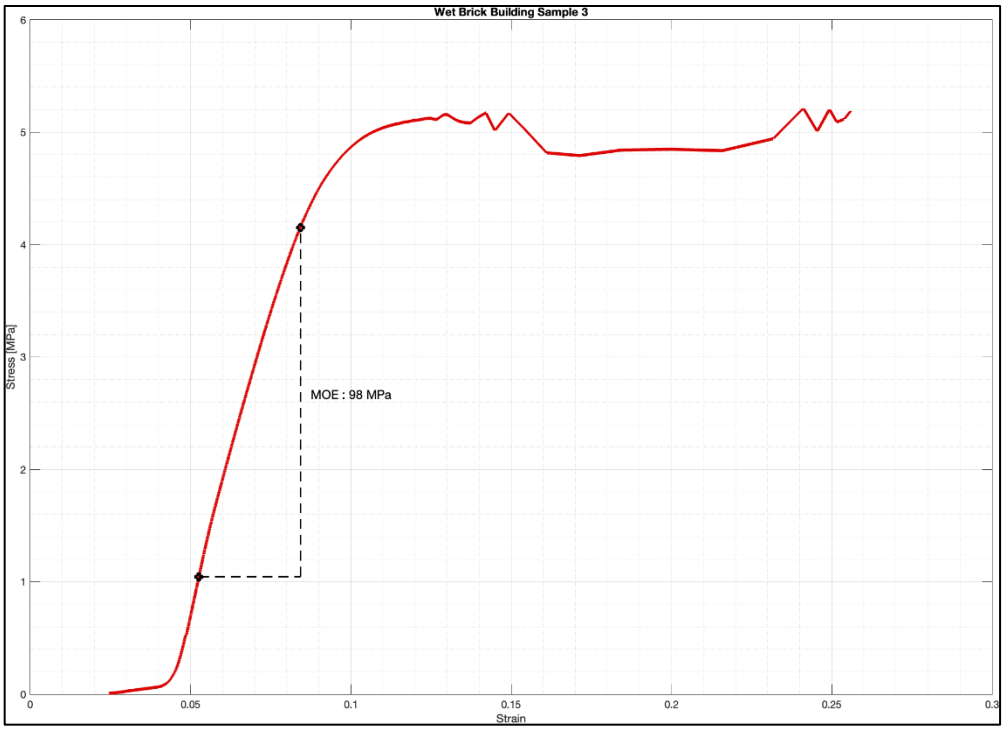
Wet Brick Building Sample 3
Stress [MPa]
Strain
MOE : 98 MPa
0
1
2
3
4
5
6
0
0.05
0.1
0.15
0.2
0.25
0.3

Boston 3NG CSEB 8 Month Stress Strain Plots

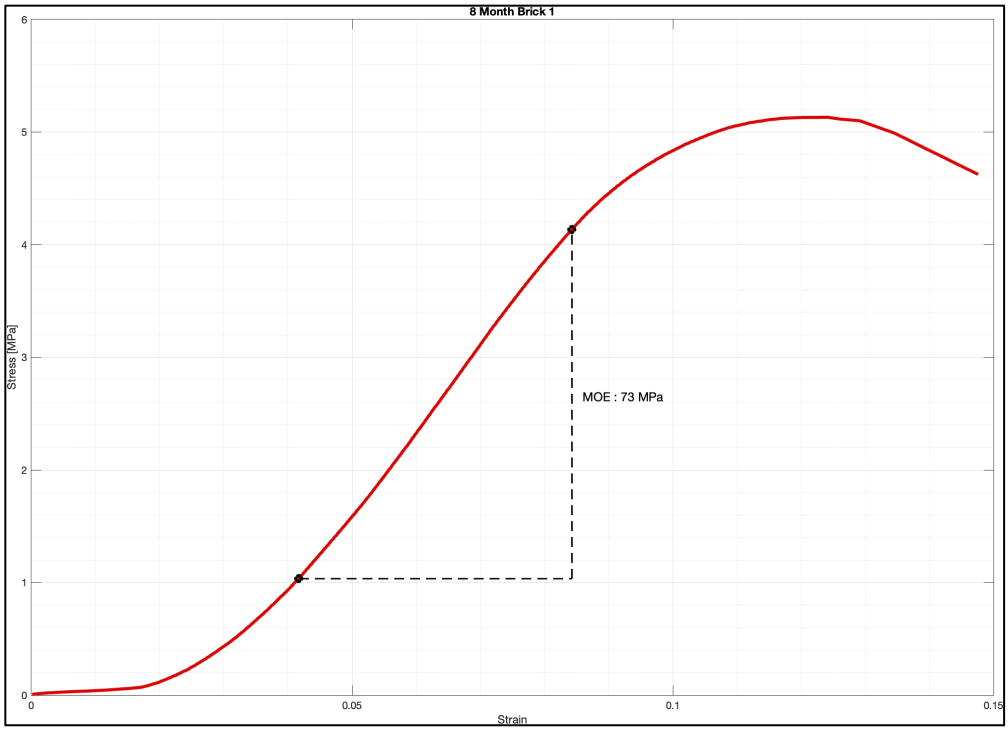

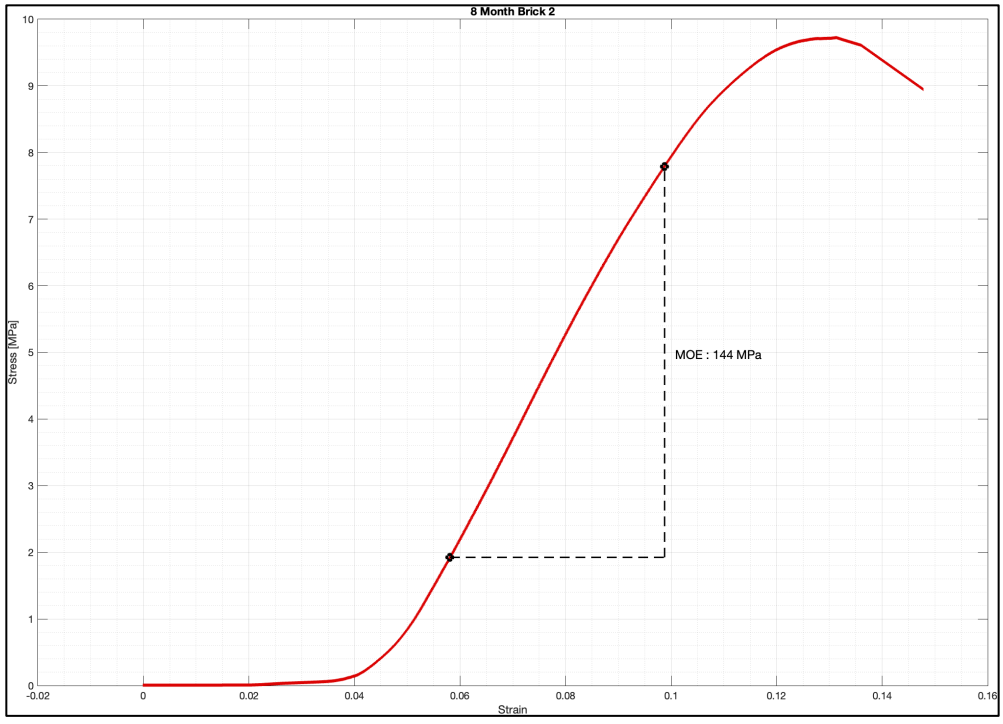

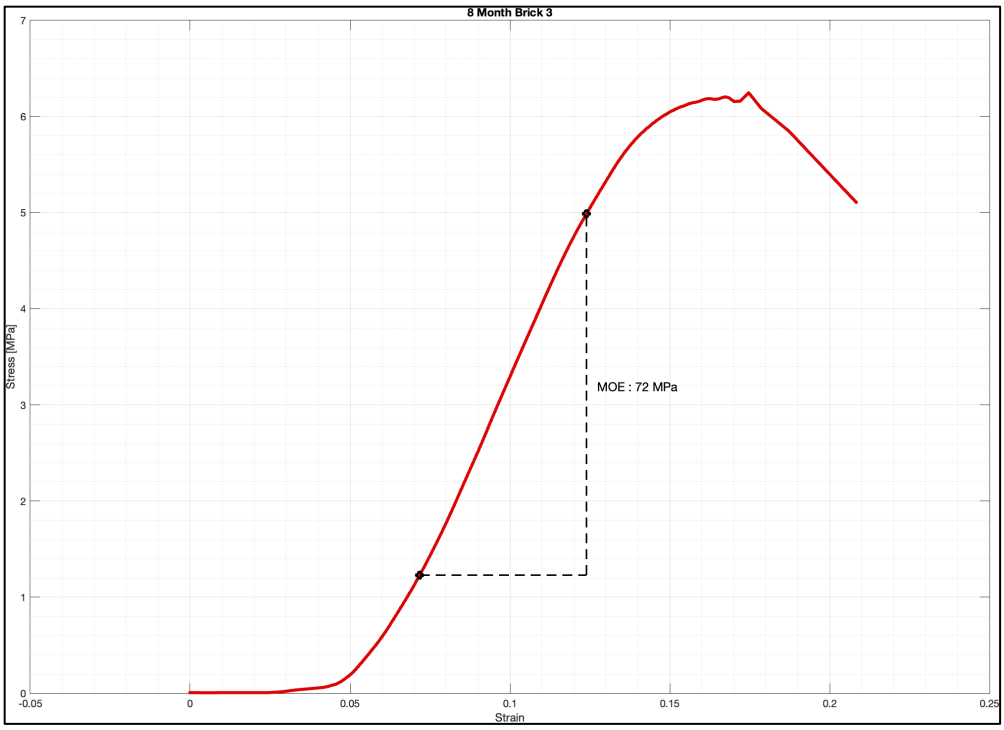

Boston CSEB Prisms Stress Strain Plots - Compression Direction

Cement Mortar

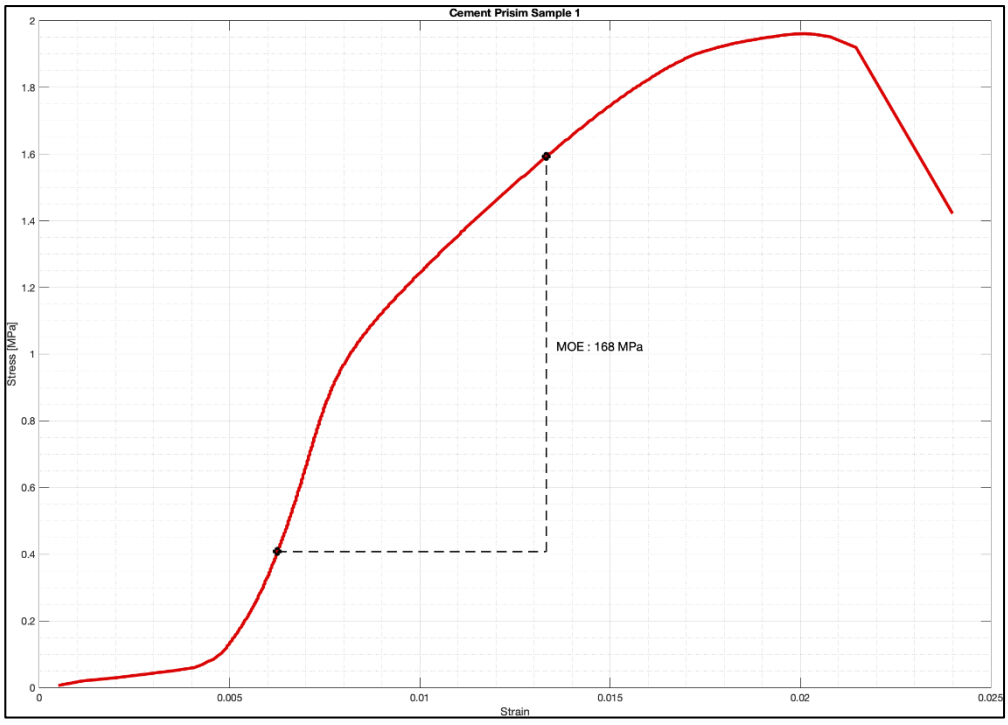

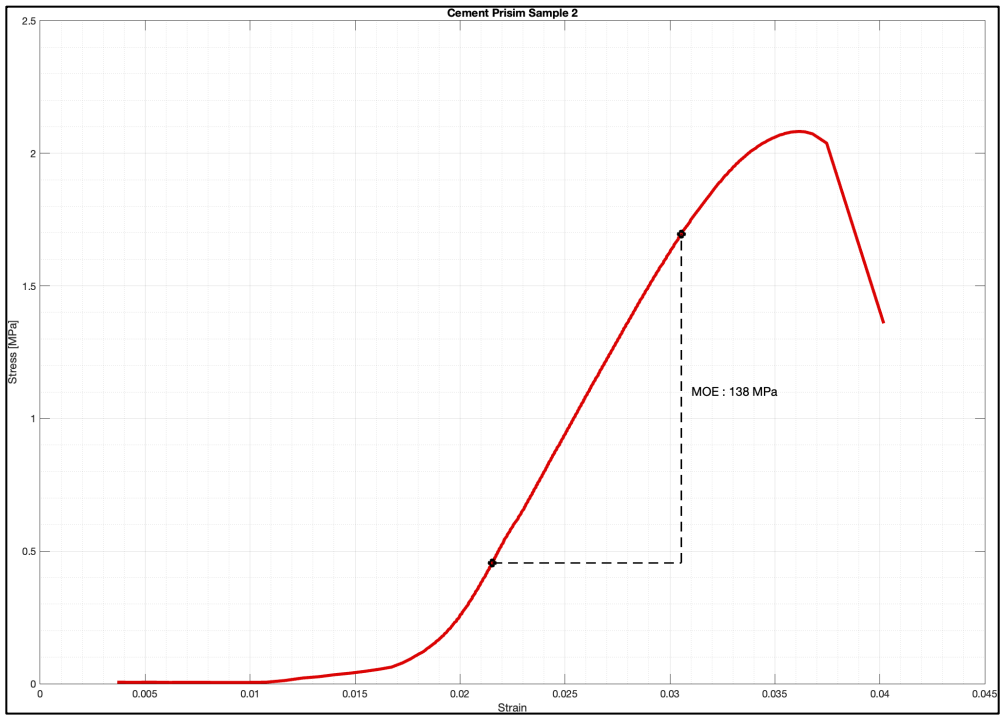
Cement Prisim Sample 2
Stress [MPa]
Strain
MOE : 138 MPa
0
0.5
1
1.5
2
2.5
0.005
0.01
0.015
0.02
0.025
0.03
0.035
0.04
0.045

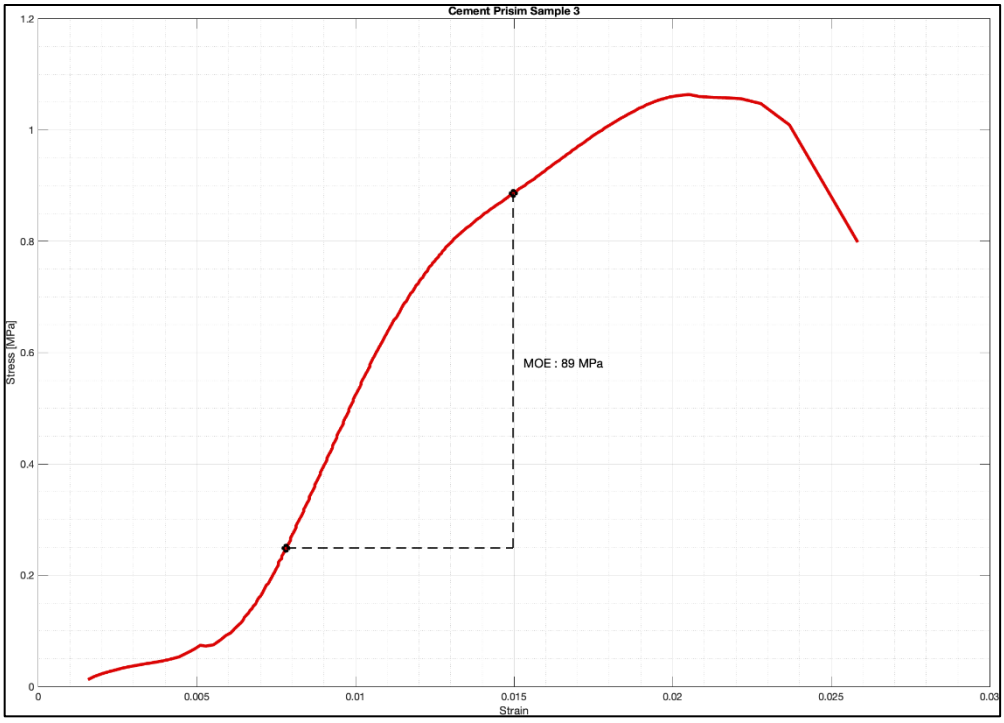
Cement Prisim Sample 3
Stress [MPa]
Strain
MOE : 89 MPa
0
0.2
0.4
0.6
0.8
1
1.2
0.005
0.01
0.015
0.02
0.025
0.03

Mud Mortar

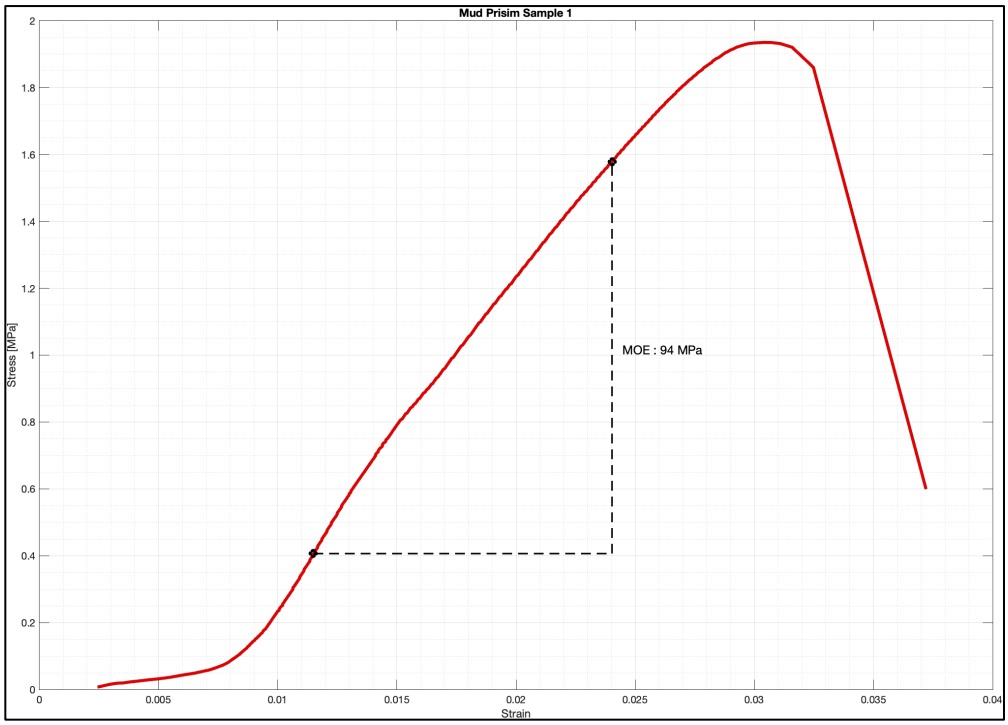
Mud Prisim Sample 1
Stress [MPa]
Strain
MOE : 94 MPa
0
0.2
0.4
0.6
0.8
1
1.2
1.4
1.6
1.8
2
0.005
0.01
0.015
0.02
0.025
0.03
0.035
0.04

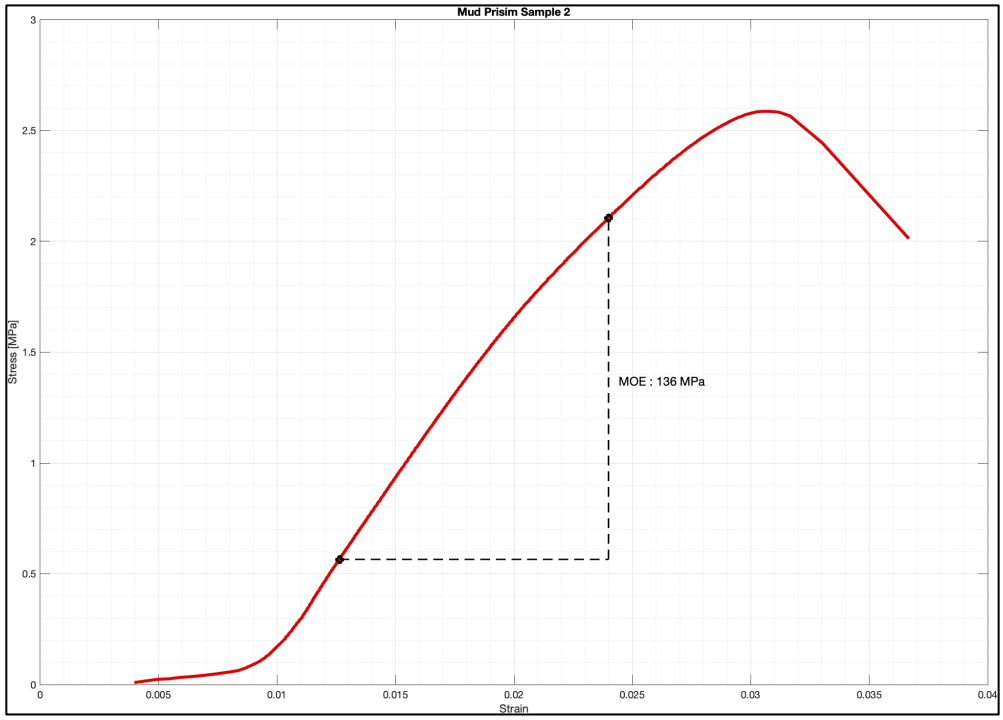
Mud Prisim Sample 2
Stress [MPa]
Strain
MOE : 136 MPa
0
0.5
1
1.5
2
2.5
3
0.005
0.01
0.015
0.02
0.025
0.03
0.035
0.04

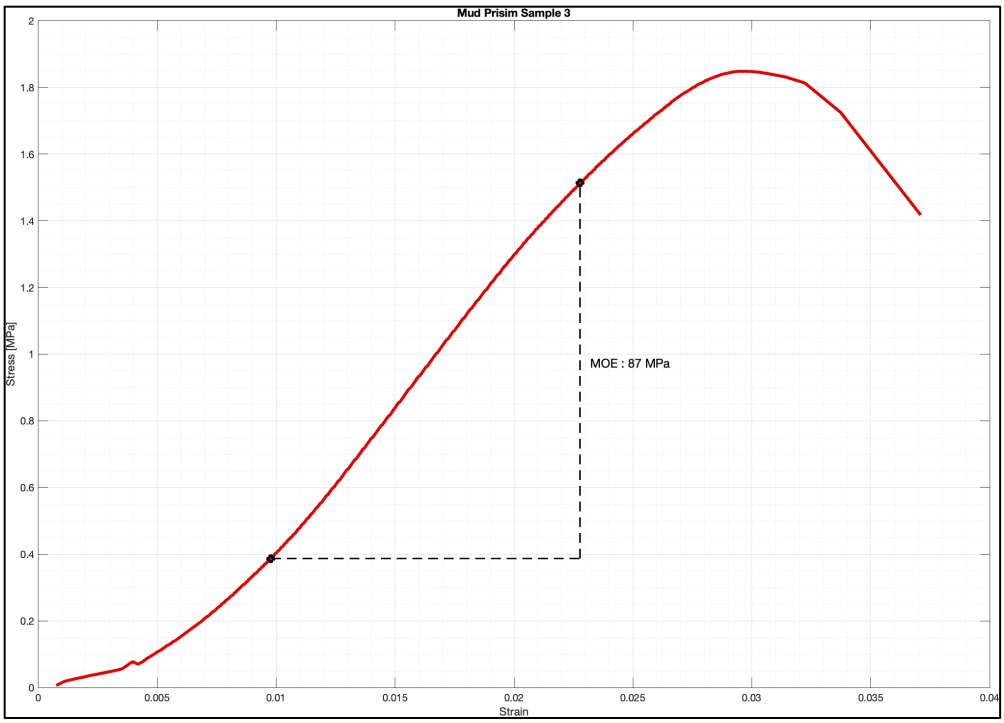
Mud Prisim Sample 3
Stress [MPa]
Strain
MOE : 87 MPa
0
0.2
0.4
0.6
0.8
1
1.2
1.4
1.6
1.8
2
0.005
0.01
0.015
0.02
0.025
0.03
0.035
0.04

Ethiopian Soil Sieve Analysis

East Addis Soil Sample

Sieve Analysis

Sieve (mm)	% PASSED
37.500	100.0
25.000	100.0
19.000	100.0
12.500	100.0
9.500	100.0
4.750	99.8
2.000	99.8
0.425	92.7
0.075	82.7

Hydrometer Analysis

Smaller than (mm)	Percent
0.020	23.2
0.002	14.0
0.001	13.8

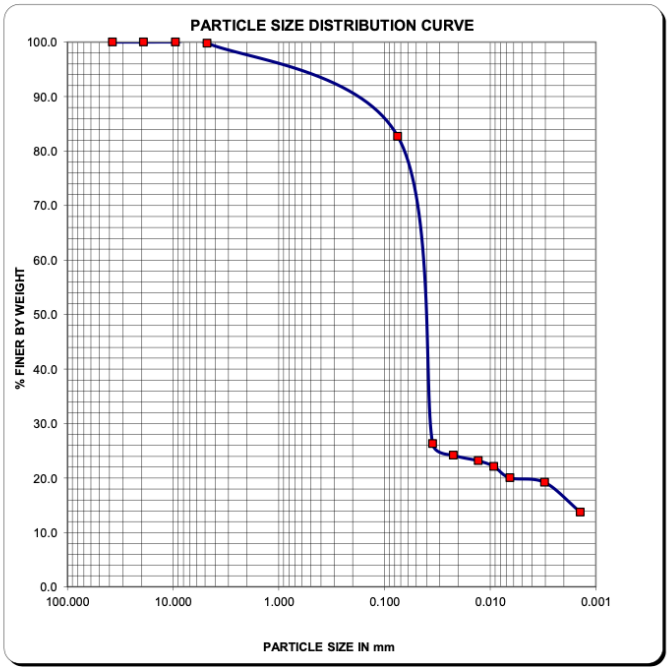

SIZE PROPORTIONS

Particle larger than 2.00 mm, %	0.2
Sand (2.00mm-0.075mm), %	**17.1**
Silt (0.075mm-0.002mm), %	**68.7**
Clay (less than 0.002), %	**14.0**

Sieve Analysis

Sieve (mm)	% PASSED
37.500	100.0
25.000	100.0
19.000	100.0
12.500	100.0
9.500	100.0
4.750	99.8
2.000	99.8
0.425	92.7
0.075	82.7

Hydrometer Analysis

Smaller than (mm)	Percent
0.020	25.3
0.002	18.0
0.001	13.8

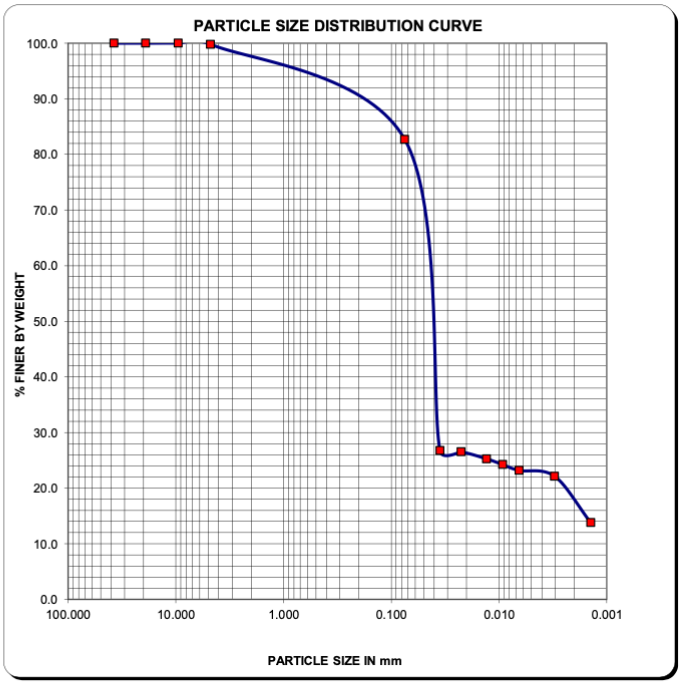

SIZE PROPORTIONS

Particle larger than 2.00 mm, % 0.2

Sand (2.00mm-0.075mm), % **17.1**

Silt (0.075mm-0.002mm), % **64.7**

Clay (less than 0.002), % **18.0**

North Addis Soil Sample

Sieve Analysis

Sieve (mm)	% PASSED
37.500	100.0
25.000	100.0
19.000	100.0
12.500	100.0
9.500	100.0
4.750	100.0
2.000	100.0
0.425	90.2
0.075	79.6

Hydrometer Analysis

Smaller than (mm)	Percent
0.020	17.8
0.002	19.7
0.001	10.5

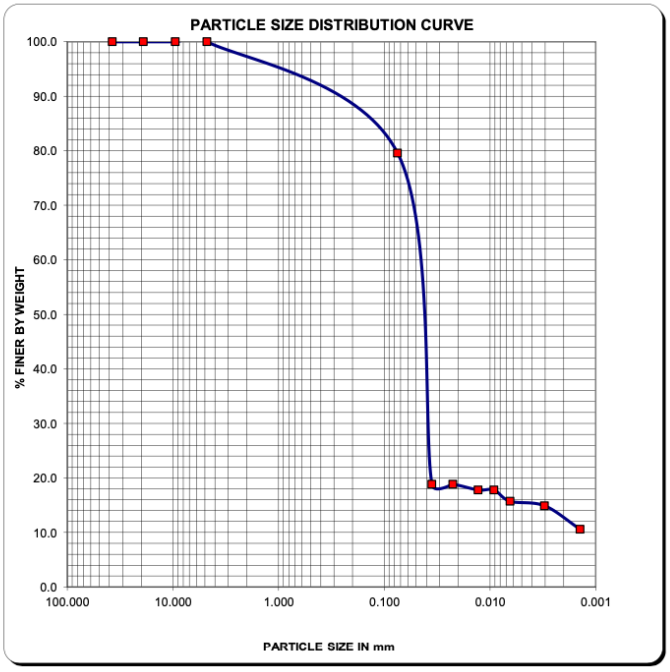

SIZE PROPORTIONS

Particle larger than 2.00 mm, % 0.0

Sand (2.00mm-0.075mm), % **20.4**

Silt (0.075mm-0.002mm), % **59.9**

Clay (less than 0.002), % **19.7**

Sieve Analysis

Sieve (mm)	% PASSED
37.500	100.0
25.000	100.0
19.000	100.0
12.500	100.0
9.500	100.0
4.750	100.0
2.000	100.0
0.425	90.2
0.075	79.6

Hydrometer Analysis

Smaller than (mm)	Percent
0.020	17.8
0.002	19.1
0.001	10.5

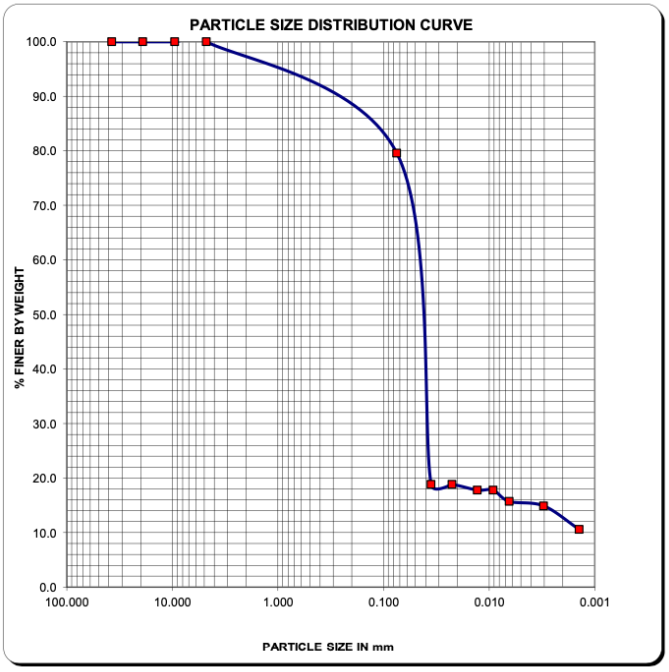

SIZE PROPORTIONS

Particle larger than 2.00 mm, % 0.0

Sand (2.00mm-0.075mm), % **21.2**

Silt (0.075mm-0.002mm), % **59.7**

Clay (less than 0.002), % **19.1**

Appendix B – Prototype Structural Analysis

2D Equilibrium Analysis of Prototype

Symmetrical Building Code Live Load

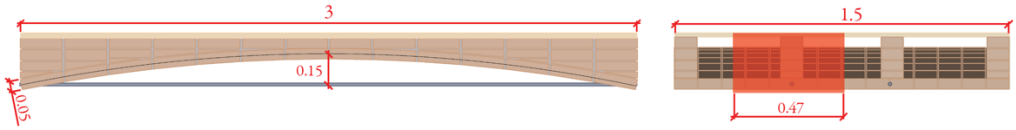

Live Load

Surface Load = 2 kN /m²

Tributary Width = 0.47 m

q_{Live} = 0.94 kN /m

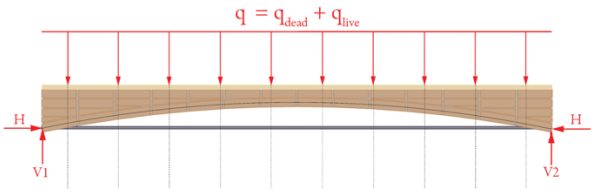

Dead Load

Primary Vault Volume = 0.227 m³

Tributary Vault Volume = 0.071 m³

Single Stiffening Wall Volume = 0.03 m³

CSEB Desnity = 2000 kg/m³

CSEB Dead Load = 1.98 kN

Plywood Volume = 0.09 m³

Tributary Plywood Volume = 0.028 m³

Plywood Desnity = 700 kg/m³

Plywood Dead Load = 0.19 kN

Total Tributary Dead Load = 2.17 kN

q_{Dead} = 0.72 kN /m

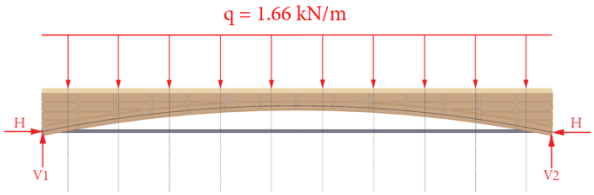

V1 = V2 = 2.5 kN

$= qL/2$

$= (1.66\ kN/m)(3m)/2$

H = 12.5 kN

$= qL^2/8y$

$= (1.66\ kN/m)(3m)^2/(8)(0.15m)$

Resultant = 12.7 kN

$= (V1^2 + H^2)^{1/2}$

$= (2.5^2 + 12.5^2)^{1/2}$

Max Stress = 0.54 MPa

= Resultant / Tributary Area

= (12.7 kN)/(0.47m*0.05m)/1000

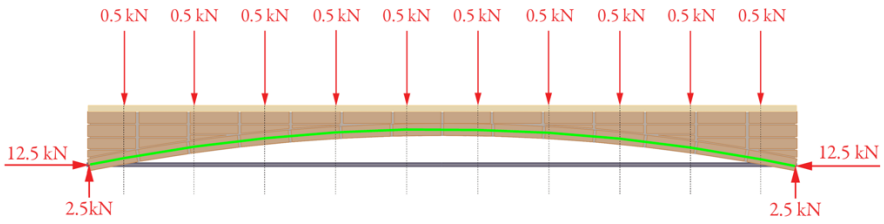

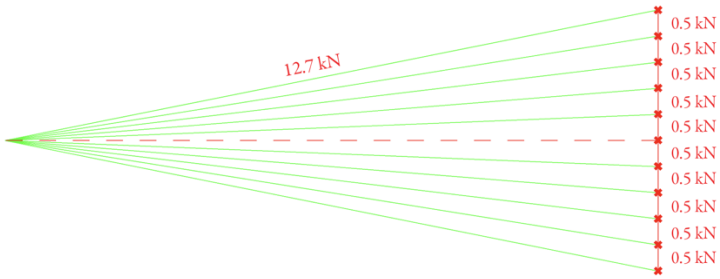

Asymmetrical Building Code Live Load

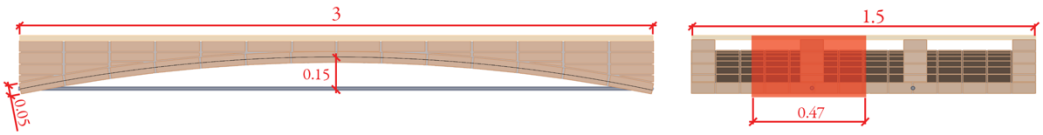

Live Load

Surface Load = 2 kN /m^2

Tributary Width = 0.47 m

q_{Live} = 0.94 kN /m

Dead Load

Primary Vault Volume = 0.227 m^3

Tributary Vault Volume = 0.071 m^3

Single Stiffening Wall Volume = 0.03 m^3

CSEB Desnity = 2000 kg/m^3

CSEB Dead Load = 1.98 kN

Plywood Volume = 0.09 m^3

Tributary Plywood Volume = 0.028 m^3

Plywood Desnity = 700 kg/m^3

Plywood Dead Load = 0.19 kN

Total Tributary Dead Load = 2.17 kN

q_{Dead} = 0.72 kN /m

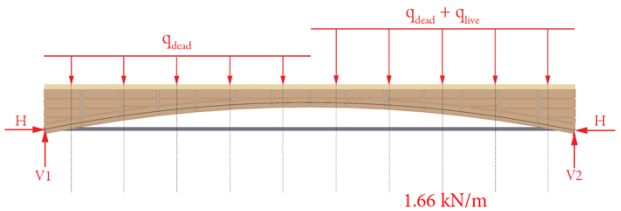

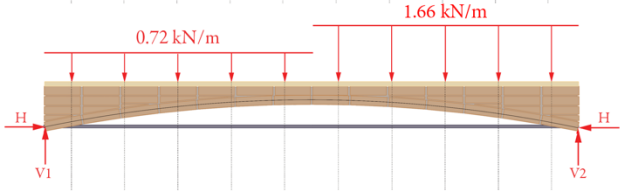

V1 = 1.44 kN

$= (q_{dead}L/2) + (q_{Live}L/8)$

$= (0.72\ kN/m * 3m/2) + (0.94\ kN/m * 3m/8)$

V2 = 2.41 kN

$= (q_{dead}L/2) + (3q_{Live}L/8)$

$= (0.72\ kN/m * 3m/2) + (3*0.94\ kN/m * 3m/8)$

H = 8.94 kN

$= (L^2/16y)[2q_{Dead} + q_{Live}]$

$= [(3m)^2/(16)(0.15m)][4.04\ kN/m]$

Resultant = 9.2 kN

$= (V1^2 + H^2)^{1/2}$

$= (2.41^2 + 8.94^2)^{1/2}$

Max Stress = 0.39 MPa

= Resultant / Tributary Area

= (9.2 kN)/(0.47m*0.05m)/1000

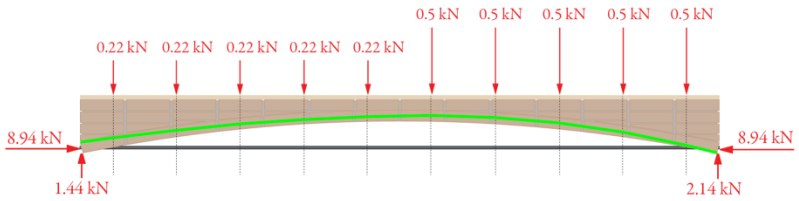

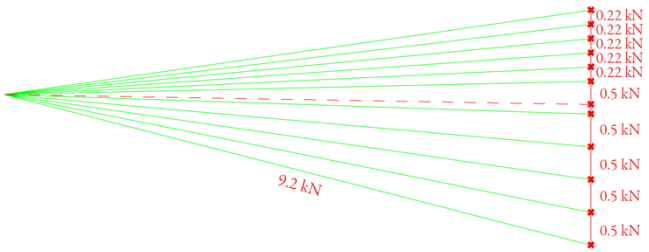

Symmetrical Double Building Code Live Load

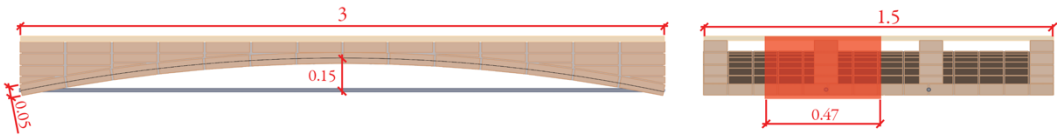

Live Load

Surface Load = 4 kN /m^2

Tributary Width = 0.47 m

q_{Live} = 1.88 kN /m

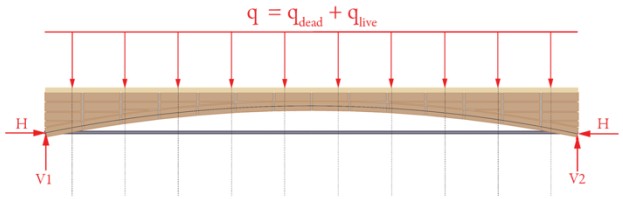

Dead Load

Primary Vault Volume = 0.227 m^3

Tributary Vault Volume = 0.071 m^3

Single Stiffening Wall Volume = 0.03 m^3

CSEB Desnity = 2000 kg/m^3

CSEB Dead Load = 1.98 kN

Plywood Volume = 0.09 m^3

Tributary Plywood Volume = 0.028 m^3

Plywood Desnity = 700 kg/m^3

Plywood Dead Load = 0.19 kN

Total Tributary Dead Load = 2.17 kN

q_{Dead} = 0.72 kN /m

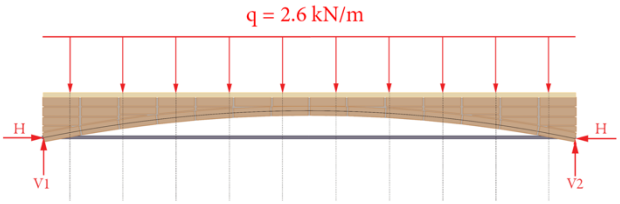

V1 = V2 = 3.9 kN

= qL/2

= (2.6 kN/m)(3m)/2

H = 19.5 kN

= $qL^2/8y$

= (2.6 kN/m)(3m)^2/(8)(0.15m)

Resultant = 19.9 kN

= $(V1^2 + H^2)^{1/2}$

= $(3.9^2 + 19.5^2)^{1/2}$

Max Stress = 0.85 MPa

= Resultant / Tributary Area

= (19.9 kN)/(0.47m*0.05m)/1000

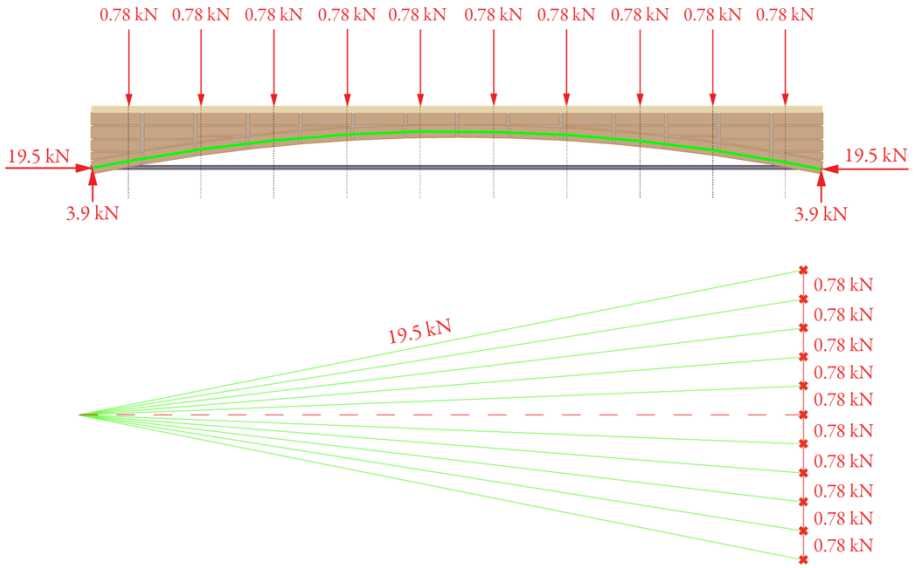

Asymmetrical Double Building Code Live Load

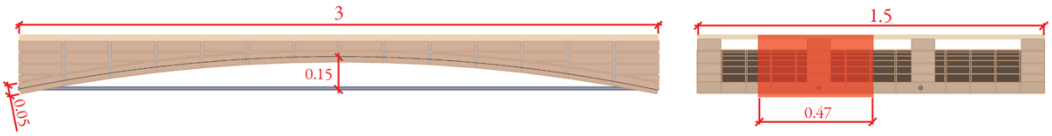

Live Load

Surface Load = 4 kN /m^2

Tributary Width = 0.47 m

q_{Live} = 1.88 kN /m

Dead Load

Primary Vault Volume = 0.227 m^3

Tributary Vault Volume = 0.071 m^3

Single Stiffening Wall Volume = 0.03 m^3

CSEB Desnity = 2000 kg/m^3

CSEB Dead Load = 1.98 kN

Plywood Volume = 0.09 m^3

Tributary Plywood Volume = 0.028 m^3

Plywood Desnity = 700 kg/m^3

Plywood Dead Load = 0.19 kN

Total Tributary Dead Load = 2.17 kN

q_{Dead} = 0.72 kN /m

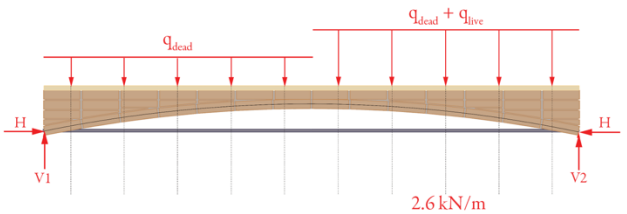

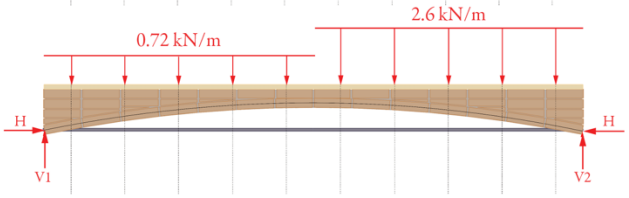

V1 = 1.8 kN

= (q_{dead}L/2) + (q_{Live}L/8)

= (0.72 kN/m * 3m /2) + (1.88 kN/m * 3m /8)

V2 = 3.2 kN

= (q_{dead}L/2) + (3q_{Live}L/8)

= (0.72 kN/m * 3m /2) + (3*1.88 kN/m * 3m /8)

H = 12.5 kN

= (L^2/16y)[2q_{Dead} + q_{Live}]

= [(3m)^2/(16)(0.15m)][4.04 kN/m]

Resultant = 12.9 kN

= ($V1^2$+ H^2)$^{1/2}$

= (3.2^2+ 12.5^2)$^{1/2}$

Max Stress = 0.55 MPa

= Resultant / Tributary Area

= (12.9 kN)/(0.47m*0.05m)/1000

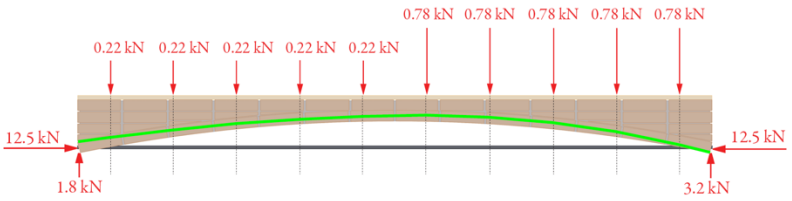

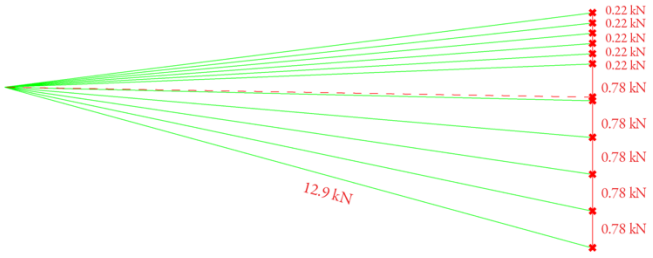

Sizing Steel Ties

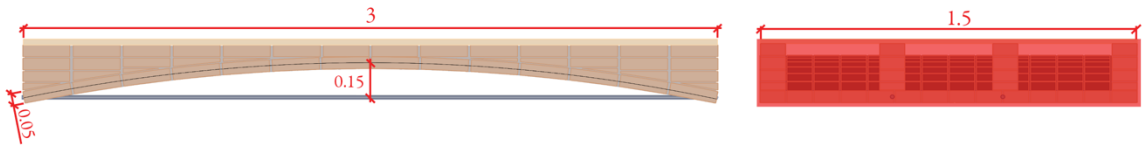

Live Load

Surface Load = 4 kN /m^2

Tributary Width = 1.5 m

q_{Live} = 6 kN /m

Dead Load

Primary Vault Volume = 0.227 m^3

Single Stiffening Wall Volume = 0.03 m^3

Total Stiffening Wall Volume = 0.12 m^3

CSEB Desnity = 2000 kg/m^3

CSEB Dead Load = 6.81 kN

Plywood Volume = 0.09 m^3

Plywood Desnity = 700 kg/m^3

Plywood Dead Load = 0.62 kN

Total Tributary Dead Load = 7.43 kN

q_{Dead} = 2.5 kN /m

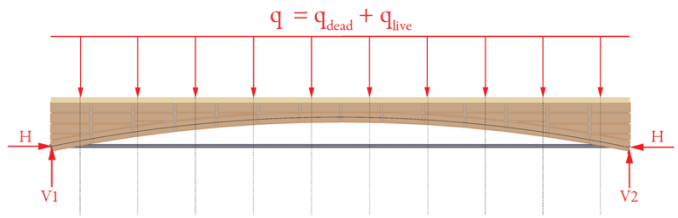

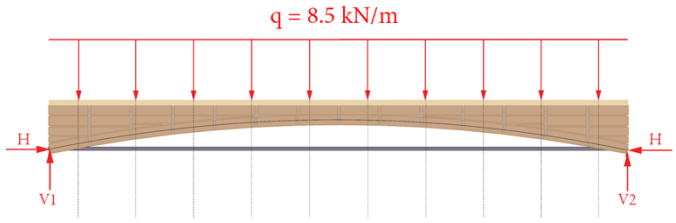

V1 = V2 = 12.75 kN

= qL/2

= (8.5 kN/m)(3m)/2

H = 63.75 kN

= qL^2/8y

= (8.5N/m)(3m)^2/(8)(0.15m)

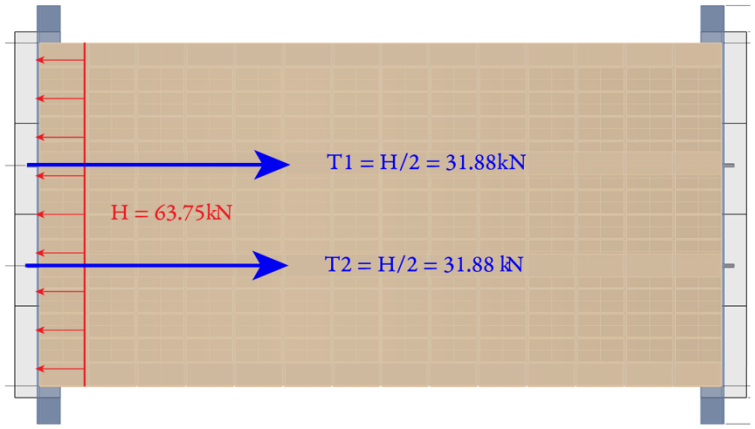

Tie Size

345 MPa Threaded rods are used; Yeild Strength 210 MPa

(24.375 kN / 210 MPa) / 1000 = 116 mm^2

Required Diamter = 12.2 mm (~1/2")

Picked Rod Diamter = 15.8 mm (~5/8")

Verifying Steel Angle Deflection

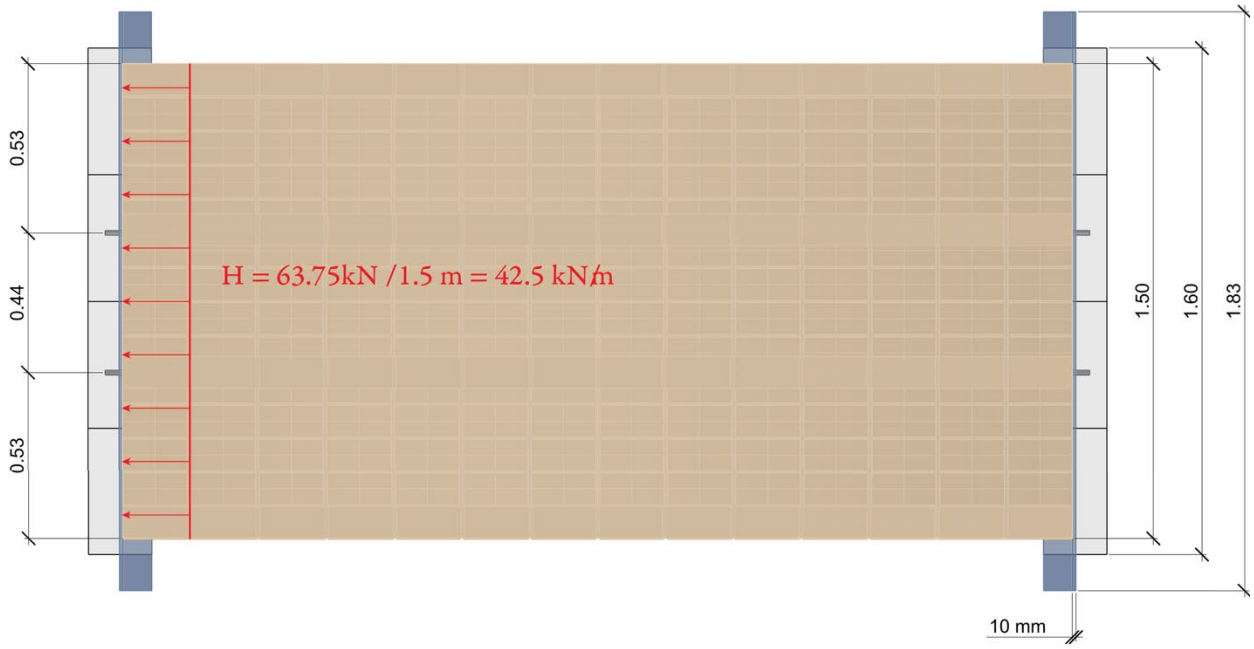

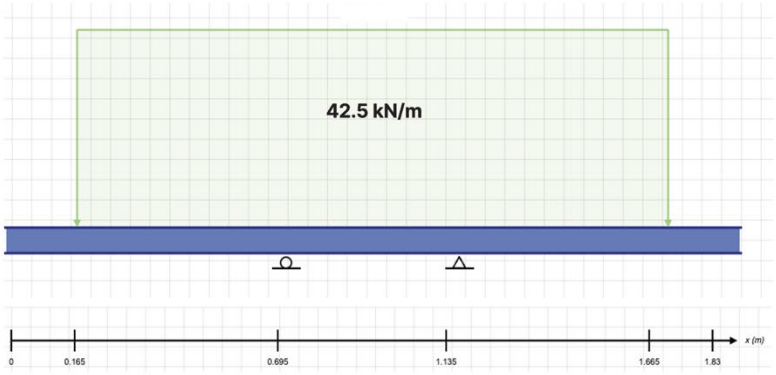

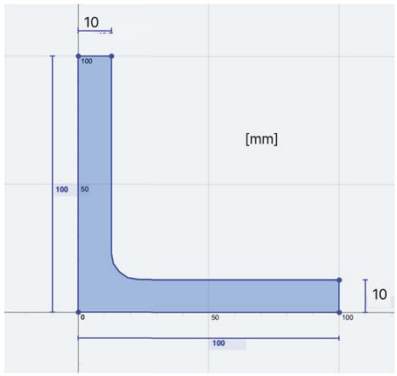

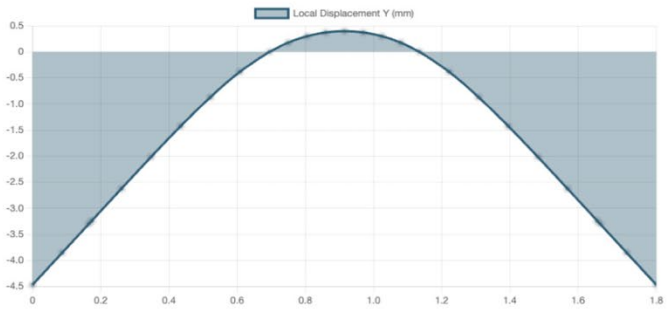

Location (m)	Total Deflection (mm)
0	5.171 mm
0.695	0 mm
0.915	0.457 mm
1.135	0 mm
1.83	5.171 mm

Prototype Deflection Analysis

Unloaded & Asymmetrical 2 kN/m²

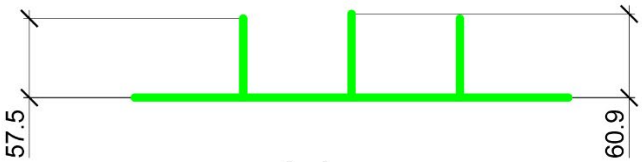

Symmetrical Loading 2 kN/m²

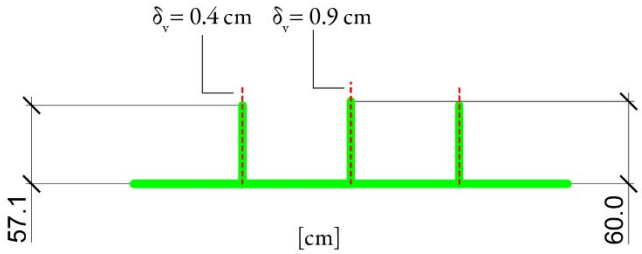

Symmetrical Loading 2 kN/m² + 1.25 kN Point Load at Center

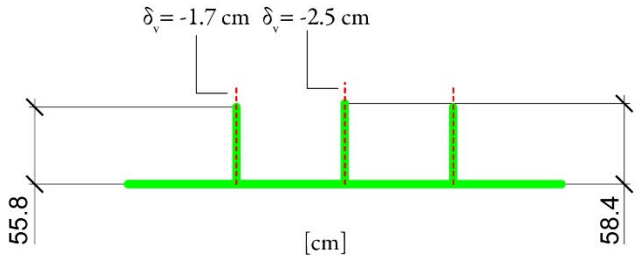

Asymmetrical Loading 4 kN/m² Right before faliure

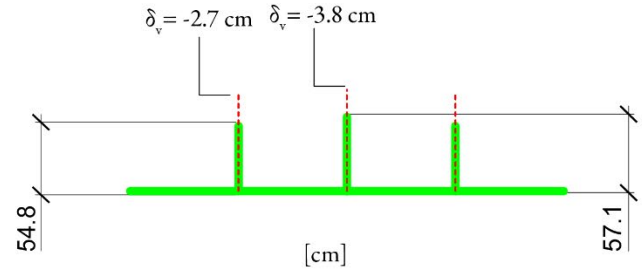

Asymmetrical Double Building Code Live Load – Deformed Geometry

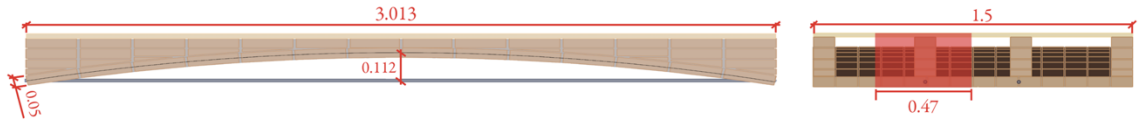

Live Load

Surface Load = 4 kN /m^2

Tributary Width = 0.47 m

q_{Live} = 1.88 kN /m

Dead Load

Primary Vault Volume = 0.227 m^3

Tributary Vault Volume = 0.071 m^3

Single Stiffening Wall Volume = 0.03 m^3

CSEB Desnity = 2000 kg/m^3

CSEB Dead Load = 1.98 kN

Plywood Volume = 0.09 m^3

Tributary Plywood Volume = 0.028 m^3

Plywood Desnity = 700 kg/m^3

Plywood Dead Load = 0.19 kN

Total Tributary Dead Load = 2.17 kN

q_{Dead} = 0.72 kN /m

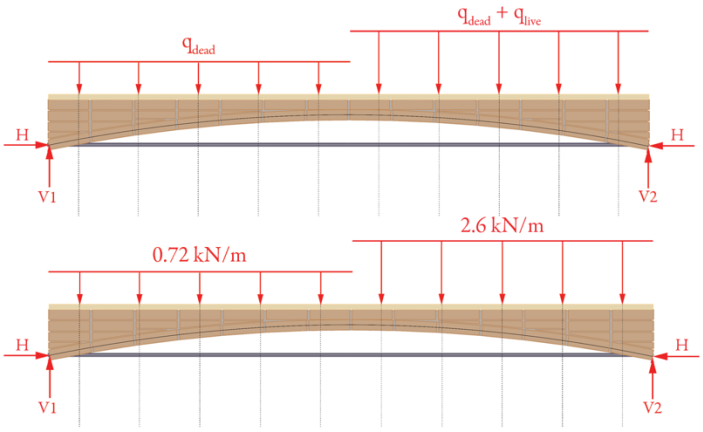

V1 = 1.8 kN

= (q_{dead}L/2) + (q_{Live}L/8)

= (0.72 kN/m * 3.01m /2) + (1.88 kN/m * 3.01m /8)

V2 = 3.2 kN

= (q_{dead}L/2) + (3q_{Live}L/8)

= (0.72 kN/m * 3.01m /2) + (3.01*1.88 kN/m * 3m /8)

H = 16.6 kN

= (L^2/16y)[2q_{Dead} + q_{Live}]

= [(3.01m)^2/(16)(0.112m)][4.04 kN/m

Resultant = 16.9 kN

= ($V1^2$+ H^2)$^{1/2}$

= (3.2^2+ 16.6^2)$^{1/2}$

Max Stress = 0.72 MPa

= Resultant / Tributary Area

= (16.9 kN)/(0.47m*0.05m)/1000